INVESTIGATION INTO THE LOAD SHARING AND JOINT STABILISING FUNCTIONS OF A KNEE-ANKLE-FOOT ORTHOSIS

by

LAURA FINNEY

September 1997

Thesis submitted in partial fulfilment of the requirements for the degree of Master of Science in Bioengineering, University of Strathclyde

Bioengineering Unit

University of Strathclyde

Glasgow

COPYRIGHT

ABSTRACT

Knee-ankle-foot orthoses (KAFOs) are commonly prescribed in the management of knee instability and in a limited capacity, to reduce the loading on the pathological anatomy. Conventional leather and metal KAFOs provide poor cosmesis but provide a wide choice for orthotic prescription. In contrast, the more cosmetic plastic and metal KAFOs now customarily administered provide a more lightweight design but with reduced stiffness and loading capabilities. As such mechanical failure, usually due to fracture of one of the metal uprights, is a common occurrence. To date, design of KAFOs has been largely empirical, with only limited evaluations into the their biomechanical performance.

This research evaluated the loads applied to the medial and lateral uprights at the orthotic knee joint of two cosmetic KAFOs, during normal level walking. A further investigation employing kinetic and kinematic data recording equipment was used to calculate total intersegmental loads. This information, together with the orthotic loading data, enabled a full biomechanical analysis of the joint stabilising and weight bearing capacity of the orthoses to be completed.

Two custom built, six-channel load transducers, designed during previous work at the Bioengineering Unit were used to replace the medial and lateral knee joints of the KAFOs. A computerised video system (VICON) recorded the 3D co-ordinates of body markers while a force plate measured the total ground reaction forces for the leg/KAFO complex. This allowed the derivation of gait characteristics like timing parameters and intersegmental forces and moments at the knee joint. Meanwhile the transducers measured the six loads applied to the KAFO at the orthotic knee joint. Conversion of the orthotic and total loads into the local reference system of the shank using the kinematic data enabled the loading data to be compared and allowed the biomechanical performance of the orthosis to be studied.

The results obtained from the two subjects tested varied in both the magnitude of the loads and the nature of the loading patterns. However, comparison of the total and orthotic moments for both patients clearly indicated that the KAFO adequately performs it joint stabilising function, by preventing the knee joint from buckling during the early part of stance. For the first patient wearing a high brimmed KAFO, the axial force results suggest that the orthosis relieved the anatomy by up to 90% during early stance, declining to approximately 20% during late stance. The other patient exhibited intense lateral trunk bending which caused a tensile force on the medial upright but a compressive force on the lateral one. When vectorially added the results showed that practically no weight bearing relief was offered by the KAFO of this patient. The high loads recorded for the patient wearing the high brimmed KAFO occasionally exceeded the maximum design loads for the transducer in the medio-lateral direction, indicating the need for stronger transducers to be constructed.

ACKNOWLEDGEMENTS

I would like to take this opportunity to express my gratitude and appreciation to all those involved in the completion of this project.

Firstly my supervisor, Stephan Solomonidis for his support and guidance throughout the project not to mention his endless enthusiasm which was of great encouragement.

The EPSRC for the grant which enabled me to study at the Bioengineering Unit.

Mariëtta van der Linden for her Matlab programs and her invaluable trouble shooting role during the data processing.

Ian Tullis for his assistance with the electronics and the staff of the mechanical workshop for their technical support.

Elaine Figgens and Brendan McHugh of the National Centre for Training and Education in Prosthetics and Orthotics for organising the patient tests and to the two patients for participating in the study.

My friends: Alice, Runi, Greg, Stuart, Steve, Neil and Shahrooz for both advice and laughter during the many long nights spent in the computer room and also to Chrissy and Raquel for their social support.

Finally to my family for their tireless moral support throughout.

TABLE OF CONTENTS

CHAPTER 1: INTRODUCTION

1.1 BACKGROUND

Orthoses are used in the treatment of a wide range of lower limb disabilities They are used where support, correction or immobilisation of the impaired structure is required. The present study concentrates on knee-ankle-foot orthoses (KAFOs) which are commonly prescribed in the management of knee instability and in a limited capacity, to reduce the loading on the pathological anatomy.

Despite the need for orthotic appliances far exceeding that for prosthetic ones, advances in the two fields have not been equal. In the case of prosthetics, the removal of the anatomical structure provides the manufacturer with the freedom to design a highly functional and cosmetic device. However, with an orthotic appliance where the same functional and cosmetic properties are required the designer is restricted by the need to interact with the underlying pathology. In spite of these problems, an extensive range of orthotic devices now exist, e.g. the 'Craig-Scott' orthosis and the 'Salford calliper', which use basic biomechanical principles in an aim to meet the functional requirements.

In the last 20 years the designs have gradually moved away from the traditional metal and leather designs first used over 100 years ago, to ones manufactured from a combination of metal and thermoformed plastic which provide lighter more cosmetically acceptable alternatives. With only basic design standards in existence the design of these devices has largely been empirical, manufactured by trial and error rather than by evaluating the structures biomechanically. This has often resulted in over designed structures which are heavier than required but which are still deficient in the critical areas, e.g. around the knee joint, where they are often prone to failure. Gozal (1986) investigated the loading of the orthotic knee joint of a KAFO that had failed twice, in both cases when the subject was stepping off a kerb. He observed that the KAFO provided an unintended load-relief from the anatomy of about 30% of body weight. It therefore seems probable that the loads on the KAFO, which resulted in fracture were a result of its weight bearing capabilities. Examination of this aspect of biomechanical analysis dates as far back as 1969 when Kirkpatrick (1969) examined the load relieving characteristics of an ischial load-bearing KAFO. Force plates and transducers recorded the total and orthotic loads respectively while cine cameras were used to determine the orientation of the leg relative to the laboratory reference system. Again it was found that the appliance transmitted up to 30% of body weight. However due to the limitations of their equipment they were unable to resolve the transducer loads into the reference system of the leg, leading to inaccuracies in their analysis. Similar studies by Lehmann *et al.*(1970) and Lehmann & Warren (1973) investigated different designs of weight-bearing KAFOs. They determined that the optimum design employed a quadrilateral thigh shell with fixed knee and ankle joints. However their research only concentrated on the axial force and was liable to the same inaccuracies of Kirkpatrick *et al.* (1969), detailed above. A complete three-dimensional (3D) analysis of the forces transmitted through a conventional KAFO was performed by Trappitt & Berme (1979) and Lim (1985). The load bearing abilities of the KAFOs were also investigated and the results indicated that the KAFOs were not overdesigned as had been previously assumed. Again these studies failed to determine the load sharing at the critical knee joint area.

1.2 OBJECTIVES OF THE STUDY

This study was a pilot study investigating the 3D load sharing capability of a cosmetic type KAFO, between the anatomy and the orthosis. The KAFOs under analysis were prescribed and manufactured for two post-poliomyelitis patients experiencing lower limb instability. The orthotic knee joints were replaced by two six-channel load measuring strain gauge transducers designed during previous research at the Bioengineering Unit. Measurement of kinetic and kinematic data during the experiments enabled a full biomechanical analysis of the orthotic gait patterns exhibited by the patient. The objectives of the study are:

1. Determine the loads applied through the medial and lateral uprights at the orthotic knee joint of a cosmetic type KAFO using strain gauge transducers.

2. Record kinematic data for the lower leg and KAFO using a computerised video system (VICON), and kinetic data, i.e. ground reaction forces and moments, using a triaxial force plate.
3. Combine the kinetic and kinematic data to calculate the intersegmental forces and moments transmitted through the total leg/KAFO complex in the reference system of the lower leg.
4. Use the kinematic data to convert the orthotic loads recorded by the transducers into the reference system of the lower leg.
5. Compare the loads calculated using the force plate data with those recorded by the transducer as an indication of the KAFOs ability to stabilise the knee joint and reduce loading on the anatomy.

A further investigation into the amount of deformation of the KAFO during weight bearing is possible by determining the ankle joint angle over the stance phase during gait.

1.3 ORGANISATION OF THE THESIS

The second chapter provides a comprehensive description of the use of biomechanical principles in the analysis of orthotic gait. To achieve this, the first part of the chapter introduces the subject of orthotics and in particular various designs of KAFOs. It then describes normal gait, pathological gait and parameters used to analyse the differences between the two gait patterns. The final part provides a review of the loading investigations carried out on KAFOs to date. Chapter 3 describes the instrumentation used in this study together with a description of the theory involved in the calibration of the equipment and the calibration procedure used. Chapter 4 describes the experimental methods employed during the patient tests. The theory used to analyse the results is detailed in Chapter 5 together with an outline of the computational methods employed to process the data. Chapter 6 presents the experimental results obtained which are discussed in greater detail in Chapter 7. Finally the conclusions together with recommendations for future work are presented in Chapter 8.

CHAPTER 2: LITERATURE REVIEW

2.1 ORTHOSES

2.1.1 Introduction

The term orthotics originates from the Greek words 'ortho' and 'statikos' which mean 'straight' and 'to cause to stand' (AAOS, 1952). The term 'orthotics' covers not just the physical appliances, but also includes the complete theory and practice of designing, casting, fabricating and fitting an orthosis (Dittmer, 1993). Different types of orthoses are used for different parts of the body depending on the shape and pathology of the section in question. Lower limb orthoses were previously known by a variety of names, including: brace, calliper, surgical appliance; and by names derived from their inventor, promoter or place of origin. This created a confusing situation whereby functionally similar orthoses, prescribed for identical conditions were known by entirely different eponyms.

In the early 1970s, the International Committee on Prosthetics and Orthotics devised a system which attempted to eliminate this confusion by standardising the terminology used in orthotics (Harris, 1973). For the limbs, the orthoses would be described by the joints which they encompass followed by the word orthosis. For example, the traditional 'long leg brace' stretching from the thigh, across the knee and ankle joints and down to the foot would now be called a knee-ankle-foot orthosis (KAFO). Likewise a 'short leg brace' extending from the calf to the foot would be renamed an ankle-foot orthosis (AFO). An orthosis was defined by the International Standards Organisation, TC168 WG1 as 'an externally applied device to modify structural and functional characteristics of the neuromusculoskeletal system in order to support, correct or protect the body part'. In practice, orthoses are mechanical devices which achieve their function through the application of forces and as such, engineering principles may be applied to their design and development to produce the optimum performance in terms of mechanical functional requirements.

2.1.2 History

The first direct evidence of the use of orthotics in medicine dates back to the Byzantine period. During excavation of the Nubian desert, a wooden splint which had been used to re-align a fractured ulna, was found in the grave of a young girl (AAOS, 1985). Prior to his death in 370 BC, Hippocrates described reducing and splinting methods in great detail however Galen (131-201 AD) was probably the first to use dynamic bracing in the treatment of scoliosis and kyphosis. The next 1000 years saw little development in splinting or bracing techniques and it wasn't until the work of Paré in the 16th century that any real advances were made.

Over the next few centuries nearly every famous physician was involved in altering existing devices. The most renowned was Hugh Owen Thomas (1834-1891), who produced orthotic designs for almost every joint. Indeed the functional concept behind his 'long hip splint' which incorporated an ischial tuberosity weight-bearing ring has remained virtually unchanged since its initial format and is still with us today. Throughout this century advances in materials and manufacturing techniques, together with a much needed stimulus resulting from the two World Wars led to a prolific period of orthotic research. Traditional metal and leather orthoses were abandoned in favour of their lighter, more cosmetically acceptable plastic counterparts. During the last 20 years this impetus has declined with many designers believing that the development has reached a natural plateau. It has been over 20 years since a substantially new design has appeared and with much room for improvement in the design, form and function of KAFOs, innovation in this area is long overdue (Platts, 1989).

2.1.3 Function of Orthoses

Developments in orthoses have mainly been material orientated with improvements in design resulting from trial and error rather than from a theoretical engineering analysis. Conventional KAFOs have not undergone much fundamental change since their introduction over a century ago. In essence they consist of double metal uprights of aluminium or steel, incorporating hinged knee joints and interconnected

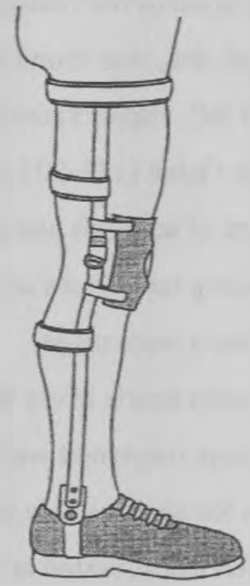

Figure 2.1
Conventional metal and leather KAFO (AAOS, 1952)

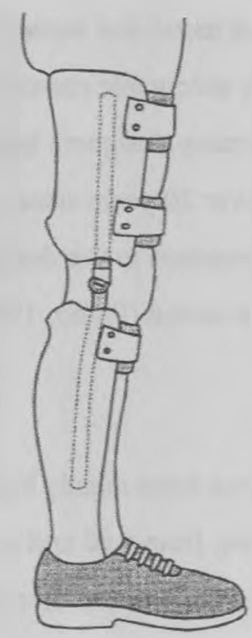

Figure 2.2
Cosmetic metal and plastic KAFO (Trautman, 1980)

by curved transverse bands which provide structural support (fig. 2.1). The padded bands are covered with leather which acts as the interface between the limb and the device. The KAFO attaches directly to the shoe via a variety of spurs, pins and stirrups thus making shoe interchangability near impossible. These designs were weighty and cumbersome and created difficulties for the patient in donning and doffing. Furthermore, most patients found them to be hard to clean and aesthetically unacceptable.

As mentioned earlier, new materials led to the development of thermoplastic orthoses (fig. 2.2). The leather components were replaced by two vacuum thermoformed plastic shells. The upper section covered the thigh segment while the lower one extended from the upper shank to the foot. Again the sections were interconnected by metal uprights. A major benefit of this design was that shoe interchange-ability was now permitted since the footpiece could be inserted inside a conventional, shop bought shoe. Intimate contact with the limb was increased which improved the force distribution over the anatomy. Patients also found the orthoses to be lighter and less obtrusive and deemed the new design to be more cosmetically acceptable. These designs also enabled the orthotist to have direct control over their function. For example, ankle dorsi flexion could be controlled by altering the stiffness of the ankle section, either by employing a thicker material during manufacture or by changing the trimline around the malleoli.

Orthotic treatment is primarily aimed at improving the ambulatory ability of the patient by producing a safer and more natural gait. This may be achieved by a variety of methods depending on the patient pathology, for example:

(i) *control* motion of a limb segment by opposing undesired musculature activity,
(ii) *compensate* for weakened or absent muscle power,
(iii) *correct* deformities by re-aligning the limb,
(iv) *support* anatomical structures from weight-bearing, often to relieve a painful joint.

The choice of orthotic prescription should be determined from the patients functional impairment and not from the clinical diagnosis. Biomechanically the function of conventional and cosmetic orthoses is the same with the former applying the controlling forces through the transverse bands whereas this is achieved via the plastic shells for the

Figure 2.3
Ortholen posterior leaf spring orthosis (McHugh, 1987)

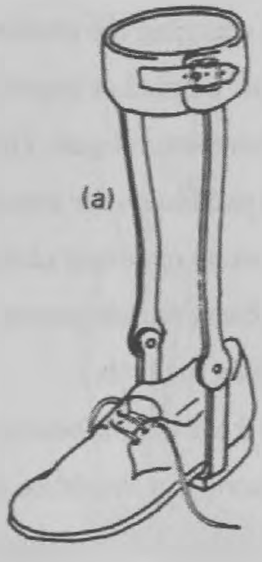

Figure 2.4
Conventional AFO with double side bars (McHugh, 1987)

latter.

In both orthotic designs (excluding those applied solely to the knee), the shoe is an integral component of the device which can directly affect its function. Depending upon the stiffness of the orthosis, the shoe upper can provide a counter measure to resist inappropriate plantar and dorsi flexion of the ankle joint. Stability of the limb can be altered by utilising a variety of shoe modifications including heels of differing density and those with medial or lateral flares. An obvious functional requirement from a design viewpoint is the provision of a mechanism which allows knee flexion during sitting for a locked knee KAFO. A KAFO can be considered as a combination of a knee orthosis (KO) and an AFO. Thus the next section detailing different KAFO design will begin with a brief review of current AFO practice.

2.1.4 Ankle Foot Orthoses

The AFO is probably the most commonly prescribed lower limb orthosis. It is primarily prescribed for conditions which result in muscle weakness or joint instability of the ankle-foot complex. Orthotic selection for various disorders is considered below.

<u>Inadequate dorsiflexion</u>

The biomechanical requirement includes dorsiflexion assistance to change the ankle joint angle at the end of stance phase from a plantar flexed to a neutral position, to prevent foot drag during swing. A controlled resistance to plantar flexion after heel strike is also required to prevent foot slap. The Ortholen™ posterior leaf spring orthosis, figure 2.3 is commonly used to manage this condition. The ankle section may be re-shaped by trimming either anteriorly or posteriorly to the malleoli to provide the degree of stiffness required. Other variants include the Engen-TIRR polypropylene AFO which resists plantar flexion while allowing limited dorsiflexion and practically no medio-lateral stability to the foot (Lehmann, 1979). Inadequate dorsiflexion produces an abnormal gait pattern with an extended heel strike duration hence an alternative design incorporating a plantar flexion stop into an articulated AFO was tried in an effort to normalise heel strike.

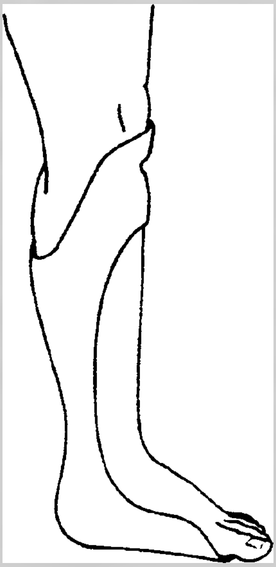

Figure 2.5
Floor reaction AFO (McHugh, 1987)

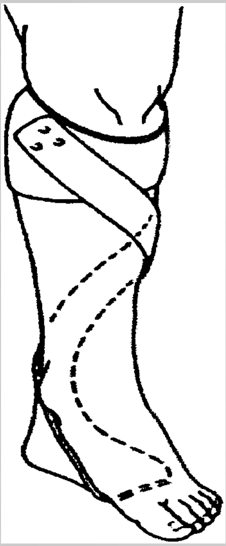

Figure 2.6
Spiral orthosis (McHugh, 1987)

A conventional AFO with double side bars and a spring-loaded dorsiflexion assist mechanism will fulfil the same functional requirements, figure 2.4.

Inadequate plantarflexion

In this case orthotic intervention is required to prevent passive dorsiflexion at the end of stance phase and provide an active push-off. For plastic AFOs, a relatively anterior trimline is needed to resist deformation on weight-bearing. This can cause patient discomfort due to the magnitude of the posteriorly directed force acting below the patella and if so the 'floor reaction orthosis' may be prescribed (fig 2.5). This design applies force to the pressure tolerant patellar tendon area but its rigid construction completely prevents plantar flexion. A conventional AFO incorporating a dorsiflexion stop will also achieve the same function (McHugh, 1987).

Subtalar instability

Weakness of the pronators will result in a varus position of the foot during swing phase and likewise weakness of the supinators will cause valgus foot during stance. Conventionally constructed orthoses attempt to correct this impairment using T-straps positioned over the appropriate malleolus and attached to the contralateral upright (Condie, 1993). Polypropylene AFOs with anteriorly trimmed ankle sections will provide effective subtalar stability but will also affect gait by eliminating all natural rotational motion. The spiral ankle-foot orthosis was specifically designed to avoid this problem (fig. 2.6). The spiral unwinds on weight bearing to permit plantar flexion and rewinds during swing thus causing dorsiflexion of the foot. Subtalar stability is controlled through a three point pressure system inherent in the spiral configuration (Lehneis. 1969).

2.1.5 Knee-ankle-Foot Orthoses (KAFOs)

A KAFO has been defined in BS2574: Part 2 (1985) as, "a device applied directly and externally to the patient's leg, extending from above the knee to the heel or beyond, with the object of, for example, correcting or compensating for a deformity or weakness". Patients suffering from post poliomyelitis syndrome probably make up the largest group of KAFO users in Britain (15,000) (Platts, 1989). The next biggest group

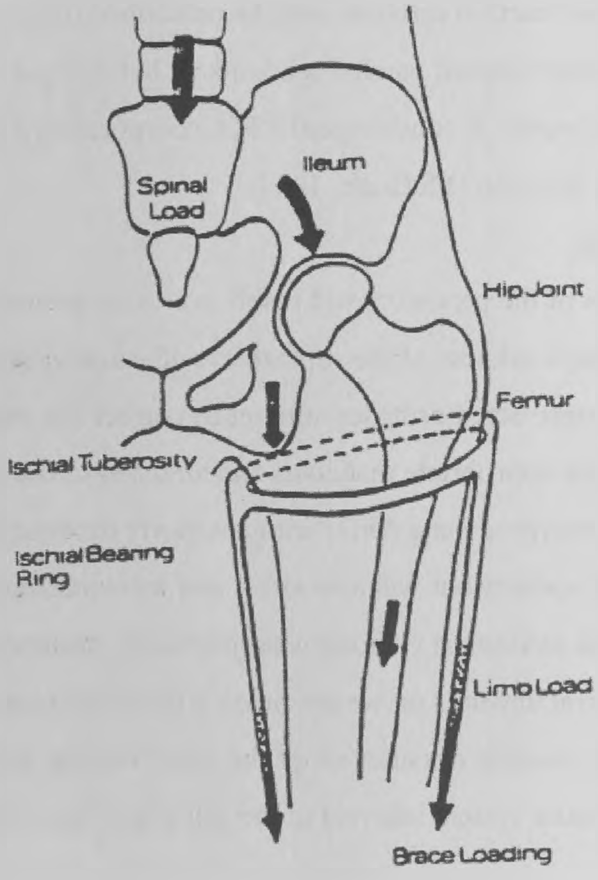

Figure 2.7
Ischial loading by an orthosis (Anderson, 1977)

would be those suffering from spina bifida, followed by a range of other disorders including muscular dystrophy, motor neurone disease, multiple sclerosis, spinal injuries, failed knee arthroplasties, etc. There is both an increased success rate and better acceptance for patients with polio than with most other conditions. This is undoubtedly because of the nature of the disease and the residual state of the limbs, i.e. flaccid paralysis, generally of the lower extremities and with some musculature remaining. Indeed many polio patients have been using KAFOs for 30-40 years. KAFO designs may be divided into two functional categories, namely joint stabilising KAFOs and weight bearing KAFOs.

Joint stabilising

This group is designed to stabilise the knee and ankle joints in the medio-lateral (M-L) or anterior-posterior (A-P) planes. For example, in the case of a post polio patient presenting with knee instability due to paralysis of the quadriceps muscles, a locked knee KAFO would prevent unwanted knee flexion during early stance, is often prescribed. A design which fully encased the ankle and foot would also provide optimum mediolateral stability, in proportion to the KAFO's ability to resist twisting and mediolateral deformation (Lehmann, 1979; Lehneis 1972). However, if the ankle is secured inside a rigid orthosis then at heel strike, the normal shock absorbing mechanism of controlled plantar flexion is eliminated causing the leg and foot to pivot forward together. The flexor bending moment that such an action produces must be compensated through muscle force or by an orthosis which will absorb part of the torque.

Other methods to control joint motion include the prevention of genu recurvatum (knee hyperextension) during weight bearing by limiting limb segment movement or by emulating push-off with the provision of a dorsiflexion stop and a foot plate which extends to the metatarsal head. Overall, all KAFOs should perform by substituting for the deficiency without hindering any remaining limb functions. The final orthotic design will be a compromise between strength, weight, comfort, reliability and cost.

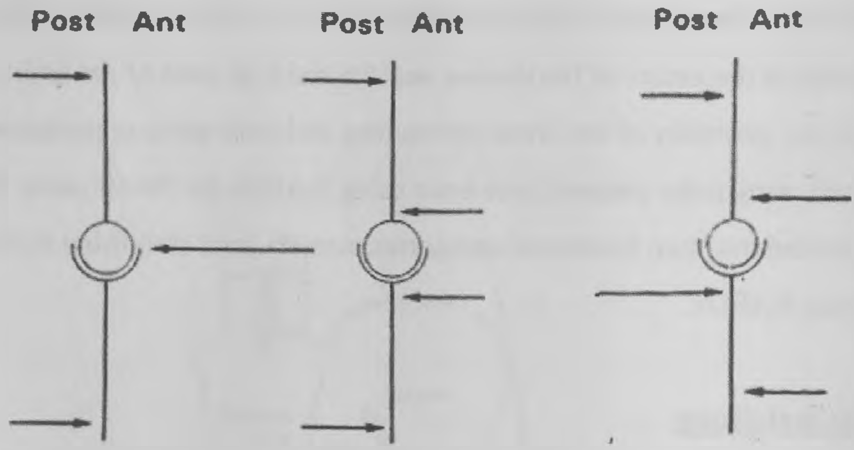

Figure 2.8
Three different force systems used to stabilise anterior-posterior motion at the knee joint (Condie, 1987)

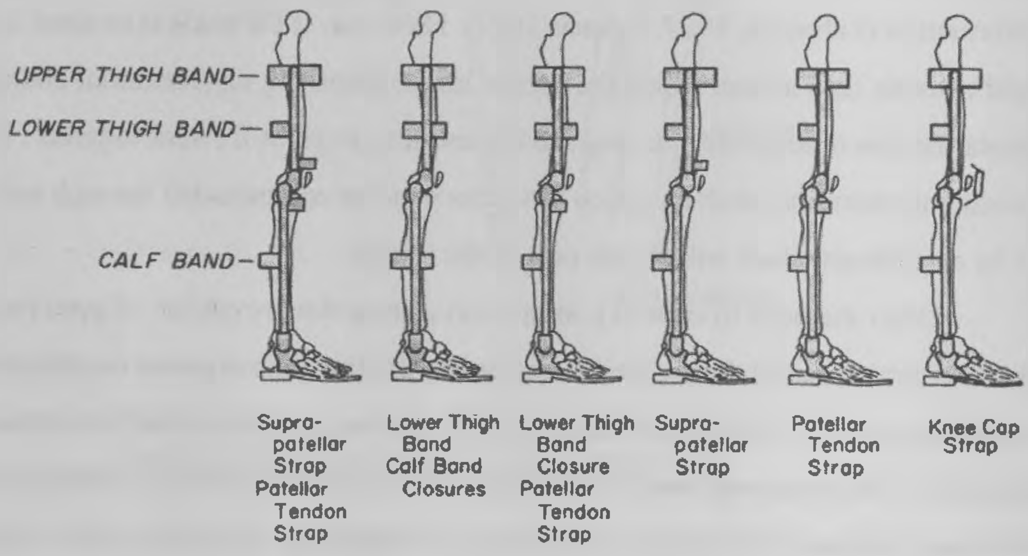

Figure 2.9
Six variants of the conventional KAFO design (Merritt, 1987)

Weight-bearing

These KAFOs function by relieving the anatomy from axial loading resulting from the ground reaction forces in addition to performing the stabilising role detailed above. Complete load relief is only possible using a patten bottom design which suspends the limb within the orthosis. Most designs function by transferring body weight directly to the pelvis, thereby bypassing the limb (fig. 2.7). Indications for use include joint instability, pain from trauma or disease and slow healing fractures. Henshaw(1970) recognised the importance of weight bearing relief for poliomyelitis patients when he designed his new cosmetic type calliper. He stated that the load should be borne by the ischial tuberosity so that the patient is effectively sitting on the orthosis. Korsah (1990) considered that use of an ischial bearing-ring or quadrilateral top was only necessary for patients with flail hip whereas those with paralysis of the quadriceps muscles could bear weight if supported correctly. Traditional designs, such as the Thomas splint employ a padded ring to transfer the load. More contemporary designs use a quadrilateral brim (Condie, 1987) similar in nature to those used for above knee prostheses. In these designs, the force is shared between the ischial seat and the thigh and inside of the socket with the view to providing better pressure distribution. However any closely fitting KAFO will relieve a proportion of the loading (Bowker, 1987) with the degree of fit critically influencing the performance. Also since the tightening of the straps will alter the fit, the patient can have a great influence over the effectiveness of the orthosis.

A three-point force system is then used to provide M-L and A-P stability in the coronal and sagittal planes respectively. The forces required to control knee stability are illustrated in figure 2.8. The central knee force is usually split into two components, applied on either side of the knee joint which prevents pressure on the patella. Extra bands at the thigh, calf, suprapatellar and patellar tendon may be added to dissipate force and reduce skin pressure and subsequent tissue damage. Figure 2.9 illustrates six variants of the traditional KAFO design which have little effect on the biomechanical function (Merritt, 1987).

The first practical KAFO used was the Thomas splint. This conventional device was designed in the 19th century and employed the Thomas ring as described above. One of the first improvements to this original design was the Scott-Craig KAFO (Scott, 1971; Lehmann *et al*,1976). This orthosis, designed for use by spinal cord injured patients, featured a minimum number of straps and bands for ease of application. The UCLA 'functional long leg brace' was designed with the intention of providing an alternative mechanism to counter the knee flexion moment during early stance (Condie, 1987). A hydraulically controlled plantar flexion motion controlled the ankle joint while the posteriorly offset knee joint altered the position of the ground reaction force to increase stability. Similarly, the IRM hydrapneumatic knee-ankle control system described by Lehneis (1969, 1972) used the same principles to prevent the knee from buckling during the critical period from heel strike to mid stance. This design offered advantages in improving energy efficiency and gait but was heavy with poor cosmesis.

The Salford KAFO was specifically designed to reduce weight-bearing while providing stability to patients paralysed by poliomyelitis (Henshaw, 1970). This design utilised plastic materials but only as a cosmetic covering over the metal uprights. The first real structural use of plastic was reported by Lehneis (1969, 1972) for his supracondylar KAFO. The unitised plastic laminate orthosis encased the knee mediolaterally and extends from a point 7cm above the malleoli to a position 4cm above the anterior border of the patella, thus effectively controlling genu recurvatum. The design combines previous orthotic devices with above-knee prosthetic alignment principles to produce a device that stabilises the knee during stance without the need for a mechanical lock.

The Stanmore KAFO (Tuck, 1974) is one of the early designs of plastic orthoses, still widely prescribed today. The thigh and shank sections are moulded from polypropylene and interconnected by aluminium or stainless steel uprights. Traditional leather straps are replaced by velcro bands providing a lightweight, cosmetic orthosis. Recently new designs have emerged based on material and manufacturing advances. One such example is the fully plastic modular orthosis, described by Engen (1989). Constructed from mass-produced plastic extrusions and attached with minimal straps and fasteners, the orthosis offers considerably reduced weight, delivery time and cost. Finally, Granata *et al.* (1990) designed a carbon fibre reinforced plastic KAFO for myopathic patients. They successfully reduced the weight of the orthosis by 40% compared to typical polypropylene orthoses. However unlike thermoplastics, carbon fibre materials cannot be re-shaped by heating to allow for minor adjustments after initial fitting.

2.2 GAIT ANALYSIS

Ambulation (or walking) is the most energy efficient method used by the human body to move from one position to another. It is a rhythmic symmetrical movement involving alternating motion of the trunk and extremities (Esquenazi, 1994) that requires the complex co-ordination of a variety of motor and sensory units under the direction of the central nervous system (Perry, 1967) to complete the action in a smooth, controlled manner.

A variety of methods are used in gait analysis, with the technique depending upon the information required. These range from straightforward observational analysis used by clinicians for a preliminary assessment and diagnosis of the pathological gait to more complicated biomechanical analysis used by engineers. Temporal parameters are often best measured using foot switches, instrumented walkways and cinematography or more commonly videography (Dittmer *et al*, 1994). Kinetic data dealing with forces, moments and power are traditionally acquired using transducers either in the form of force plates or by direct attachment to specially designed orthoses. The importance of relating forces, moments and joint angles to time-distance variables, frequently leads to a combination of methods used to analyse gait. The gait cycle is generally broken down into its separate stages. This next section details some of the terminology used to describe and evaluate normal gait.

2.2.1 Gait parameters

Gait involves the motion of the body by alternative re-location of the feet. In this context, it will be used to define walking with the condition that one foot must always be

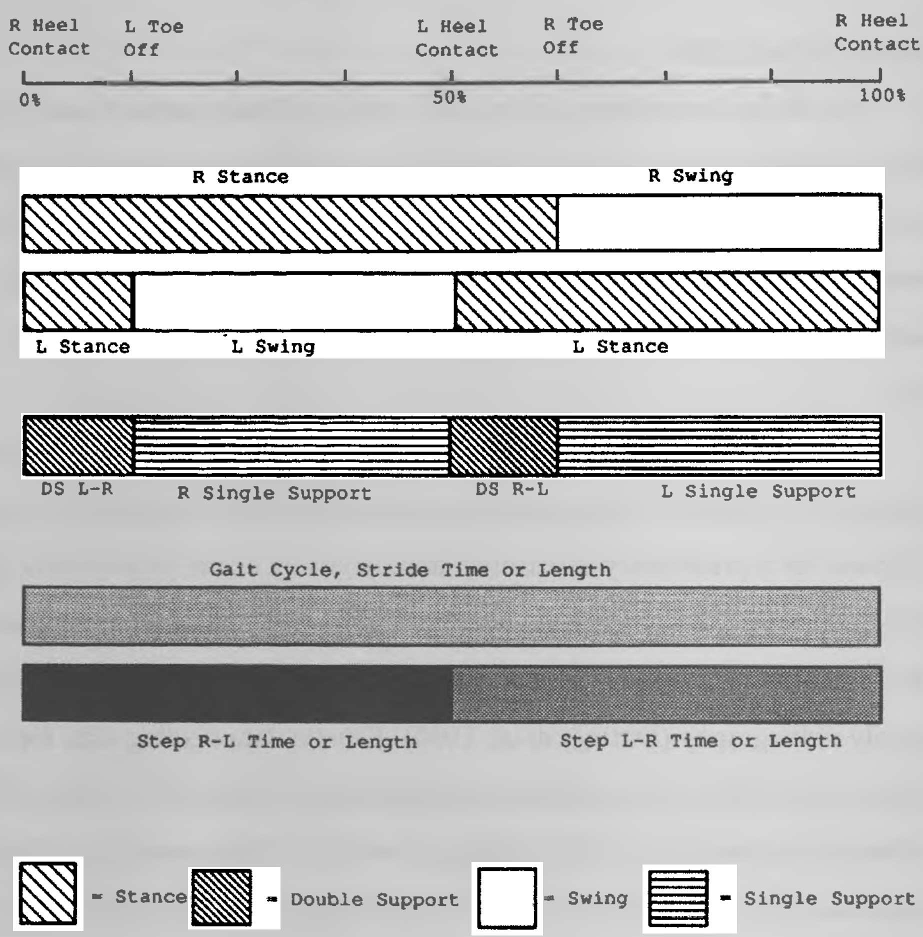

Figure 2.10
Temporal parameters of the gait cycle (Smidt, 1990)

in contact with the ground. It is a recurrent cycle that can be characterised by discrete temporal and distance factors which are crucial to understanding the complete gait cycle.

The gait cycle (fig. 2.10) is generally considered as the interval between successive ipsilateral foot contact. A step time is defined as the time between consecutive feet contacts and so a stride time, which is the completion of one gait cycle, consists of two steps. It is useful to normalise data to the stride time so that temporal parameters within and between patients can be compared. Another useful division of gait cycle is consideration of the time that each foot is in contact with the floor. This is termed the stance time and occupies about 62% of the cycle at 1m/s (Nicol & Paul, 1988) with the remainder of the cycle, known as swing time occupying 38%. Double foot support occurs twice in the cycle from 0-12% and 50-62%, with single foot support occupying the remainder (Smidt, 1990; Nicol & Paul, 1988).

These gait cycle ratios relate to a normal subject walking at moderate pace. When the pace is increased, the stance and swing time both reduce and the duration of the double support period slowly decreases until it completely disappears. Technically, at this point the subject is running.

The analysis may be further sub-divided by concentrating on the anatomical position of the foot as the cycle progresses. For example:

<u>Heel strike</u>: This, being the first contact of the heel with the ground, usually defines the beginning of the cycle. Although in some forms of pathological gait the forefoot is the first point of contact and initial foot contact would be a more accurate definition.

<u>Foot flat</u>: As the name suggests the foot is in full contact with the ground.

<u>Toe off</u>: Last contact of the foot with the ground in nearly all cases occurs at the toes.

These events are separated by identifiable intervals which relate to complex musculature activities of the limb. These intervals are associated with performing the functional activities involved in walking, namely shock absorption, momentum control and forward propulsion; single limb balance; and limb length adjustment (Perry, 1967).

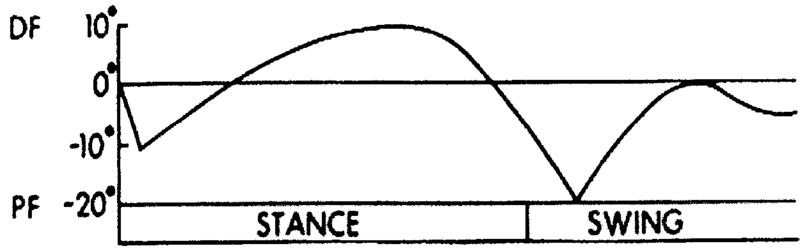

Figure 2.11
Ankle angle during the gait cycle: dorsiflexion (DF); plantar flexion (PF). (AAOS, 1985)

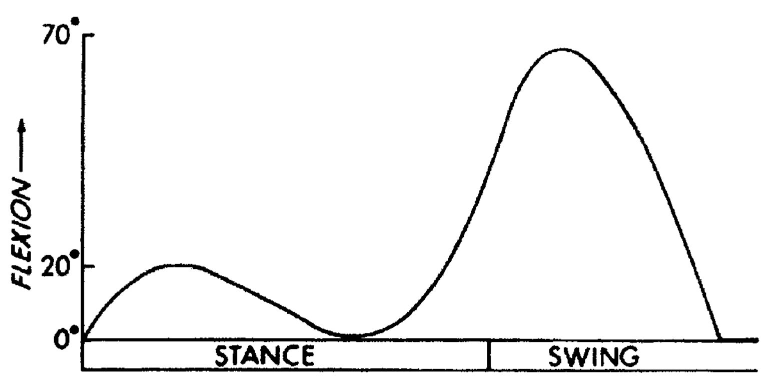

Figure 2.12
Knee angle during the gait cycle (AAOS, 1985)

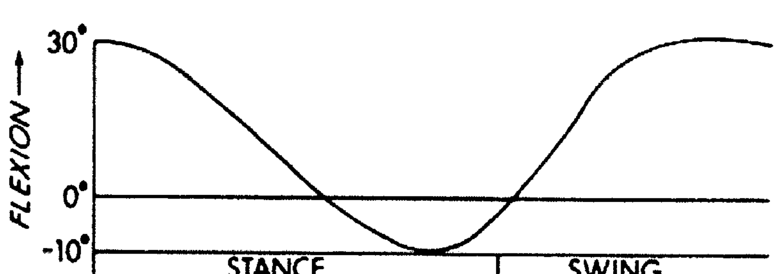

Figure 2.13
Hip angle during the gait cycle (AAOS, 1985)

2.2.2 Joint Angles

Joint angles are important parameters in gait analysis. When plotted for healthy individuals a clearly recognisable pattern emerges that is used as a standard to which a pathological gait can be compared. Values are generally calculated for the hip, knee and ankle joints with each displaying a distinct pattern.

Immediate plantar flexion occurs as the heel strikes the ground but action of the dorsiflexor muscles prevents foot slap (fig. 2.11). The forward momentum of the body is absorbed through rapid knee flexion to 15° by action of the quadriceps, and the hip is at maximum extension. The ankle moves into a slight dorsiflexion position as the body continues its forward travel, now supported on a single limb. The hip and knee return to their maximally extended position as the body is at its highest position. The plantar flexors become active next as they prepare to push the foot up and propel the body forward. As weight is transferred to the contralateral limb, rapid passive knee flexion (0-50°) occurs without evident knee flexor activity (Perry, 1967). This early swing phase is characterised by flexion of the hip, knee and plantar flexion at the ankle as the limb is picked up off the ground to prevent foot drag. The knee is now extended (fig. 2.12) and the hip is further flexed (fig. 2.13) as the limb stretches through ready for load bearing. The foot returns to a plantar flexed position in preparation for another heel strike, and the cycle is complete.

2.2.3 Ground Reaction Forces

Force is a vector quantity having magnitude and direction. It is the product of mass and acceleration. The external forces acting on a body will be related to its acceleration, both gravitational and resulting from the velocity and direction of its path through space and to its mass. Tri-axial force platforms measure the three orthogonal forces which the body exerts on the ground. When plotted against the gait cycle a distinctive pattern corresponding to certain physical events is produced. The vertical component (fig. 2.14) starts at zero at heel strike rising to a peak just greater than body weight for average walking speed. The next peak occurs as the leg pushes the body up

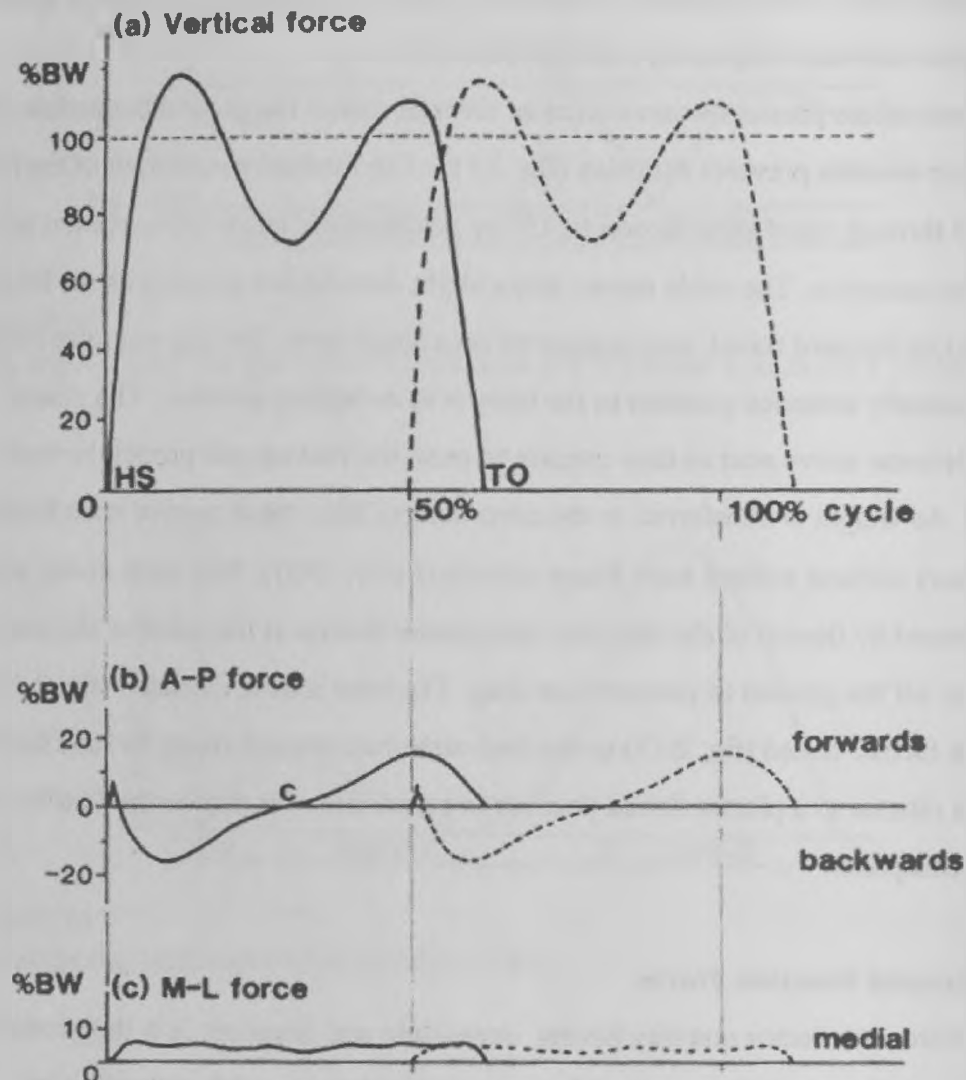

Figure 2.14
The three components of the ground reaction force acting on the foot during the gait cycle (Nicol and Paul, 1988)

just after the heel leaves the ground. The trough separating the peaks occurs at mid stance resulting from the upward acceleration of the contralateral limb. The initial spike displayed on some graphs, relates to the impact of the body on the ground (Mann, 1988).

The forces along the direction of walking are measured by the anterior-posterior shear and follow the pattern displayed in figure 2.14. An initial backward shear reverses direction at midstance causing a forward force on the foot no greater than 20% body weight (Henshaw, 1969). The small medio-lateral forces are directed medially on each foot over the cycle (Nicol & Paul, 1988).

2.2.4 Moments

A moment is the product of forces and the perpendicular distances from the pivot to the line of action of the force. Hence if the joints are considered to act as pivots the ground reaction forces will cause a moment about the joints which must be resisted by the muscles. Although moments are three-dimensional by nature, the sagittal plane moment dominates during gait and is predominately used for analysis (Smidt, 1990). This type of analysis neglects inertial moments resulting in different values than those obtained using inverse dynamics. For the ankle however, the mass and inertia are low and the moments will be similar to those calculated.

Loading of the knee is variable among individuals and difficult to predict. In contrast the hip moments although easy to predict, are difficult to calculate since small inaccuracies in the moment arm will produce large moment errors due to the large forces experienced. At heel strike the GRF passes anteriorly to the hip and knee, and posteriorly to the ankle. This tends to flex, extend and plantar flex these joints respectively. As the stance phase progresses the GRF moves behind all joints (fig. 2.15)and quadriceps activity is required to control flexion of the knee. As the trunk continues to glide forward, first the ankle and then the knee and ankle remain positioned posterior to the force and active plantar flexion is required for ankle stability and push-off (fig. 2.16).

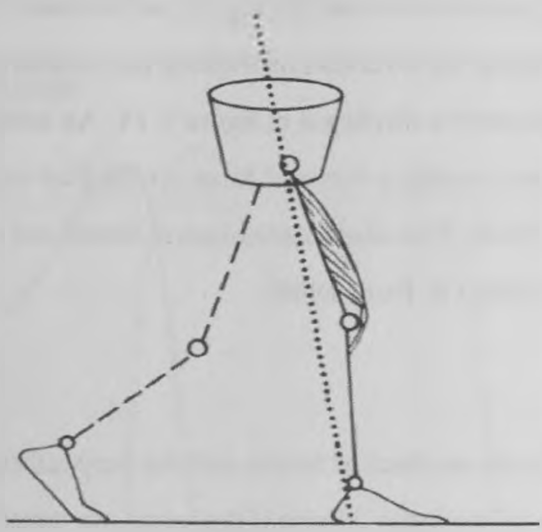

Figure 2.15
Position of the ground reaction force during early stance (AAOS, 1985)

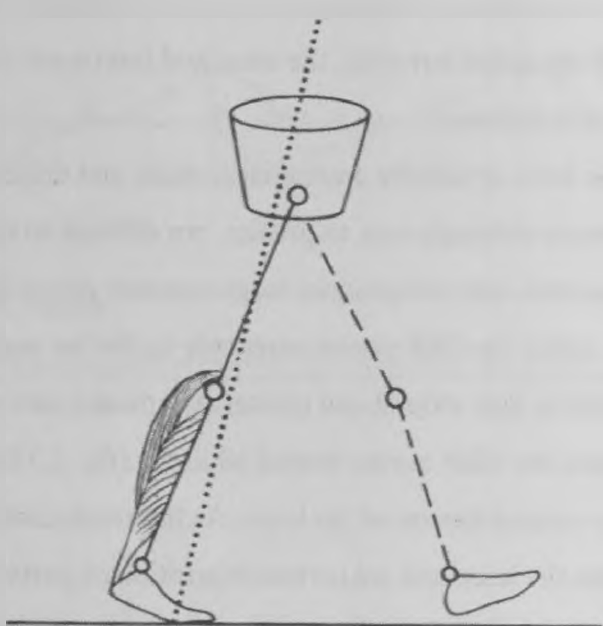

Figure 2.16
Position of the ground reaction force during late stance (AAOS, 1985)

2.2.5 Normal Gait

For most healthy individuals, gait is a natural skill performed sub-consciously in a highly uniform manner. It is a safe action accomplished with the optimal conservation of physiological energy. All individuals exhibit their own unique gait patterns, easily recognisable to their close friends. These patterns depend not only on the person but also on the situation, with changes in speed, activity and terrain causing unrecognisable differences. The average values for these individual patterns for level moderate walking are assembled together to produce the typical force/moment/joint angle curves commonly used to analyse the gait of 'normal' subjects. Through a detailed knowledge of normal gait and the deviations displayed by pathological conditions the corresponding deficits can be understood and corrective measures taken.

2.2.6 Post-poliomyelitis Gait

A detailed literature search reveals that despite comprehensive research into normal gait patterns, little of this has been directed towards analysis of post-polio gait. This is perhaps due to the lack of a typical paralysis pattern, with muscles affected ranging from weakness in just a few to total paralysis of all four extremities. However, one of the most common problems is flaccid paralysis of the lower limb extensors. This effect is best examined by considering the position and direction of the GRF during a gait cycle. At heel strike the GRF vector passes anterior to the knee generating an extension moment that stabilises the joint. As the body advances, the GRF is directed posterior to the knee producing a flexion moment. Weakened quadriceps muscles will be unable to prevent knee flexion thus producing an unstable gait. The patient with a unilateral impairment often tries to overcome the deficiency by adopting compensatory gait deviations. Manually pushing the thigh posteriorly will force the knee into extension. Alternatively, trunk flexion during stance creates a stabilising extension moment by repositioning the GRF in front of the knee. These unsightly manoeuvres produce high energy consuming gait patterns which require orthotic correction in the form of a KAFO as described in section 2.1.5.

The precise orthotic gait pattern will depend on the orthosis with great variability among cases, e.g. the infinite stability provided by a locked knee KAFO is at the expense of a stiff-gait pattern with high metabolic energy costs (Merritt, 1987). Another disadvantage with these typical KAFOs which prevent knee flexion is the associated problems with foot clearance during swing phase. Hip hiking, lateral trunk sway, circumduction and plantar flexion of the contralateral limb are examples of some techniques used by patients to overcome this problem. Nevertheless, a well designed orthosis should not cause additional abnormalities.

Other factors which influence gait are firstly, unlike a prosthesis, the orthotic device is worn over the limb and will thus add extra weight to an already weakened leg. Secondly, the post polio patient has full proprioception and consequently can make optimum use of the remaining muscles and knowledge of joint position to substitute for missing functions and compensate for his/her impairment. A simple gait evaluation could examine cadence, since in their analysis of orthoses for hemiplegic patients, Dittmer *et al* (1994) viewed that an effective orthosis should increase patient cadence. Finally, in evaluating amputee gait, van der Linden (1995) raised some important questions which can be applied to any pathological gait, such as: why does the deviation occur? i.e. due to orthosis or pathology. Also is the deviation a solution to the original problem or should it be changed? Answering these questions should help to evaluate the gait and aid in assessing the effectiveness of the orthotic prescription.

2.3 LOADING

2.3.1 Introduction

Evaluation of KAFO loading may be divided into three categories in relation to the instrumentation used. The first group employs force plates to measure the ground reaction forces being transmitted through the whole limb. This type of analysis will provide information on the loading on the complete foot/orthosis complex. The second category aims to determine the forces taken by the orthosis, usually by a number of force measuring transducers incorporated into the KAFO structure. This information provides useful design data for determining the required strength of the orthosis but reveals little about the effectiveness of the orthosis on the loading of the limb. These data are obtained by the final group who, by using a combination of transducers and force plates can perform a simple subtraction that enables them to calculate the anatomical loading. A search of the literature reveals that while sporadic attempts have been made over the last 30 years to measure both total and orthotic loading, limited research has been conducted into anatomical loading. Thus, at present a considerable lack of information on comprehensive anatomical load analysis exists.

KAFO loading is a complex function which depends on the KAFO, the patient and the activity being performed (Platts, 1988; Lim, 1985). Each patient is different in size, shape and walking style and since KAFOs are custom made to suit the individual patient then their design is subject to much variation. Indeed even the same KAFO prescribed for two almost identical patients may be subjected to very different loads depending on the wearers style of walking (Lim, 1985). Most of the analysis to date has been empirical, with advances in materials and technology being tested by trial and error rather than through a quantitative engineering analysis, involving theory and mechanical testing. Design has often concentrated on satisfying medical demands, often leaving aspects such as strength and safety to chance. This has led to either problems with failure during use or heavy over-designed KAFOs which contain more metal than required but are still not strong enough in the critical areas.

2.3.2 Failure of Orthoses

The average KAFO lasts about 9-12 months before failure or patient changes mean a new orthosis is required. Scothern *et al* (1984) believed that many cases of KAFO failure went unreported perhaps because they were not considered as failures, e.g. when an orthosis needed re-aligned due to yielding. Failure should cause minimal injury to the patient and they suggested that if KAFOs were constructed from materials which failed in a ductile manner then lighter orthoses could be used without risk of catastrophic failure. Anderson *et al* (1977) reported four cases of mechanical failure from a test group of 36 during their clinical assessment of the Salford KAFO. All patients were male none of which were physically injured and the failures occurred in cases of over-loading. This team believed that it was impossible to design for all loading situations, e.g. patient tripping, since the resulting orthoses would be too heavy. Anderson also performed a static load analysis on an experimental Thomas ring KAFO in an attempt to relate the orthosis length to its weight bearing capabilities (Elias, 1994). Calibrated springs incorporated into the orthotic uprights measured the KAFO loading while the ground reaction force was measured using conventional bathroom scales. Twenty patients with unilateral paralysis due to poliomyelitis were investigated. He found that although loading was not directly proportional to the length of the orthosis, the KAFO unloaded the leg by approximately 84% when equal to leg length, i.e. ischial tuberosity to floor, and was completely unloaded when reduced to 80% of limb length. He also reported that loads on the lateral uprights were always less than those on the medial.

2.3.3 KAFO Weight Sharing Capability

Kirkpatrick *et al* (1969) were one of the first groups to attempt a full dynamic engineering analysis of the division of loads between the leg and the orthosis. Force plates were used to measure the ground reaction forces while strain gauge transducers mounted in the lower part of the KAFO near the ankle were used to measure KAFO loading. Both the force plates and the transducers could measure forces in three orthogonal directions. A cine-camera recorded the kinematic data, allowing the angle of the leg to be calculated during all phases of gait. By matching the instant of heel strike on the film with that recorded by the transducers, the force plate data could be resolved into axes fixed with respect to the leg and a comparison between total and orthotic loading made.

The orthosis used was an ischial weight-bearing KAFO. They found that the axial force borne by the orthosis never exceeded more than about 30% of body weight and hence does not fulfil its designed purpose of weight relief. The cine-camera data were used to convert the ground reaction forces into the reference system of the leg. However the difference between the orthotic axis in which the orthotic loads were measured and the anatomical axis of the leg into which the total loads were resolved was neglected. Also since the camera used could only record the leg position in one plane then the unaccounted difference between the two sets of force measurements are likely to be quite substantial unless the leg motion was accurately maintained in the sagittal plane.

An evaluation of the changes in axial loading due to the differing designs of ischial weight-bearing KAFOs was also performed by Lehmann *et al* (1970). Using the same instrumentation set-up and analysing techniques as Kirkpatrick *et al* (1969), with the same associated problems as mentioned above, they performed a dynamic analysis of seven types of KAFOs on the one volunteer. They found the quadrilateral shell to provide more weight relief than the Thomas ring design. In terms of the ankle and knee joint designs they concluded that the anatomical loading was progressively decreased with: (1) The quadrilateral shell with fixed knee and free ankle; (2) The same design with fixed ankle; (3) The same design with rocker bottom which could nearly provide complete weight bearing relief. An interesting point to note is that voluntary muscle action, i.e. plantar and dorsi flexion will vary the anatomical loading. Thus careful training into the proper use of the orthosis can significantly alter the loading characteristics.

Lippert (1971) investigated the loading properties on 19 different versions of an experimental KAFO. The ischial weight bearing orthosis was custom-built to record all six components of the forces and moments. However the additional instrumentation meant its mass was 5kg, some 2-3kg heavier than a normal design. After preliminary measurements which illustrated that the maximum leg angle was 14° in the sagittal plane and 5° in the coronal plane, Lippert considered conversion of the ground reaction forces to the KAFO axis unnecessary. Quoting from the paper, "the difference is too small to justify more complicated photographic methods of angle measurement". His investigations found that KAFOs with shoe attachments failed to completely unload the leg with their use becoming more ineffective as the stance phase progressed. He cited this to be partly due to leg muscle activity working against the orthosis and also considered this to explain the swing phase loading pattern. Strain gauge transducers at the calf section were aligned to measure Fx and Fz shear forces. Similarly gauges on the uprights at the ankle measured the axial force, Fy.

The results indicated that 50% of body weight was borne by the KAFO uprights, with the average A-P and M-L forces being 50N and 35N respectively. Moments were calculated at the thigh bands and the ischial seat with the latter position displaying higher loads. In contrast to Lehmann *et al.* (1970), Lippert found that free ankle joints offered more weight relief than fixed types. He further commented that greater loads were experienced on the medial upright when compared to the lateral side. Lippert also considered that orthoses were over-designed, a view shared by Lehneis (1969),who believed that KAFOs were "over-designed to prevent breakage ... and heavier than they need to be".

Lehmann & Warren (1976) performed a biomechanical evaluation on six conventional double upright KAFO designs. The KAFOs were instrumented with strain gauge transducers to determine the distribution of forces on the limb as well as the effect on anatomical knee shear. They identified that the forces required to stabilise the knee were minimised when the leg was maintained as straight as possible, with the stabilising forces applied beneath the knee but as close to the joint centre as possible. A similar investigation performed by Lehmann *et al* (1976) on the Scott-Craig orthosis reached the same conclusions.

2.3.3 Loading during Ambulatory Activities

Researchers at the University of Strathclyde, Bioengineering Unit have spent considerable effort evaluating the biomechanical performance of KAFOs during normal ambulatory activities. Trappitt (1979) designed and manufactured four six-channel load measuring strain gauge transducers to record orthotic loading (Trappitt & Berme, 1981). The transducers could be incorporated above and below the knee joint of a conventional double upright KAFO. He found that the medial upright was generally loaded more than the lateral side, especially with regards to axial force. This agrees with the studies done by Anderson (1977, 1974) and Lippert (1971). He tested two post poliomyelitis subjects during normal level walking but found little agreement between the two sets of results. The heavier subject carried 50% of the body weight through the orthosis compared with 68% for the 20N lighter subject. The KAFO designs were different in that one had a fixed ankle joint while the other was free to dorsiflex. The higher axial loads were recorded for the fixed joint which agrees with the findings of Lehmann *et al* (1970). The maximum A-P and M-L forces were 100N and 50N respectively. Although these values were within the design limits for the KAFO, moments of 23Nm and 13Nm were recorded in the A-P and M-L direction which exceeded the design strengths of the KAFO. This questioned the belief that conventional KAFOs were over-designed.

Lim (1985) produced the most useful research on KAFO loading when he evaluated the loading properties of non weight-bearing KAFOs. Eight post-poliomyelitis patients with uni-lateral impairment were fitted with the locked knee, free ankle conventional KAFOs. Four newly designed, six-channel transducers were incorporated into the proximal and distal KAFO uprights. In addition four other transducers sensitive to A-P and M-L forces were attached to each of the two straps on the KAFOs. Force plates measured total limb loading while two orthogonal cine-cameras recorded kinematic data. This system meant that markers on the medial upright orthosis are hidden from the side camera and those on the posterior of the pelvis are hidden from the front camera. Lim determined their positions from the known co-ordinates of other markers. For example the orientation of the medial upright was determined from the markers on the lateral upright, assuming that the uprights were parallel to each other. Other inaccuracies in Lim's work resulted from the perspective effect of the cine-photography and the scaling corrections required. Investigations were conducted for both normal level walking and during simple ambulatory tests which simulated differing loading conditions, e.g. walking around a bend, walking up and down steps. The results obtained can be summarised as follows:

- There is no correlation between body weight and axial loading (Fy) with the lightest subject recording the highest axial force. The highest value occurred just after heel strike and was generally borne by the lateral upright more than the medial one.

- The maximum A-P forces tended to flex the orthosis about the knee joint and thus reactionally extend the limb about the knee. Hence the KAFO performed its knee stabilising role. Larger forces were seen on the medial upright, occurring just after heel strike.
- Both the axial moment (or torque) and mediolateral bending moment acted in opposite directions on each of the two uprights. The magnitude and direction of the results obtained for these two moments and for the M-L force varied greatly between patients. This is true for most of the loads measured and as such, creates many difficulties in predicting loads for design purposes.
- The weight-bearing relief of the KAFOs ranged between 10-38% however large KAFO axial loading did not necessarily indicate smaller anatomical loading since the greatest orthotic loads were often from the lighter subjects.

Lim believed that the subjects walking style greatly influenced the loading pattern, with higher loadings being recorded for more ‘aggressive’ walkers. Furthermore, he commented that when the same patients were tested on different days, different loads were recorded and he suggested that the physiological and psychological conditions may influence the subjects gait.

Gozal (1986) investigated the loading characteristics on the orthotic knee joint of a post-poliomyelitis patient with the same instrumentation as used by Lim. The lateral knee joint of the cosmetic KAFO had already failed twice whilst the patient was stepping off a kerb. The study indicated that the lateral upright was indeed more highly loaded and this was increased when stepping off a low platform, explaining the failure. Gozal also noted an unintended load relief of 30% body weight.

The most recent study in the Unit was conducted by Maqsood (1996) who used Lim’s transducers to measure the KAFO loading during walking tests representative of daily ambulatory activities. Three post-poliomyelitis patients were fitted with cosmetic KAFOs in which the orthotic knee joints were replaced by the six-channel load measuring transducers. Maqsood reported greater axial loadings in the lateral upright, agreeing with

Gozal (1986). Small loads were recorded during the swing phase which, like Lim (1985), were attributed to strapping forces rather than muscle activity as suspected be Lippert (1971).

Finally, a study by Bergmann *et al* (1994) approached the subject of load sharing ability of an ischial weight-bearing orthosis from a completely different slant. The forces were measured *in vivo* in a patient with two instrumented endoprostheses. Their results showed that the orthoses reduced the hip joint loading by about 30%, independent of the orthotic design and of the position in which the femur was held.

CHAPTER 3: INSTRUMENTATION

3.1 INTRODUCTION

The primary objective of this study was to determine the load sharing capability of a KAFO. For a full three-dimensional biomechanical analysis it was necessary to record kinematic data so that the orientation of the limb and of the transducers in space could be determined. This information was used to convert the kinetic data, recorded from the force plate and strain gauge transducers into the anatomical axis of the shank so that a comparison between the two could be justified.

This chapter describes the data gathering system employed in the tests. Both kinematic and kinetic data are required. The instrumentation may be sub-divided into its three component systems, which are:

1. An orthotic load measuring system consisting of two six-channel strain gauge transducers, twelve amplifiers and a data collection computer.
2. A force platform, responsible for measuring the ground reaction forces applied to the leg/KAFO complex.
3. A video recording system which registered the kinematic data enabling the three-dimensional co-ordinates of the limb and the orthosis in space to be derived.

Since the transducers required re-calibration, this instrumentation set-up is described in section 3.4 which details the complete calibration procedure.

3.2 KINETIC DATA ACQUISITION

A Kistler force platform of type 9261A was used. The platform measures the ground reaction forces and moments in three orthogonal directions. The platform consists of an upper plate supported on a lower plate by four legs. The legs are instrumented with piezo-electric quartz crystals at differing orientations which produce an output charge when a mechanical stress is applied. The platform has a surface area of 600 x 400 mm^2. For technical reasons the origin of the platform lies at an imaginary point beneath the top

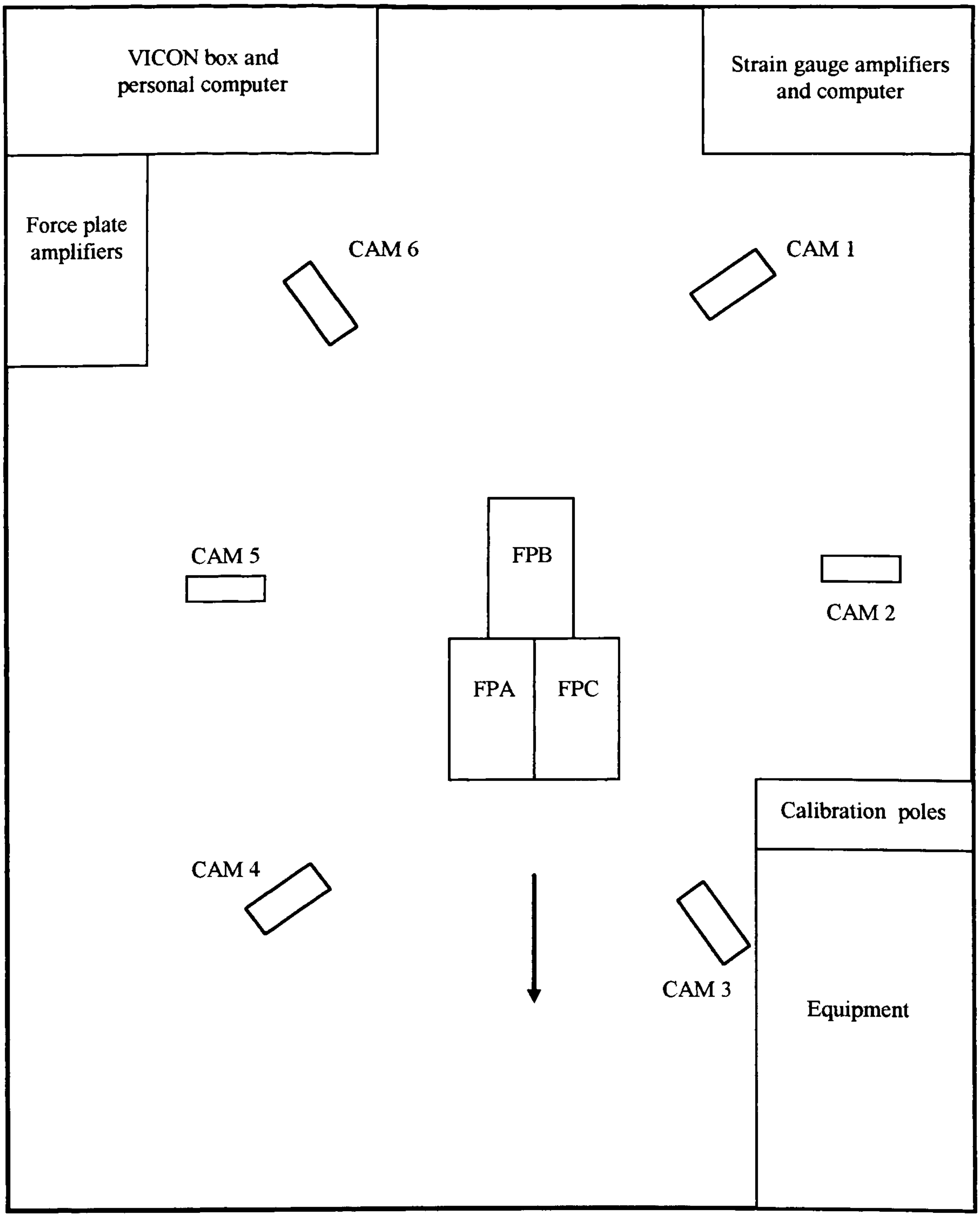

Figure 3.1
Floormap of the biomechanics laboratory illustrating the three force plates (FPA, FPB, FPC) and six cameras (CAM 1 till CAM 6)

surface. Figure 3.1 illustrates the position of the three force plates. The origin of force plate A (FPA) lies at the centre of the upper plate, 57mm beneath the top surface whereas for plates force plate B (FPB) and force plate C (FPC) the distance is 40mm. The upper surface is flush with the laboratory floor and covered with the same floor material so that it would not cause an obstruction and so it is not obviously visible to the test subjects. A series of amplifiers convert the electrical charge produced by the piezo-electric force transducers into proportional voltages. The force data acquisition and processing is performed using the VICON 370 system. This is the same system that is used to analyse the kinematic data and further details can be found in section 3.3. The force data was sampled at 50Hz with an analogue gain of 1V. The overall error possible in the measurements is ±2% (Van der Linden, 1995).

All three force plates (fig. 3.1) were available for testing and so it was originally thought that two consecutive steps could be recorded during each trial for each patient. This would allow a useful comparison between normal and orthotic limb loads to be made. However, the gait deviations exhibited by the two patients made it impractical to record two consecutive steps and so just the leg wearing the KAFO was tested. Due to problems with the equipment on the test days, FPA was used to test patient X and FPB for patient Z.

3.3 KINEMATIC DATA ACQUISITION

Kinematic data was gathered using the VICON 370 gait analysis system (Oxford Metrics Ltd.).The VICON system uses the ADTECH AMASS software to convert the two-dimensional (2D) co-ordinates of body markers recorded using six cameras, into three-dimensional (3D) co-ordinates of the limb in space.

3.3.1 Cameras

The six infrared cameras (Oxford Metrics Ltd.) were positioned in the gait laboratory (fig. 3.1). The infrared light emitted by the cameras is reflected by the markers back to the cameras. Each camera is linked via an etherbox to the microcomputer allowing each camera image to be viewed separately on the screen. VICON displays any markers detected as small circles and varies their size according to their distance from the camera. The cameras have a focal length of 4m and are manually positioned and rotated to obtain the best image. The light sensitivity of the cameras may be adjusted through VICON. This permits either clearer marker images or alternatively, the elimination of undesired images or reflection, e.g. from other cameras.

3.3.2 Camera Calibration

The cameras are calibrated through the VICON computer package prior to data collection. Four calibration poles each of which has 5 reflective markers attached, are required. The poles are hung from suspension wires arranged at pre-determined positions in the laboratory. The cameras are positioned until each camera can clearly view all 20 markers and the VICON calibration program is started. It is important that the poles are evenly spaced and that the image covers the whole screen for the calculated residual errors for each camera to be low. The VICON program will reject the camera positions until the calibration errors are satisfactorily small.

3.3.3 Markers and Calibration Stick

All markers used in the study, including those used for camera calibration were made from light weight spheres of 16mm diameter. The markers were covered with a special light reflecting material: 3M Scotchlite Brand High Gain 7610 (3M Company). This material contains small spheres which reflect the infrared light back to the cameras thus facilitating easy marker detection. The body markers were mounted on short sticks, of about 5mm length, to aid detection. The eight markers were attached to the subject using double sided tape. The calibration stick used to identify the anatomical landmarks (see section 5.1.3) was constructed from a 350mm metal rod with two markers fixed onto the stick 200mm apart. The calibration poles were the standard ones used in the gait laboratory, each having five reflective markers fixed at pre-determined positions.

3.3.4 Data Acquisition and Processing

Data acquisition, including controlling the sample rate and synchronising the cameras is performed by the etherbox. From here, the data were transferred to the Sun microcomputer where it is stored. Data processing using the VICON 370 package can be performed on any PC linked to the Sun station. The VICON software contains programs to name and identify each marker and to reconstruct the marker paths on screen. The system enables the user to 'fly' around the image to get a full three-dimensional view. Further manipulation of the data enables graphs of ground reaction forces and joint angles to be plotted. Like the kinetic data, the kinematic data were also sampled at 50Hz and processed using the same software, both systems were fully synchronised. The ASCII files containing matrices of the video and force plate data were processed further using the Matlab® software package (version 4.1, The Mathworks, Inc) on an IBM compatible personal computer.

3.4 CALIBRATION

The strain gauges were first calibrated in 1983 following construction by Lim (1985). A further calibration was undertaken by Maqsood (1996) for her analysis on the loads at the orthotic knee joint as a KAFO wearer performed normal ambulatory activities. Re-calibration is not normally required within a 5 year period unless the transducers were mishandled (Gozal, 1986). However, examination of Maqsood's results revealed evidence that the maximum service load had been frequently exceeded and on occasions so had the minimum overload capacity, hence re-calibration is required. This section details the complete re-calibration of both transducers, referred to as Mark II transducers in accordance with the original notation used by Lim.

3.4.1 Transducers

The two main requirements when designing transducers is to have robust measuring devices that will accurately record orthotic loading but can also be easily attached to the KAFO metal uprights. However since strength is directly related to the

Channel	Maximum service load allowed	Minimum overload capacity	Maximum loads previously recorded
Fx	200N	400N	270N
Fy	800N	1600N	260N
Fz	200N	400N	450N
Mx	25Nm	50Nm	9Nm
My	15Nm	30Nm	6Nm
Mz	35Nm	70Nm	48Nm

Table 3.1
Design load ratings together with the maximum loads recorded by Maqsood (1996) for transducers 2 and 3

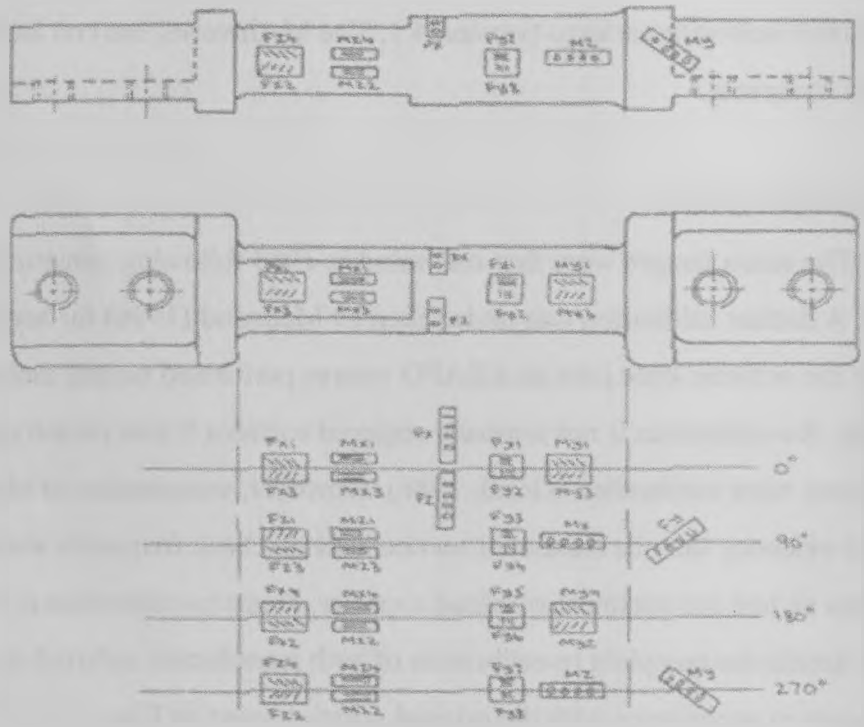

Figure 3.2
Strain gauge positions on transducer

cross sectional area and the sensitivity is also indirectly related, then these two fundamental properties are conflicting in nature. Lim (1985) considered that the optimum transducer design was achieved by using a hollow metal cylindrical bar onto which the foil grid, polymer backed gauge elements are attached. The positions of the strain gauges are illustrated in figure 3.2. Deflection of the bar produces an electrical resistance in the gauge which is directly proportional to the original strain. By careful positioning of the 20 gauges used, all three forces (Fx, Fy and Fz) and moments (Mx, My and Mz) can be recorded simultaneously. The design load ratings for the Mark II transducers Lim (1985)are noted in Table 3.1 along with the maximum load recorded in Maqsood's (1996) tests .

Ideally when a load is applied to one channel, only the strain gauge designed to measure that channel will record an output voltage. However output is often displayed in all six channels. This effect, known as cross-talk is an intrinsic property of all transducer design. Libertiny (1975) listed some causes to be due to improper transducer geometry, poorly located gauges and improper calibration, but complex design and difficulties in alignment make these problems virtually impossible to eliminate. Calibration is used to take these cross-talk effects into account. The gauges are connected in a full Wheatstone bridge arrangement both to compensate for temperature induced apparent strain, a significant error source at raised temperatures, and to provide accurate measurement of low gauge output. Other sources of error include hysteresis, creep, non-repeatability, non-linearity, zero shift, poor resolution and noise (Lim 1985), many of which can be detected and taken into account during calibration.

3.4.2 Theory of Transducer Calibration

Calibration is the process whereby an accepted standard is compared against an unknown quantity and used to determine its value. Hence the accuracy of the calibration is a direct function of the accuracy of the calibrating procedure and errors from the tools and techniques used will have a cumulative effect. Essentially a static calibration consists of adding known loads along a specific transducer axis and recording the output voltage.

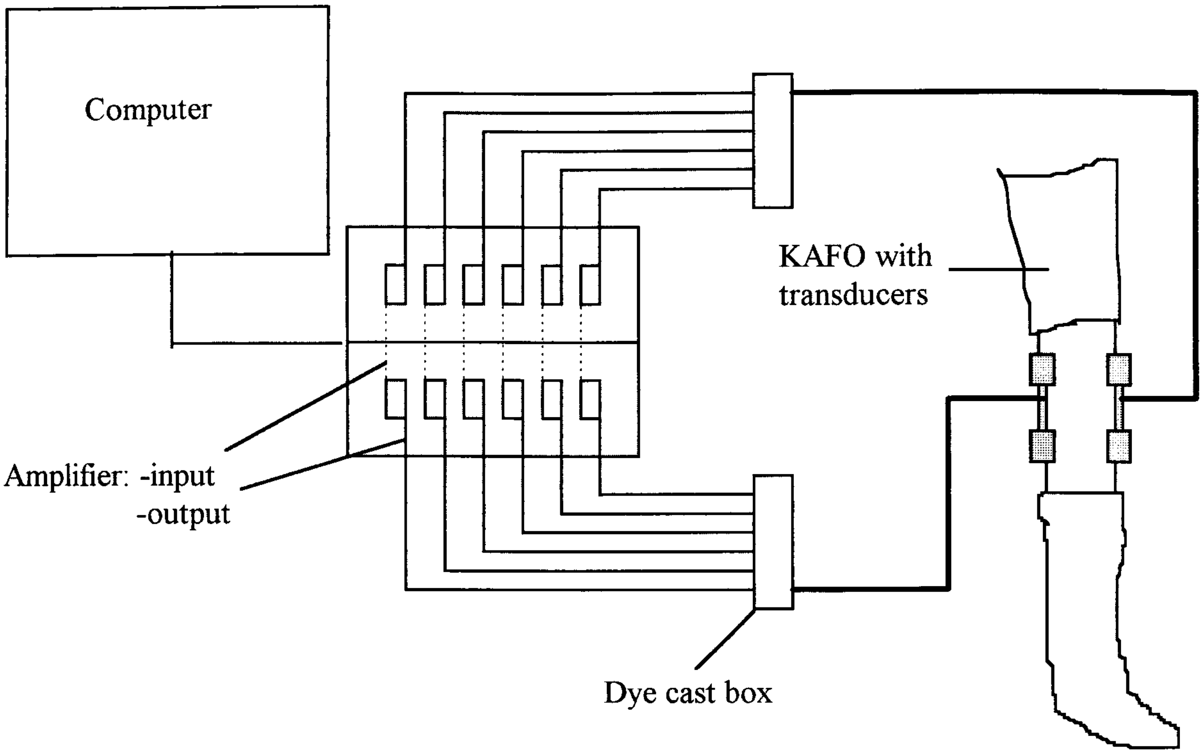

Figure 3.3
Circuit diagram of equipment used to calibrate the transducers

Channel	Bridge voltage	Gain
Fx	3V	2000
Fy	6V	1000
Fz	3V	2000
Mx	3V	500
My	3V	200
Mz	3V	500

Table 3.2
Gain and bridge voltage settings for calibration of transducers 2 and 3

The loads are usually known weights of 10 times greater accuracy than that required from calibration and the measured output will supply information on the magnitude of each calibration coefficient for the channel measured.

For a six-channel transducer, the output signal S_i (i=1,6), i.e. the measured output voltage, is a direct function of the input signal F_j (j=1,6), i.e. the applied load. An accurately designed transducer will produce a first order output, which can be expressed mathematically as:

$$S_i = \sum_{j=1}^{6} C_{ij} F_j$$

Equation 4.1

In matrix notation:

$$[S]=[C][F]$$

Equation 4.2

where: [S] = column matrix (6x1) of output signal voltages

[C] = square matrix (6x6) containing calibration factors C_{ij} determined from calibration data

[F] = column matrix (6x1) of input applied loads.

Hence written matrically:

$$\begin{bmatrix} SFx \\ SFy \\ SFz \\ SMx \\ SMy \\ SMz \end{bmatrix} = \begin{bmatrix} C_{11} & C_{12} & C_{13} & C_{14} & C_{15} & C_{16} \\ C_{21} & C_{22} & C_{23} & C_{24} & C_{25} & C_{26} \\ C_{31} & C_{32} & C_{33} & C_{34} & C_{35} & C_{36} \\ C_{41} & C_{42} & C_{43} & C_{44} & C_{45} & C_{46} \\ C_{51} & C_{52} & C_{53} & C_{54} & C_{55} & C_{56} \\ C_{61} & C_{62} & C_{63} & C_{64} & C_{65} & C_{66} \end{bmatrix} \begin{bmatrix} Fx \\ Fy \\ Fz \\ Mx \\ My \\ Mz \end{bmatrix}$$

This matrix may be broken into the 6 component mathematical equations for example SF_x may be expressed as:

$$SF_x = C_{11}F_x + C_{12}F_y + C_{13}F_z + C_{14}M_x + C_{15}M_y + C16M_z$$

Equation 4.3

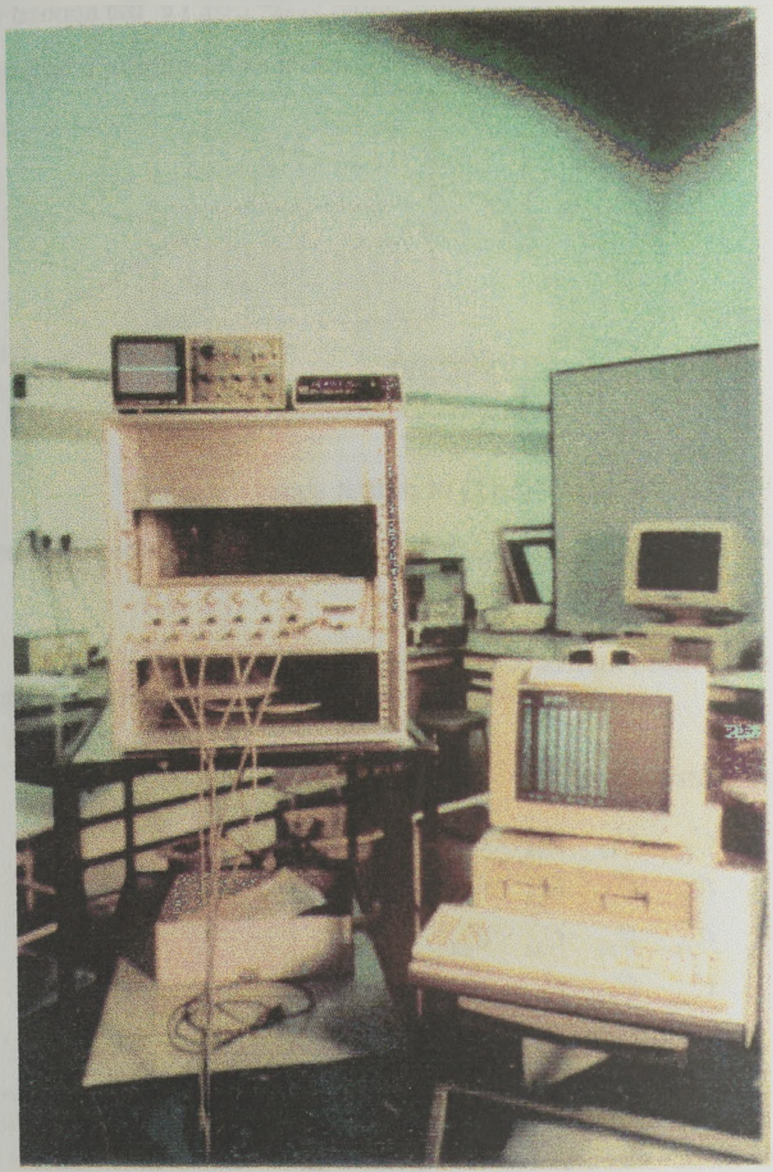

Figure 3.4
Arrangement of equipment

Applying a load to the Fx channel will generate the undesired cross talk signals (SF_y, SF_z, SM_x, SM_y, SM_z) in addition to the desired SF_x signal. This allows the first column in the calibration matrix to be calculated and allows the magnitude of the sensitivity coefficient and the five calibration factors for that channel to be determined. This is repeated for all six channels to produce the full calibration matrix.

During operation the loads applied to the KAFO are unknown. These are obtained by inserting the measured output voltages and the pre-determined calibration factors into the re-arranged form of equation 4.2:

$$[F]=[C]^{-1}[S] \qquad \text{Equation 4.4}$$

where: $[C]^{-1}$ is the inverse of the calibration matrix [C].

3.4.2 Calibration Instrumentation

Calibration takes place on a calibration bench which consists of specially designed rig created to support the transducer as static loads are applied. A bank of six amplifiers was used for calibration, with each transducer channel being connected to a separate amplifier so that Fx, Fy, Fz, Mx, My, Mz corresponded to amplifiers 1, 2, 3, 4, 5, 6 respectively. The Mz channel experiences relatively high loads and thus the transducer requires a large enough cross sectional area to resist failure due to fatigue. However a large area will increase the stiffness of the transducer, particularly in the axial direction and yet the Fy load is much higher than the Fx or Fz loads. To overcome this problem the sensitivity of this channel is doubled by using two resistors in series in each leg of the Wheatstone bridge. For this reason the strain gauges for all channels had a resistance of 120Ω apart from Fy whose resistance was 240Ω. A 3V bridge voltage was supplied to all channels apart from Fy which required 6V due to the additional resistor. The six channels of the transducer were connected via a dye cast box to the six amplifiers. These in turn were connected to a computer onto which Signal Centre, a data collection package had been installed. Figure 3.3 illustrates a circuit diagram of the equipment. This set-up is

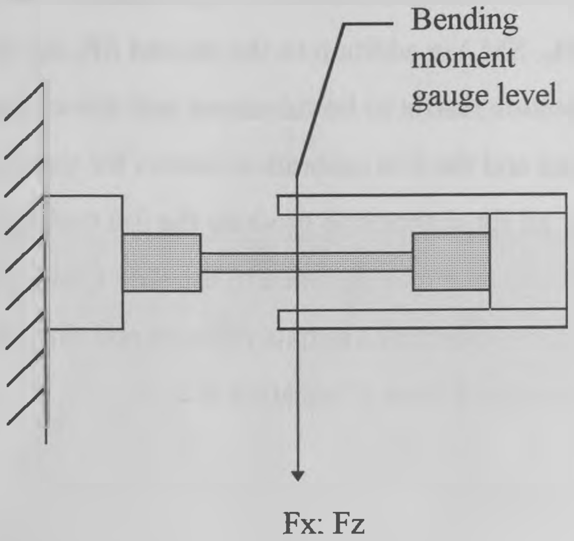

liagram of method used to calibrate Fx, Fz channels

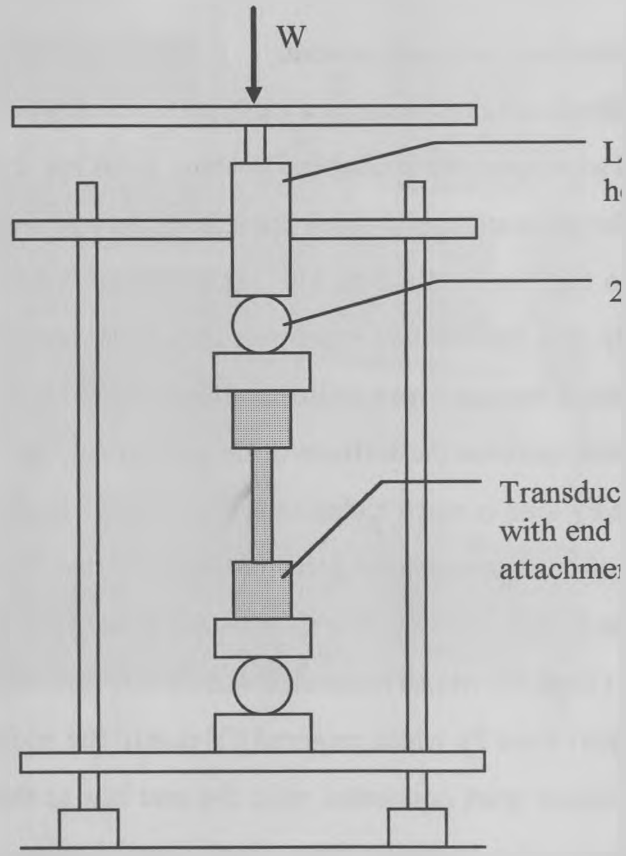

diagram of axial loader used to calibrate Fy channel used during testing and allows the signal output from each channel to be viewed simultaneously as shown in figure 3.4. The output signals could also be measured using a standard digital voltmeter (DVM). Initially both measuring techniques were used to compare their accuracy and viability.

Before beginning it is important to determine the orientation of the device, i.e. proximal and distal end, and in which direction the load is being applied, e.g. +Fx or -Fx. It is important to remember that a positive signal output does not necessarily correspond to a positively applied load. Each transducer has an 'origin' which is an imaginary point where the line of action of the resultant forces can be considered to pass through. For these devices it is along the central axis at the level of the Mx and Mz gauges.

The amplifiers had gain settings ranging from 20 to 2000. These were adjusted so that all channel outputs were approximately of similar magnitude, and then compensated for during calculations. Table 3.2 lists the bridge voltage and gain settings used for both transducers during calibration. Since both patients tested were right leg KAFO wearers it was decided to calibrate transducer 2 and 3 for location in the medial and lateral upright respectively with loading applied in a positive direction at the distal end. A right handed sign convention is used throughout, details of which are given in appendix A1.

3.4.4 Methodology

The transducer was located horizontally in the calibration jig and connected to the amplifiers and computer. The bridge voltages are set and the gains are increased from zero to their pre-determined values. The bridge on the amplifier is then balanced to give zero output. The transducer was then left to warm-up for at least 2 hours to allow the zero-drift to be observed. The channel to be calibrated was pre-loaded at the distal end in both positive and negative directions to remove any irregularities in the strain gauge and at the coupling of the jig and transducer.

Channel Fx: Before commencing, the output of the signal for each channel was re-set to zero if a slight drift in its mean value had occurred. The initial 'zeroed' value was noted

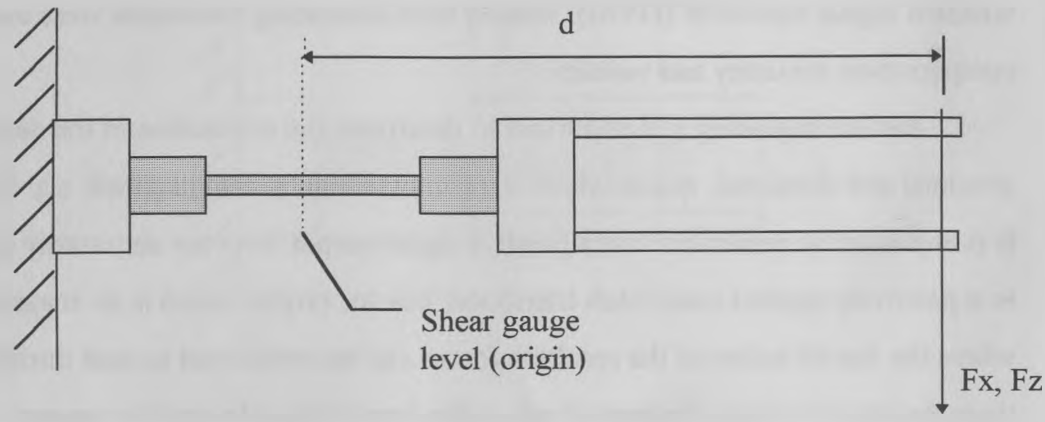

Figure 3.7
Schematic diagram of method used to calibrate Mx, Mz channels

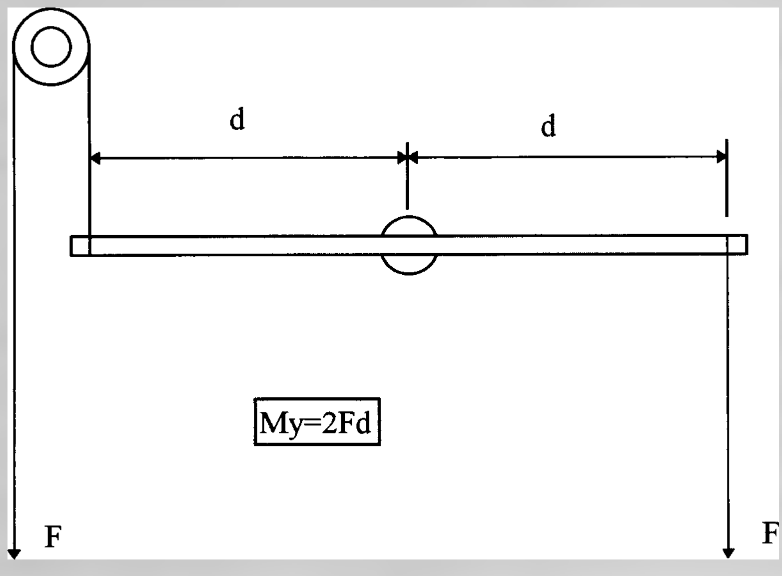

Figure 3.8
Schematic diagram of method used to calibrate My channel

on the DVM and the data collection computer. The weight carrier was hung over the origin at the level of the moment gauges and the reading for all six channels was noted on both measuring devices, figure 3.5. This method of loading will actually induce some bending moments as well as shear due to the different level of the gauges, but this is assumed to be negligible. The first weight was placed on the carrier and a similar recording made. This method was repeated for each of the 9 weights used until a maximum load of 98.4N had been applied. Measurements were again recorded as the weights were removed and a comparison of ascending and descending signal output allowed any problems to be observed. Examination of the initial and final reading was used to ensure that the transducer had not yielded.

Channel Fy: The transducer was positioned vertically into an axial loader, see figure 3.6, with the proximal end above the distal end. The apparatus applied pure compression to the device as weights were added in 9 steps up to 97N and the output voltage noted.

Channel Fz: The transducer was rotated by 90° so that loads were applied over the correct gauges and a calibration was repeated similar to that for the Fx channel (fig. 3.5).

Channel Mx: The transducer was rotated to the position used to calibrate Fz. Weights were added up to a maximum of 98.4N at 250mm from the transducer origin (fig. 3.7).

Channel My: The distal end of the transducer was rigidly fixed to the jig. Two lever arms extending radially from the central axis of the transducer were attached to the transducer's distal end (fig. 3.8). This allowed forces equal in magnitude but opposite in direction to be applied at equal distances from the transducer axis and hence supplying a pure torque. The sets of weights were added to a maximum of 60.9N in six steps at 120mm from the central axis.

Figure 3.9 (a) till (f)
Calibration graphs of the voltage output when each channel of transducer2 was loaded and unloaded in turn.

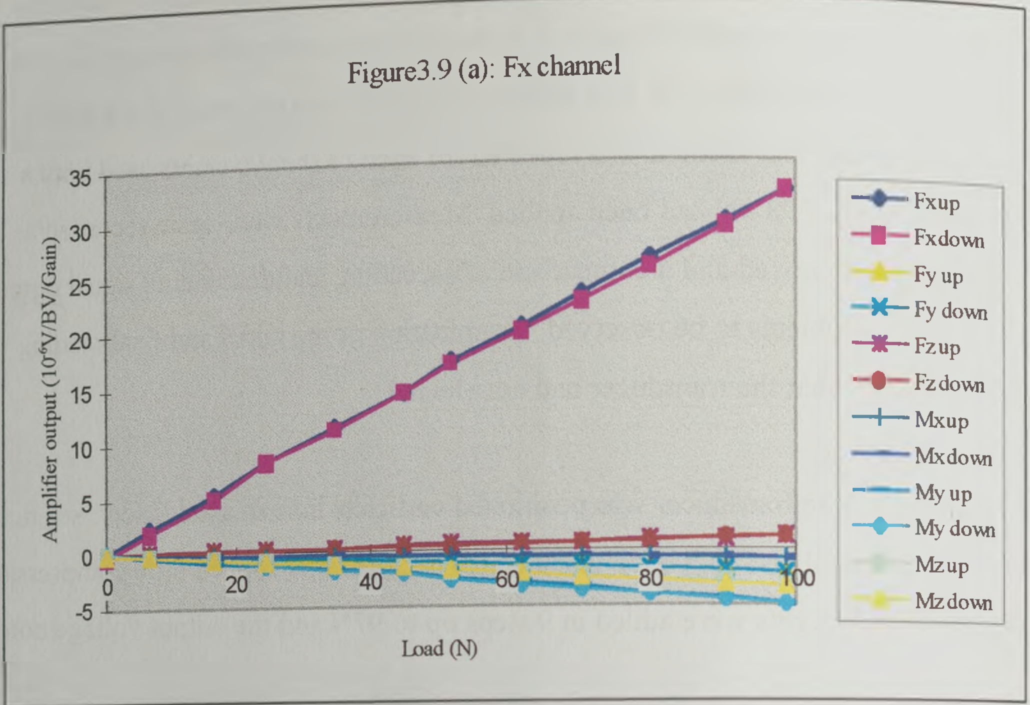

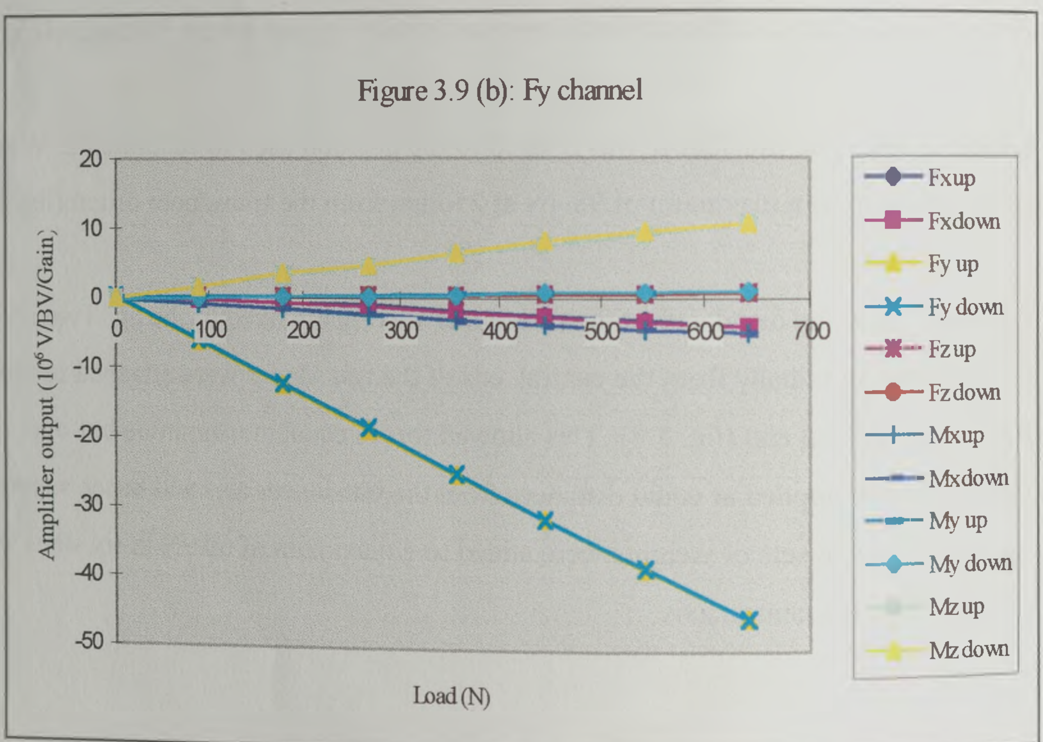

Channel Mz: The transducer was rotated to the position used to calculate the Fx channel and a similar calibration using a maximum 98.4N load at 250mm was repeated (fig. 3.7).

3.4.5 Results

The numerical output from the DVM and the Signal Centre package on the computer was in millivolts. This was adjusted to take account of the bridge voltages and gains for each channel. A calculation for each signal output was then performed to obtain the desired calibration factors in units of V/N(m)/bridge voltage/unit gain for each channel. An example calculation for each channel is shown in appendix A2. The calibration matrices obtained using the DVM values are given in table 3.3 (a) and (b). Graphs of signal output against load were plotted to show the degree of cross-talk effect for each channel. A regression line was fitted to the principal calibration coefficient to check for linearity and hysteresis. The voltage output was plotted against the input load to check for linearity, hysteresis, etc, figures 3.9 (a) to (f).

3.4.6 Discussion

The signal output from the transducer rapidly fluctuated around its mean value both when a load and when no load was applied. The values ranged from ±5mV which suggested problems with noise which could originate from a variety of sources including: mains, transistors, radio signals, etc. The problem was most apparent when the computer was used to record the signals as the fluctuating values were more difficult to read. This small amount of noise was impossible to eliminate and was considered to have a negligible effect on the accuracy of the results since the transducer output at maximum loading was around 2V. In terms of equipment accuracy, similar results were obtained using the computer or DVM for the maximum loadings. However at low or zero loading the DVM recorded values to a maximum accuracy of ±0.05mV whilst the maximum computer accuracy was ±0.5mV but with unreadable fluctuations. For these reasons the DVM was used to calibrate the transducers .

Figure 3.9 (d): Mx channel

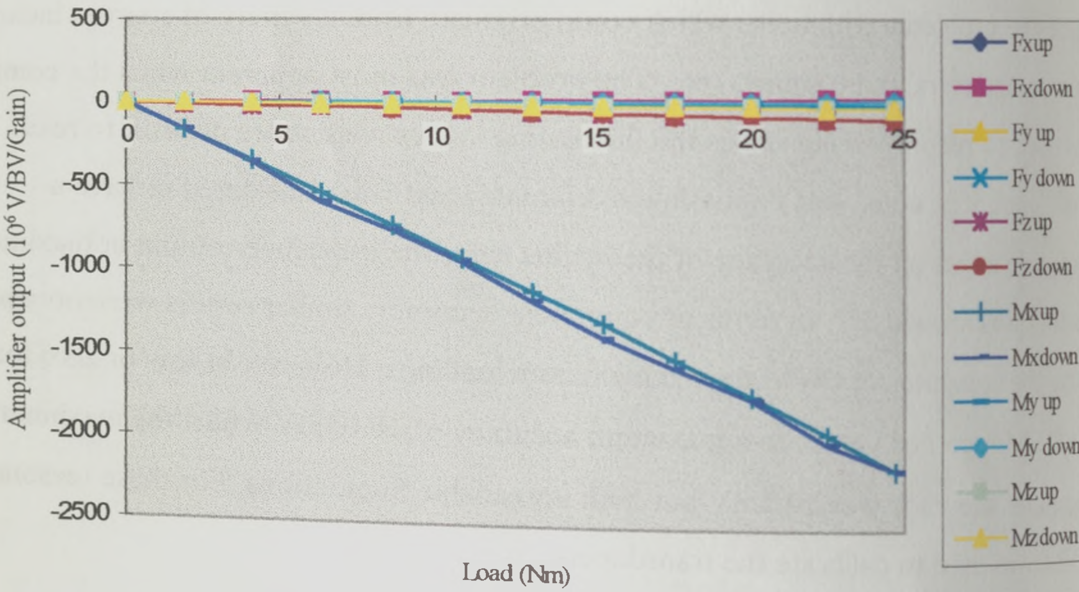

Figure 3.9 (c): Fz channel

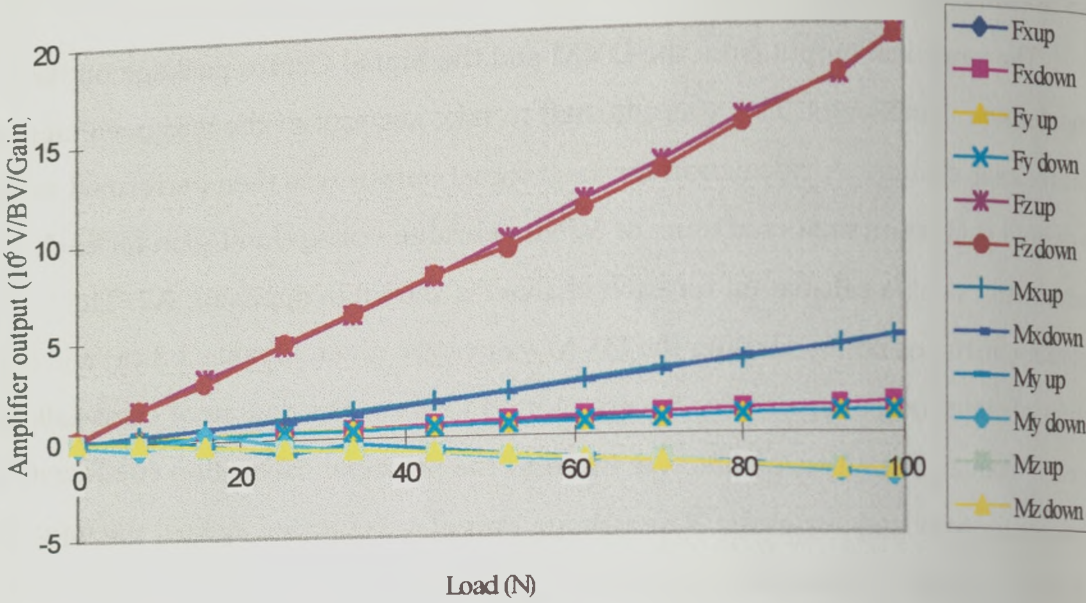

Figure 3.9 (e): My channel

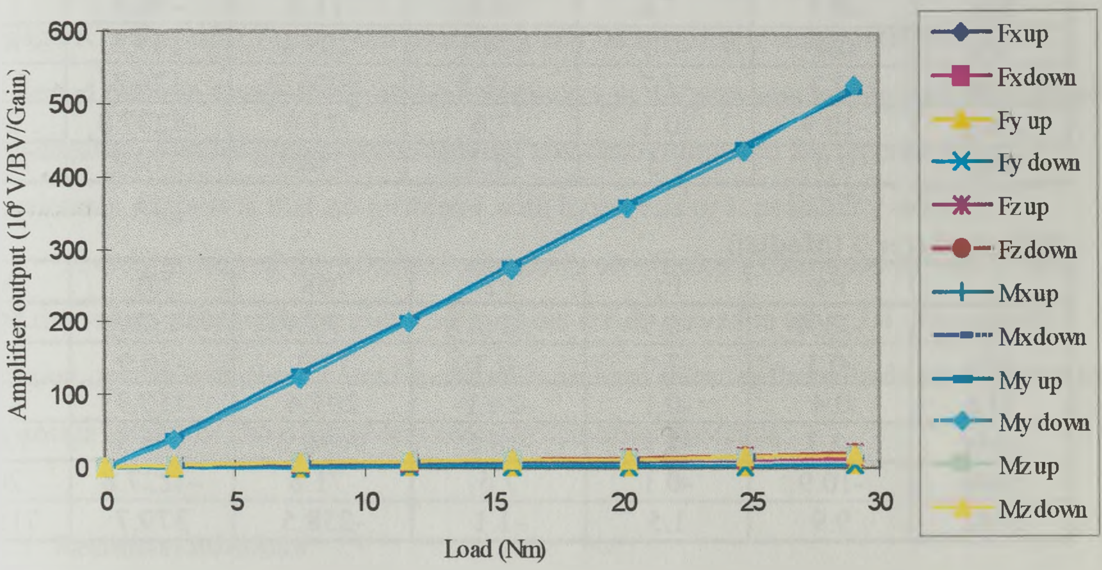

Figure 3.9 (f): Mz channel

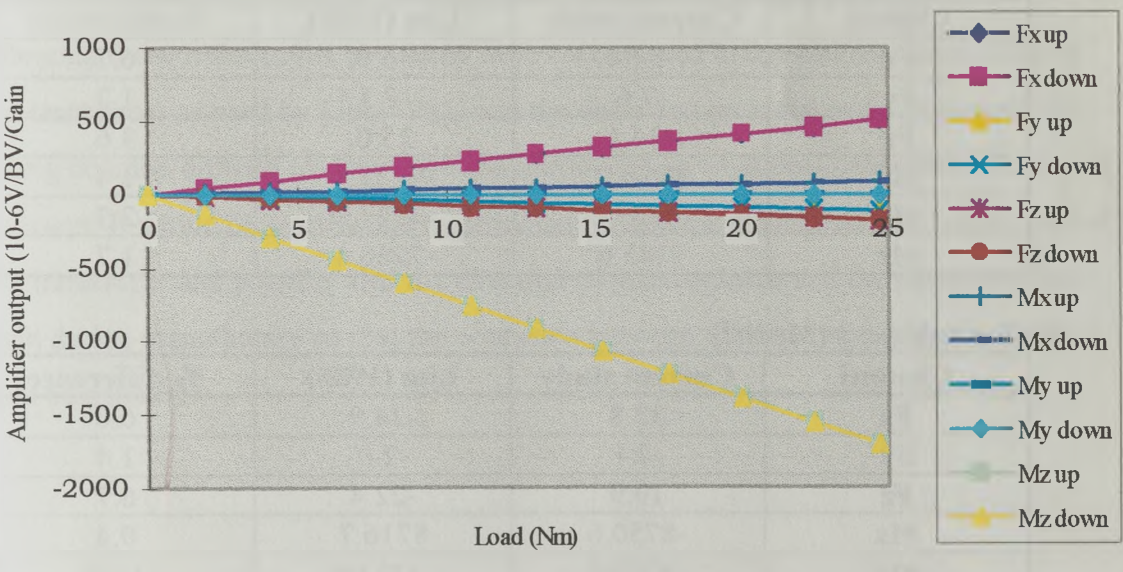

Table 3.3
Calibration matrices obtained using DVM values for all channels

(a)Transducer 2 (Lateral)

	Fx	Fy	Fz	Mx	My	Mz
SFx	-33.4	-0.5	2.6	179.4	-338.5	-396.4
SFy	-0.3	-7.6	-0.3	11.2	-36.9	11.9
SFz	0.4	-0.1	-24.1	207.4	155.3	81.3
SMx	-2.7	-7.7	-18.5	9096.2	126.3	132.6
SMy	-10.9	-0.1	7.6	-71.6	-4227.8	20.2
SMz	9.9	1.5	-1.1	-238.5	379.7	7154.6

(a)Transducer 3 (Medial)

	Fx	Fy	Fz	Mx	My	Mz
SFx	-33.4	-0.5	2.6	179.4	-338.5	-396.4
SFy	-0.3	-7.6	-0.3	11.2	-36.9	11.9
SFz	0.4	-0.1	-24.1	207.4	155.3	81.3
SMx	-2.7	-7.7	-18.5	9096.2	126.3	132.6
SMy	-10.9	-0.1	7.6	-71.6	-4227.8	20.2
SMz	9.9	1.5	-1.1	-238.5	379.7	7154.6

Table 3.4
Comparison of the principal calibration co-efficients determined by Lim (1985) with those obtained in this study

(a) Transducer 2 (Lateral)

Channel	**Current study**	**Lim (1985)**	**% difference**
Fx	-34.4	36.9	6.7
Fy	-7.6	-7.5	1.3
Fz	-24.1	25.0	3.6
Mx	9096.2	-9228.8	1.4
My	-4227.9	-4127.3	2.3
Mz	7145.6	-7266.4	1.7

(b) Transducer 3 (Medial)

Channel	**Current study**	**Lim (1985)**	**% difference**
Fx	32.8	-34.9	6.0
Fy	-7.1	-7.0	1.4
Fz	19.9	-22.4	6.7
Mx	-8750.6	8716.7	0.4
My	-3767.0	-4324.6	12.8
Mz	-6954.1	6818.8	1.9

A zero-drift averaging ±10mV occurred during the 2 hour warm-up period between the initial and first recorded zeroing. This insignificant amount is expected for transducers of similar physical proportions

The regression line fitted to the graphs of the principal calibration factors, gave an average R^2 value of 0.98 for both ascending and descending loading patterns. This confirmed that the overloading of the transducers in the previous testing had not affected their linearity. Similar graphs for ascending and descending and for repeating the experiments suggested that no problems with hysteresis or repeatability existed.

A comparison of the principal sensitivity co-efficients calculated by Lim (1985) with the values determined during this analysis are displayed in table 3.4. The largest variation occurs with the Fx and Fz channels perhaps because these loads come closer to the design limits for the transducers than for the other channels.

3.4.7 Recommendations

The process of calibration is such that the actual method used, for example loading the distal end with positive forces and moments is unimportant provided that it is taken account of during the calculations and testing. However it is often useful to observe a standard protocol so that results from previous calibrations can be compared. In calibrating these transducers, problems were encountered in determining the number of each transducer as used by Lim (1985) and the distal and proximal ends. This made the loading position difficult to determine and introduced an additional unnecessary source of confusion. It would be worthwhile to permanently inscribe the number and correct end of each transducer and possibly also the direction of positive loads and the position of the origin during manufacture so that the confusion between different methods of calibration could be avoided.

CHAPTER 4: METHODOLOGY

4.1 INTRODUCTION

This chapter describes the method employed to collect the kinetic and kinematic data during the tests. A brief profile of the subjects, reviewing their present condition is described. The preparation of the equipment and of the subjects for the tests is then discussed together with a detailed description of the positioning of the markers required to obtain the co-ordinate data. An outline of the test procedure and a rundown of the steps taken after the subject tests is provided. Finally, a brief summary of the data processing using the Matlab software package is supplied.

4.2 SUBJECT MEDICAL INFORMATION

4.2.1 Clinical Background

Poliomyelitis is an infectious viral disease affecting the central nervous system. Degeneration of the motor cells in the spinal cord results in muscular weakness, flaccid paralysis and ultimately muscle atrophy in one or more limbs. The muscles most commonly affected are the knee extensors and the foot flexors of the lower limbs. The virus has been virtually eliminated in developed countries due to a successful immunisation programme but is still prevalent in countries of low socio-economic status, e.g. Uganda. The last epidemic occurred in Britain in the 1950s leaving behind a generation of people requiring orthotic treatment.

The two subjects tested were right leg KAFO wearers, both employed by Maqsood (1996) the previous year in her study examining general KAFO loading. This was primarily done to allow usage of the cosmetic type custom built KAFOs manufactured the previous year to accommodate the two transducers on the medial and lateral uprights in place of the orthotic knee joint. However this will also allow for a comparative analysis of transducer loading during simple level walking recorded in both

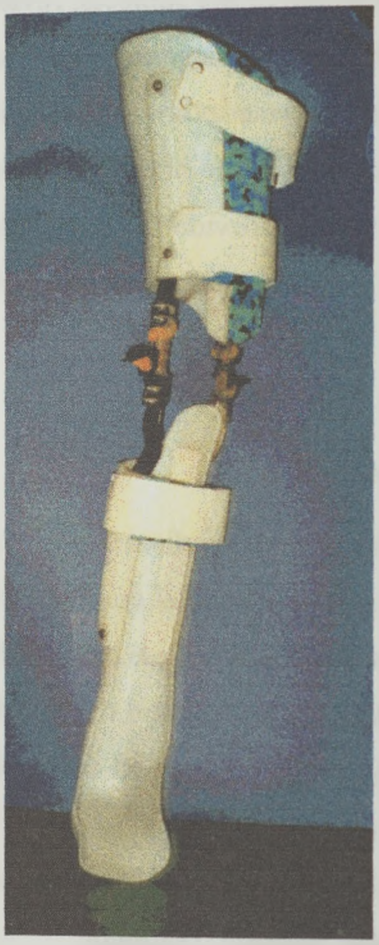

Figure 4.1
KAFO used for subject Z tests

this and the previous study. The subjects are referred to by the letters X and Z, both for reasons of confidentiality and in accordance with the original notation used by Maqsood.

4.2.1 Subject X Information

Age: 49

Height: 1715 mm

Weight: 80.5 kg (789.4N)

KAFO: Right leg, high brimmed socket

History: This subject was diagnosed as having polio in 1950 at the age of 2.5 during the height of the last epidemic. Since then he has always worn conventional long leg callipers, apart from a three years period at the age of 12 when short leg callipers were used. He currently uses a cosmetic KAFO and has a specific preference for a high brimmed socket although considered to provide no pathological benefit. The KAFO is worn for approximately 14 hours a day.

Activity: Despite redundancy from an active job this subject still manages to lead an active lifestyle, enjoying frequent foreign holidays and employing his time doing daily domestic chores.

Observations: The subject displays a valgus alignment of the right knee together with a slight flexion contracture. An operation on his sound leg was used to limit further growth, however a shorter right leg is still evident. Circulation problems has resulted in slight skin temperature variations but a strong pulse indicates no oedema. His walk is ambulatory, exhibiting minimum hip and knee flexion and lateral trunk bending during swing phase.

4.2.2 Subject Z Information

Age: 37

Height: 1695 mm

Weight: 80 kg (784.4N)

KAFO: Right leg, non weight bearing (fig. 4.1)

History: The subject was diagnosed as having polio when 18 months old and he first started wearing full length conventional KAFOs in the early 60s converting to cosmetic KAFOs in the late 80s. Attempts at using various KAFO designs, including a free knee lock with posterior stops have been met with limited success due to discomfort. However a ground reaction AFO used with walking sticks did improve the subjects gait and is now worn interchangeably with the KAFO for about 2 hours each day.

Activity: This subject leads a fairly active life, performing daily stretching exercises and attending the gym twice weekly. His routine includes weight lifting using his lower limbs which helps to both strengthen his muscles and reduce the flexion contracture at the knee of his paralysed leg.

Observations: The subject has previously undergone a Tibial Rerotational Osteotomy but external rotation of the foot is still observable, particularly when seated. Hyperextension of the right knee is exhibited. This is a direct result of knee weakness and acts to prevent adequate contralateral limb advancement. A heel raise on the right shoe helps to compensate for this condition by moving the position of the knee anteriorly. The subject has a slow ambulatory gait displaying intense lateral trunk bending during swing phase.

4.3 PREPARATION

4.3.1 Preparation of the KAFOs

The two KAFOs used in the tests were custom built for the subjects. The thigh and shank sections were manufactured from thermoformed polypropylene and connected together with standard metal uprights without orthotic knee joints. The two transducers were securely located between the uprights in place of these joints. Care was taken to position the transducers in the arrangement in which they had been calibrated for, i.e. proximal or distal end and medial or lateral side. A flat metal plate was attached perpendicular to the defined transducer axis, the reason for which is detailed in section 5.1.3. All metal parts of the KAFO which could reflect light were painted dull black so

	Subject X		Subject Z	
Setting	Bridge voltage	Gain	Bridge voltage	Gain
Fx	3	2000	3	2000
Fy	6	2000	6	2000
Fz	3	2000	3	2000
Mx	3	1000	3	1000
My	3	1000	3	500
Mz	3	500	3	500

Table 4.1
Bridge voltage and Gain settings used during the experimental trials for subjects X and Z

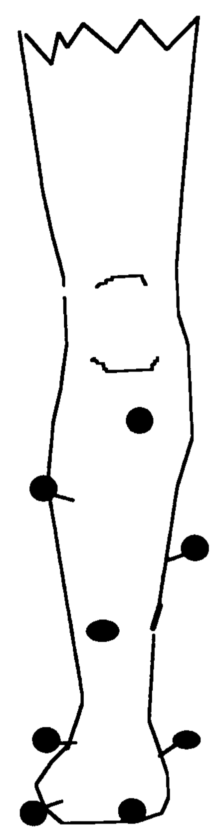

Figure 4.2
Schematic representation of the markers attached to the shank and foot

that they would not be detected as markers by VICON. The transducers were connected to the data recording computer in a manner similar to that used for calibration. The transducers were given a minimum period of two hours to 'warm-up' prior to the tests.

4.3.2 Preparation of the Laboratory

The six cameras were mounted on tripods and connected to the etherbox using separate cables. The cameras were positioned around the desired force platform, ensuring that there was a clear path for the subject to walk along on either side of the platform (fig. 3.1). The background in the laboratory was obscured by dark blue curtains and any other objects which could reflect light were removed from the view of the cameras. The four calibration poles were suspended from the ceiling. The cameras, VICON box and computer were switched on ready for calibration. The calibration program was started and each camera was repositioned until all four poles were clearly detected. When satisfactory camera errors were recorded (section 3.3.2), the parameters were stored and the cameras must remain in the same position for the duration of the tests. Since the force plate amplifiers take a long time to warm-up they remain on permanently.

4.3.3 Preparation of the Subjects

The bridge voltage and gain settings were set for all 12 channels on the amplifier at the values given in table 4.1. The course and fine gain controls were adjusted to produce an initial zero measurement from each of the 12 channels. The subject then donned the instrumented KAFO. An initial test was performed to check that the bridge voltages and gains used were appropriately set. The subject was asked to perform some simple level walking and the corresponding transducer outputs were recorded. A graphical representation was used to compare the magnitude of the loads for each channel. The subject was then given further time to become accustomed to the instrumented KAFO while an assistant walked behind, holding the cables in order that no extra stress was imposed on the electronic connections. The markers were then attached

Figure 4.3
Illustration of the pointer method' used. (From: Cappozzo *et al.*, 1995)

to the subject using double sided tape. Four markers were placed on the shoe and four on the shank (fig. 4.2). Each of the KAFOs were tightly strapped to the leg and it was assumed that there was no relative movement between the calf and the KAFO. This enabled markers to be placed directly on the KAFO as well as the bony part of the shank and the extra KAFO thickness was then taken into account ensuring data processing. Efforts were made to spread out the markers as much as possible, ensuring that no three markers were in line or in the same plane.

4.4 EXPERIMENTAL PROCEDURE

4.4.1 Anatomical Landmark Calibration

The anatomical axes of the shank and foot were calculated from particular bony landmarks on each. However attachment of markers to these landmarks is generally inaccurate due to the relative movement between the skin and bone, especially at musculative areas. For this reason the pointer method as described in Cappozzo *et al.* (1995) was used to determine the position of the landmarks. This technique makes use of the calibration stick described in section 3.3.3. The subject is fitted with the markers described above which remain in position for both the calibration and dynamic trials.

During calibration, the subject is positioned in his normal standing posture, in full view of all six cameras and the stick is used to point to the landmarks while their positions are recorded for 1s (fig. 4.3). Since both the length of the stick and the distance between the two markers are known, it is possible to calculate the 3D co-ordinates of the end of the stick which are also the co-ordinates of the anatomical landmarks. Hence the position of the landmarks relative to the markers can now be calculated for the static calibration trial. This information is then used to calculate the position of the landmarks for each frame in the dynamic trial when only the attached markers are present. It was again assumed that the tight strapping did not allow any relative movement between the shank and the KAFO. A similar technique could then be used to first calibrate the position of certain points on the transducer and then calculate the actual transducer position for each frame in the dynamic trial using the position of the detected markers. Thus markers

Table 4.2
List of anatomical and transducer landmarks recorded during the calibration trials for the foot, shank, medial and lateral transducers.

<u>Foot</u>
Distal end of first metatarsal (FM)
Distal end of fifth metatarsal (VM)
Distal end of second metatarsal (SM)
Calcaneus (CA)

<u>Shank</u>
Lateral head of fibula (HF)
Tibial tuberosity (TT)
Lateral edge of lateral malleolus (LM)
Medial edge of medial malleolus (MM)

<u>Lateral transducer</u>
Centre of lateral edge at proximal end (LTP)
Centre of lateral edge at distal end (LTD)
Lateral edge at distal end of calibration plate (LTC)

<u>Medial transducer</u>
Centre of medial edge at proximal end (MTP)
Centre of medial edge at distal end (MTD)
Medial edge at distal end of calibration plate (MTC)

directly attached to the transducer which could interfere with the subjects gait were not required. Each of the anatomical and transducer positions are recorded in turn with an initial check made after each trial to ensure all 10 markers (4-foot, 4-shank, 2-stick) were present. Table 4.2 gives a list of the anatomical and transducer points used for calibration.

4.4.2 Dynamic Trials

The patient is positioned at a starting point on the walkway and asked to walk in a straight line until 4-5 steps after the force plate with an assistant holding the cables behind him. It is useful to give the subject a distant point to focus on so that they are distracted from aiming for the force plate which would alter their normal gait pattern. If the subject does not step centrally on the correct force plate with their impaired limb, then the starting position is adjusted and procedure repeated until he does. Most users of locked knee KAFOs have great difficulty in altering their normal walking pace hence subjects were tested at only their normal level walking speed.

When the subject is ready a sign is given by the experiment co-ordinator for the subject to start walking and also to start data acquisition on the transducer computer and to start data capture for the cameras and force plate. This method provides only approximate synchronisation between the two load recording systems. However the time of heel strike is clearly visible on both recordings so this is used to manipulate the data and accurately synchronise the recordings. Data were recorded for 10s and the procedure was repeated 10 times with the subject given time to rest between trials, if required. The marker co-ordinates were re-constructed immediately after each trial to check that all markers were visible. If so, the markers were removed and the subject could doff the KAFO. A final transducer measurement was performed with the KAFO lying horizontal and unloaded to check for amplifier drift from the initial zero measurement.

4.5 Data Processing

The data is produced from VICON in ASCII format as a table for each trial which contained the 3D co-ordinates for each marker in each frame (see chapter 5).

CHAPTER 5: THEORETICAL ANALYSIS

The marker co-ordinates and the force plate loads are recorded by VICON and as such defined in the ground (or global) reference system. Similarly the transducer loads are recorded in the local transducer reference system. However the relationship between the transducer and the shank, and between the ground reference system and the shank is known from the calibration trials hence data processing is used to manipulate the data from each of the measuring reference systems into the local reference system of the shank. This allows a direct comparison between the differing loads recorded by each device to be made. The data output produced by VICON is in ASCII format and contains the co-ordinates of the markers for each frame of the experimental and calibration trials. Similarly the force plate data is in ASCII format and as such both can be saved in matrix notation as raw text files and analysed through the Matlab software package. A series of programs written in and run through Matlab are used to process the data. The first part of this chapter describes the axis systems and sign conventions used in the analysis. The chapter then outlines the function of the programs used in the chronological order of analysis. A brief description of the theory behind the transformation of the co-ordinate systems is provided together with the calculations of the joint angles, velocities and accelerations. Finally the inverse dynamics used to calculate the intersegmental forces and moments is provided.

5.1 ANALYTICAL DEFINITIONS

5.1.1 Sign Convention

The Cartesian sign convention illustrated in appendix A1 is used throughout. This system defines the directions as follows:

x-axis: horizontal- positive in the direction of progression;

y-axis: vertical- positive vertically upwards;

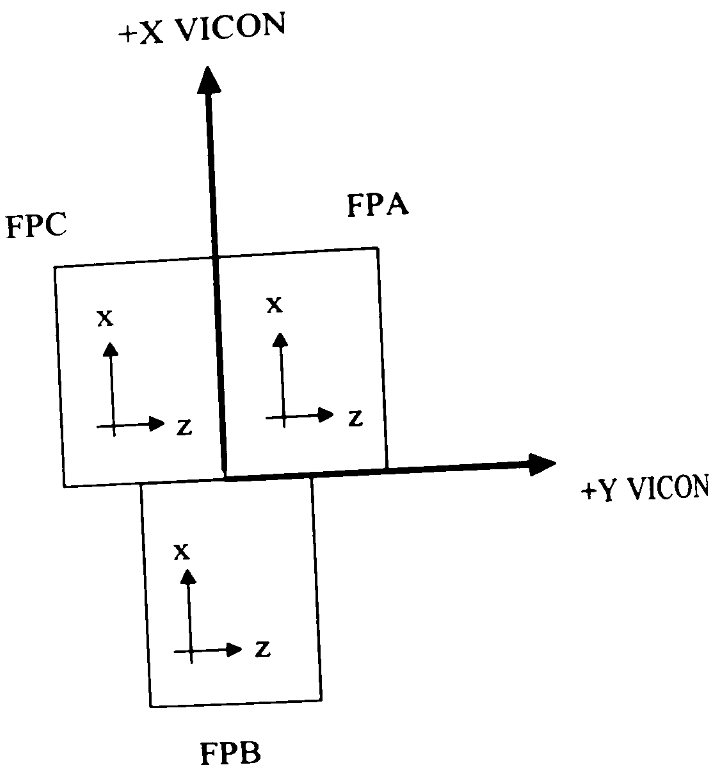

Figure 5.1
Relative positions of the local reference systems of the three force plates, FPA, FPB, FPC and VICON instrumentation

z-axis: horizontal- positive from left to right.

The Cartesian system dictates that a positive rotation is clockwise when viewed along the positive axis. A positive load is applied by an external device, e.g. ground or orthosis, to the distal end of the body segment. The transducers record loads acting from an external device onto their distal end. This sign convention applies for the anatomical loading as well as loading on the transducers. The body segments and the orthotic shank section are considered as rigid bodies and as such the position of the attached markers relative to one another will remain constant for the duration of the tests.

5.1.2 Ground Reference System

The absolute position and orientation of the body segments and transducers relative to space may be defined by the ground reference system (GRS). The co-ordinates of objects defined by this system are also known as global co-ordinates. In the biomechanics laboratory this system is defined relative to the force plates as shown in figure 5.1. The different system used by the VICON software to define the co-ordinates of the video camera data (also shown in figure 5.1) is taken into account during data processing.

5.1.3 Local Reference Systems

In a similar way to which the ground reference system (GRS) is fixed in relation to the laboratory space, the local reference systems are fixed to the segment/transducer which they define. However since the segment can move relative to the earth the local axis system will move relative to the GRS. Hence the position and orientation of the segments relative to each other may be calculated from their instantaneous positions relative to the GRS. Four local reference systems were employed in this study; the foot, the shank and the medial and lateral transducers. The anatomical systems (fig. 5.2) were defined from the co-ordinates of the anatomical landmarks recorded in the calibration trials, using the definition of Capozzo *et al.* (1995). The anatomical landmarks are easy to identify and can be located with palpation, with the soft tissue thickness being neglected.

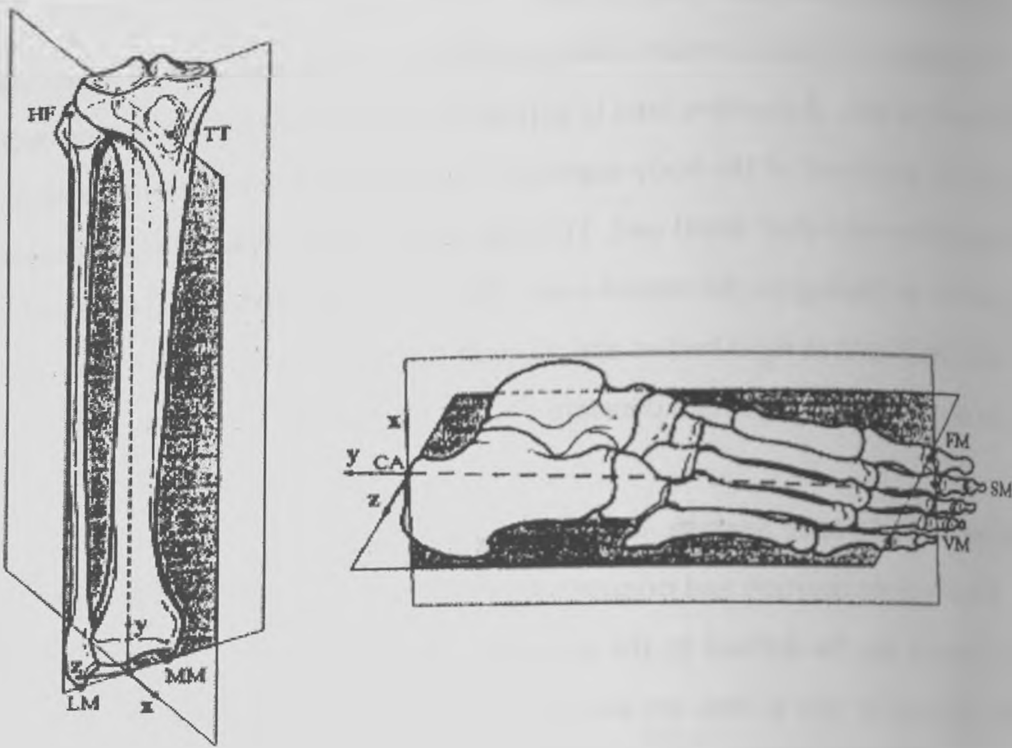

Figure 5.2
Anatomical reference system for the shank and foot. (From Cappozzo *et al.*, 1995) Abbreviations defining anatomical landmarks are listed in table 4.1

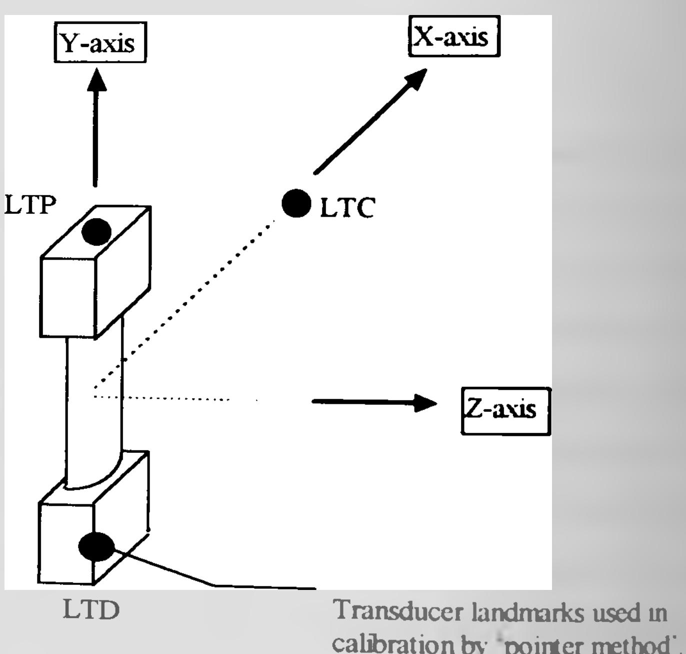

Figure 5.3
Lateral transducer local reference system defined by calibration landmarks. All markers are in the same plane. Abbreviations are listed in table 4.1

Appendix A3 provides a list of the local reference axis systems determined from the anatomical landmarks.

In a similar manner to the anatomical local systems, the local reference systems of the transducers are defined from the transducer marker points, again determined during calibration. The positions pointed to with the calibration stick may be considered to be in a triangular arrangement, as illustrated in figure 5.3. A line joining points A and B passes through the transducer central axis and thus defines the y-axis. Point C is defined from the metal plate rigidly attached to the transducer. Thus a line perpendicular to the y-axis, at the level of the transducer origin and passing through point C defines the x-axis. The z-axis is normal to the plane formed by the points A, B and C. Thus the imaginary transducer origin, used for calibration is also the origin of the transducer axis system and the axes defined are in accordance with those used to describe positive loads during the calibration procedure.

Each of the local systems are defined by an orthonormal matrix where each column represents the global co-ordinates of the local X, Y and Z axes.

5.2 MATRIX THEORY

VICON generates the co-ordinates of the markers in all trials using the GRS. However basic vector and matrix analysis enables the relationship between the GRS and each local reference system (LRS) to be calculated.

Consider a rigid body L suspended in 3D space having a LRS with axes x, y and z positioned within a GRS with axes X, Y and Z (fig 5.4). Any point on the body can be defined using either its LRS or the GRS. The transformation between the LRS and GRS may be described by a rotation matrix and a translation vector. The rotation matrix, M is of the global origin about its co-ordinate axes. The translation vector, $\overline{T}$ simply describes the vector necessary to move the global origin to the local origin relative to the GRS (subscript 'G').

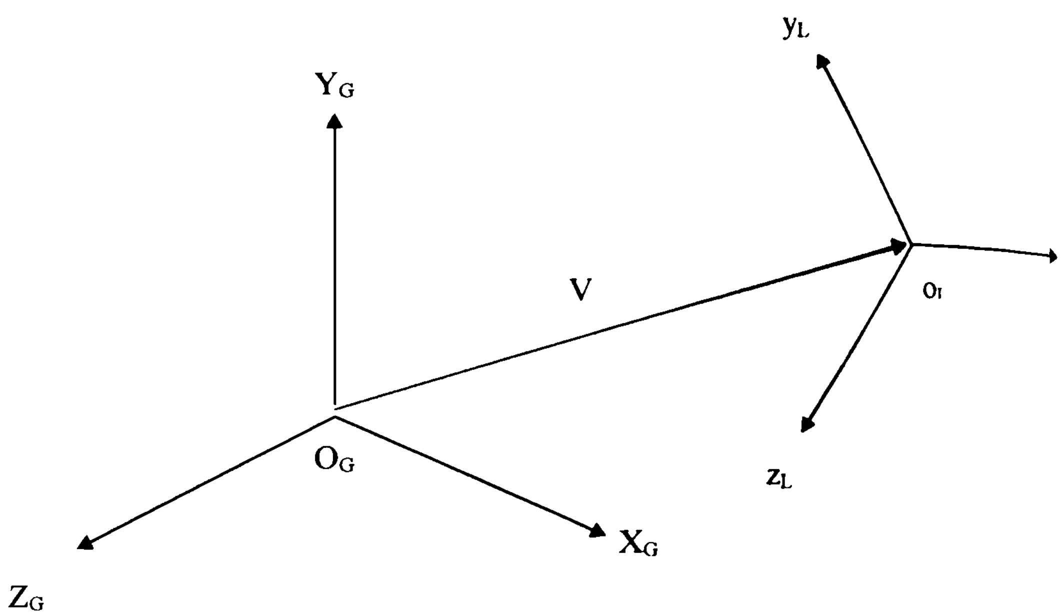

Figure 5.4
Local reference system (LRS) defined within a global reference system (GRS). Vector V represents translation from origin of GRS, O_G to origin of LRS, O_L.

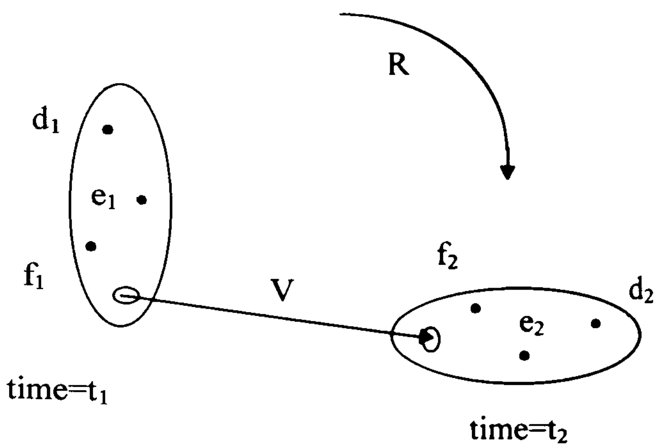

Figure 5.5
Change in position and orientation of a rigid body A fined by points d, e and f from time t_1 to time t_2. R represents rotation matrix and V the translation vector.

$$T = \begin{bmatrix} X_G \\ Y_G \\ Z_G \end{bmatrix} \qquad M = \begin{bmatrix} m_{11} & m_{12} & m_{13} \\ m_{21} & m_{22} & m_{23} \\ m_{31} & m_{32} & m_{33} \end{bmatrix}$$

This matrix may also be described by Euler rotation angles around the co-ordinate axes. Since matrix multiplication is not commutative, the angles depend on the order of rotation as well as the rotational axis about which the rotation is performed. In this study the Euler analysis described by Van der Linden (1995) was used. Again the right hand Cartesian co-ordinate system is used with rotations from X- to Y-axis, Y- to Z-axis and Z- to X-axis positive.

The rotation sequence is defined as:

$[R]=[Rz(\gamma)]*[Rx(\alpha)]*[Ry(\beta)]$ Equation 5.1

where:

R: Total rotation matrix transforming the GRS into the LRS,

Ry First rotation of angle β around the global Y axis,

Rx: second rotation of angle α around the X axis of the intermediate system resulting from the first rotation,

Rz: third rotation of the angle γ around the Z axis of the second intermediate rotation resulting from the second rotation.

If the position vector of a point in body L has co-ordinates $[xyz]_L$ relative to the LRS and co-ordinates $[XYZ]_G$ relative to the GRS then the following relationship may be used to describe the transformation of the point between the two reference systems.

$[XYZ]_L=[R]*[XYZ]_G+\overline{T}$ Equation 5.2

where: $\overline{T}$ is the translation vector

This relationship can also be used to describe the movement of a segment from one position to another over a finite time interval (fig 5.5). This requires the co-ordinates of

Table 5.1

List of Matlab programs used to analyse VICON data together with a brief summary of their function

1) lfirst: Input VICON data for experimental trials and arrange markers in separate segment files for foot and shank.
2) lfirst2: Input VICON data for calibration trials and arrange markers in separate files for foot, shank and calibration stick.
3) linpm2: Interpolates a gap of four or less markers assuming a linear trajectory.
4) lsearch: Re-calculates the co-ordinates of missed markers using the co-ordinates of the other three markers in the same segment.
5) lfilter: Filter data with a 4th order Butterworth filter
6) lintpoly: Uses a 3rd order polynomial to interpolate a gap of maximal nine missed frames.
7) lstickf; lsfickl; lsticktl; lsticktm: Calculates the transducer and anatomical landmarks from calibration stick co-ordinates.
8) lcufflmf: lcufflml; lcufflmtl; lcufflmtm: Determines the rotation matrix and translation vector from calibration co-ordinates to new orientation in each frame of experimental trial. Calculates the co-ordinates of landmarks in experimental trials.
9) lanatrdl; lanatrdm: Define reference system for each transducer.
10) ldefsyst: Define reference system of shank and foot from Cappozzo *et al.*,(1995)

the same three points on a rigid body, L for two instants in time. Two 3 x 3 matrices are generated, M_{t1} and M_{t2} for times t_1 and t_1 respectively, which are multiplied together to produce a matrix, R defining the rotation of L from time t_1 to t_2. Mathematically (Van der Linden, 1995):

$$[R]=[M_{t1}][M_{t2}] \qquad \text{Equation 5.3}$$

A similar analysis can be used to determine the position and orientation of one segment relative to another one. These methods are used in the computational analysis of the kinematic data described below.

5.3 FUNCTION OF COMPUTER PROGRAMS

5.3.1 Initial Data Manipulation

The initial matrices input into Matlab contained the co-ordinates of the eight markers detected by VICON during the experimental trials. Table 5.1 lists the Matlab programs used to analyse the VICON data in the order they were used. The matrices were split so that the markers for each segment were contained in separate files and the different axis system used by VICON was accounted for.

5.3.2 Data Processing

Markers were missing in some experimental frames but it was possible to retrieve their co-ordinates using the algorithm of Veldpaus *et al.* (1988). If the co-ordinates of four markers were known in frame A but only three in frame B then the co-ordinates of the missing marker was estimated for frame B using the rotation matrix defined from the positions of the three known markers for each frame. A recursive second order Butterworth filter of 10 Hz was used to filter the co-ordinates of the raw data. A three and five point filter was also used to filter the angular velocity and segment centre of gravity after the second and first order differentiation respectively.

5.3.3 Landmarks

A representative frame from each calibration file was used to calculate the co-ordinates of the landmarks on the segments, i.e. the foot, the shank and the transducers, from the co-ordinates of the markers on the stick. The position of the segment landmarks were now known in relation to the anatomical markers since both were recorded simultaneously for the calibration trials. However, it was necessary to know their relation to each other for each frame of the experimental trials. This would give information on the trajectory and orientation of the segments in space with respect to time. For this, another set of calculations using the method described by Veldpaus *et al.* (1988) was used. The technique used essentially describes the principle discussed in section 5.2. Thus the displacement of a set of at least four markers from one frame in the calibration file to every frame in the experimental file could be described as a rotation about the markers centre of gravity followed by a translation. By applying these transformation matrices to the co-ordinates of the segment landmarks during a representative frame in the calibration file their position in each frame of the experimental trials can then be calculated. The final outcome are the co-ordinates of the segment landmarks in every frame of the experimental files which enables the local reference systems to be defined. Mathematically this may be described as (Veldpaus *et al.* 1988):

$$\bar{p}_{\mathrm{exp}}=[R](\bar{p}_{\mathrm{cal}}-\bar{s})+\bar{s}+\bar{v} \qquad \text{Equation 5.4}$$

[R] Rotation matrix of the anatomical markers from calibration file to frame t in the experimental trials

$\bar{p}_{\mathrm{exp}}$ position vector of mean co-ordinates of markers in frame t of experimental trial

$\bar{p}_{\mathrm{cal}}$ position vector of mean co-ordinates of markers in the calibration trial

$\bar{s}$ position vector of co-ordinates of anatomical markers in the calibration file

$\bar{v}$ translation vector to translate mean co-ordinates of anatomical markers in e calibration file to their position in frame t of experimental trial

	Subject X		Subject Z	
	Shank	Foot	Shank	Foot
Segment	1.29	3.70	3.68	1.28
Mass (% body mass)	40.4	44.3	40.4	44.3
CG (% segment length)	41.6	0.38	41.3	0.38
Ix ($x10^2$ kgm^2)	1.55	3.09	1.54	3.07
Iy ($x10^2$ kgm^2)	41.9	3.06	41.7	3.04
Iz ($x10^2$ kgm2)				

Table 5.2
Calculated segment parameters. Mass and position of centre of gravity (CG) calculated from values proposed by Contini (1970). CG from heel and knee joint for foot and shank segments respectively. Moments of Inertia calculated according to McConville (1980).

5.4 KINEMATIC ANALYSIS

5.4.1 Joint Centres

Generally in a biomechanical analysis the position and orientation of the thigh during gait would also be studied which would provide information on the position of the femoral epicondyles, used to define the knee joint. However it was considered beyond the scope of this study to analyse the thigh position since the KAFOs used had locked knees. For this reason the knee joint centre was defined as the midpoint of the line connecting the origins of the lateral and medial transducers. The ankle joint centre was defined as the midpoint of the line connecting the medial and lateral malleoli.

5.4.2 Joint Angle Calculation

Joint angle time curves are one of the basic tools used in gait analysis. However with the use of a locked knee KAFO it was assumed that the thigh and shank sections would act as one complete body but that there might be some relative movement between the foot and shank due some flexibility in the polypropylene orthosis. Thus the ankle joint angle was calculated relative to the normal standing posture in the calibration trial with the most probable rotation around the Z-axis corresponding to dorsi/plantar flexion. The local co-ordinate matrices for the shank, S and foot, F had already been determined for each frame as described above. The method of Berme *et al.* (1990) was used to determine the rotation matrix, J between the local co-ordinates of the proximal segment (shank) to the local co-ordinates of the distal segment (foot). Mathematically expressed as:

$$[J]=[F]^{-1}[S] \qquad \text{Equation 5.5}$$

5.4.3. Segment Centre of Gravity, Angular Velocity and Acceleration

The centre of gravity of each body segment was required for calculation of the velocity and acceleration (table 5.2). For the shank its position lay on a line connecting the knee and ankle joint while for the foot a line connecting the heel and second metatarsal head was used. The values proposed by Contini (1970) were used to

Table 5.3

List of Matlab programs used to analyse the force plate data together with a brief summary of their function.

1) lforcegr; lforceca: Input force plate data, take account of force plate used and convert from 'bits' to N and Nm.
2) lsynchr: Synchronises force plate data with VICON data by reducing it to a similar size.
3) ltimes: Find the frames at heel strike and toe off and calculates the stance time.
4) ljointp: Calculates the centre of rotation for the ankle and knee joint.
5) lcalccp: Calculates the centre of gravity of each segment
6) langvel: Use rotation matrix to calculate the angular velocity of the segments.
7) langacc: Determines the angular acceleration from the 1st derivative of the angular velocity.
8) lcalcfor: Calculate the forces applied by the proximal to the distal segments.
9) lmomankl: Use previously calculated forces, mass and centre of gravity to determine the intersegmental moments at the ankle.
10) lmomknee: Use previously calculated forces, mass and centre of gravity to determine the intersegmental moments at the knee.
11) lwjoint: Determine the rotation of the foot about the ankle joint
12) lnormf; lnormm: Normalises the stance time with the intersegmental forces, moments and joint angles

determine their precise locations. The method described by Berme *et al.* (1990) was used to determine the angular velocity of the body segments relative to the LRS. For more information on how this was performed the reader is referred to the description given in Linden (1995). The velocity and translational acceleration of the body segments were derived from the first and second derivation of the filtered 3D co-ordinates of the centre of gravity of each segment, respectively. This is used to determine inertial force and thus joint loads.

5.5. KINETIC ANALYSIS

A list of the programs used to analyse the force plate data is given in table 5.3 in the order that they were used. A basic outline of the function of each program is also provided.

5.5.1 Inverse Dynamics

In the majority of engineering analyses, the forces and moments are the inputs used to determine the bodies kinematics. In contrast, the method of inverse dynamics uses the known kinematics of the body to determine the desired force and moment outputs. In this situation unknown proximal forces at each joint are determined from the known distal forces using Newtonian mechanics, i.e. forces are equal but opposite. The analysis starts at the foot where the distal external force applied to the foot is known to be the ground reaction force. The body segments are assumed to be rigidly connected to each other with hinged frictionless joints. Again using Newtonian mechanics, the unknown external force at the proximal joint can be calculated if the mass and acceleration of the centre of gravity are known. This technique assumes no other external forces act on the body. The values proposed by Contini (1970) are used to determine segment masses from percentages of total body mass.

5.5.2 Intersegmental Forces and Moments

The methods used by Linden (1995) were also used in this study to determine the intersegmental forces and moments. The approach used is described in the following section. According to Newton's second law the sum of the external forces on a body equals the product of its mass and the acceleration of the centre of gravity.

For the foot: $\Sigma F = -Fp + F_G - mg = m_f a_f$

$$Fp = -m_f a_f + F_G - m_f g \qquad \text{Equation 5.6}$$

For the shank:

$$Fp = -m_s a_s + Fd - m_s g \qquad \text{Equation 5.7}$$

where:

Fp	Reaction force at proximal joint
F_G	ground reaction force
Fd	distal joint reaction force
m_f	mass of foot
m_s	mass of shank
g	acceleration due to gravity
a_f	acceleration of centre of gravity of foot
a_s	acceleration of centre of gravity of shank

Similarly for moment calculations, the resultant external moments acting on a segment equals the product of the angular acceleration and the moment of inertia. The total moments include the inertial moments and these were derived from the regression equations of McConville *et al.* (1980). The methods described by Hof (1992) and Hardt & Mann (1980) were used to calculate the net joint moments, using the equation:

$$\begin{aligned} \Sigma M &= d(I_G w_G)/dt \\ &= [S][d(I_a w_a)/dt] \\ &= [S][I_a d(w_a)/dt + (w_a) \times (I_a w_a)] \end{aligned} \qquad \text{Equation 5.8}$$

where: ΣM Total moments

I Moment of inertia

w Angular velocity vector

S Local co-ordinate matrix of segment S

The subscripts 'G' and 'a' refer to the global and local axis systems respectively and the symbol 'x' denotes the mathematical cross product.

The total external moments were comprised of the moments at the distal (Md) and proximal (Mp) joints and the moments caused by the distal (Mfd) and proximal (Mfp) forces at these joints. These moments due to forces were calculated as the product of the reaction force at the joint and the distance between the co-ordinates of the distal (Jd) and proximal (Jp) joint centres and the co-ordinates of the segment centre of gravity (c). Mathematically:

$$Mfd = Fd\ (Jd-c)$$

$$Mfp = Fp\ (Jp-c)$$

$$\Sigma M = Mp + Md + Mfp + Mfd$$

Hence:

$$Mp + Md + Fd\ (Jd-c) + Fp\ (Jp-c) = [S][I_a d(w_a)/dt + (w_a) \times (I_a w_a)] \qquad \text{Equation 5.9}$$

From this equation the proximal joint force for each segment may be calculated. From Newtonian mechanics, this is also the force at the distal joint of the proximal segment, thus allowing the moments for each proximal segment to be calculated in turn. For the ankle moments, the term Fd is replaced by the position of application of the ground reaction force (or centre of pressure).

5.6 TRANSDUCER DATA ANALYSIS

The transducer data were sampled at 100Hz. The output generated by Signal Centre was in the form of a table, with a row for each instant sampled, and 12 columns

Table 5.4

List of Matlab programs used to analyse transducer data together with a brief summary of their function

1) lcrosst: Input the medial and lateral transducer data and perform calculations to take accoung of the bridge voltage, gain and cross-talk effects.
2) Ltzero: Synchronise transducer data with force plate data by matching the point of heel strike for each trial. Reduce transducer data to zero initial loading.
3) Lanafor; lanamom: Calculate the transformation from the axis system of the transducer to that of the shank by determining a rotation matrix and translation vector from the calibration trial to each frame in the experimental trials. Recalculate the transducer loads.
4) Ldivide: Reduce the frequency of the transducer data to that of the force plate and VICON data.
5) lnormfmt: Normalises the force recorded by the transducer over one stance phase.

for the six medial and six lateral loads. These files were saved in ASCII format for input into the Matlab software package. The matrix was split into two, one for each transducer, for ease of analysis. Next, each column was adjusted to take the bridge voltage and gain for that channel into account. The matrix was transformed so that each column now represented the six loads recorded by each transducer. These six values were then multiplied by the inverse of the cross-talk matrix for each transducer (see section 3.4.1) and this was repeated for each column in the matrix. The newly determined matrix was then transformed again to return it to its original format.

The data were plotted to enable the instant of heel strike corresponding to the force plate data collection to be determined. The load data for this gait cycle was then saved in a new file, to be analysed separately. The graphs showed a slight offset for each channel which related to the loads due to the strapping. These were reset to zero so that the transducer was assumed to be under no loads when suspended by the leg prior to heel strike. It was noticed that when both data measurements were plotted together there was often a disagreement, by a frame or two, about the instant of heel strike. Further manipulation was used to remove these obvious errors.

All parameters, including those calculated previously, were then normalised so that 100 on the time scale equals the full stance time (heel strike to toe off). A list of the programs used to analyse the transducer data is provided in table 5.4 in their chronological order.

Figure 6.1: (Subject X)
Six components of the transducer load on the medial and lateral uprights of subject X

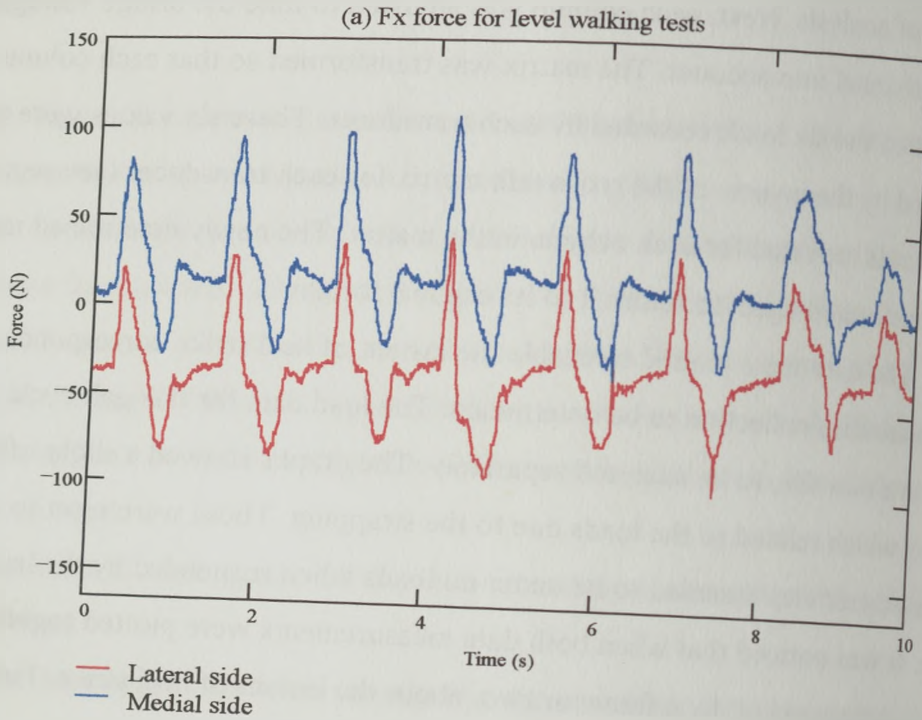

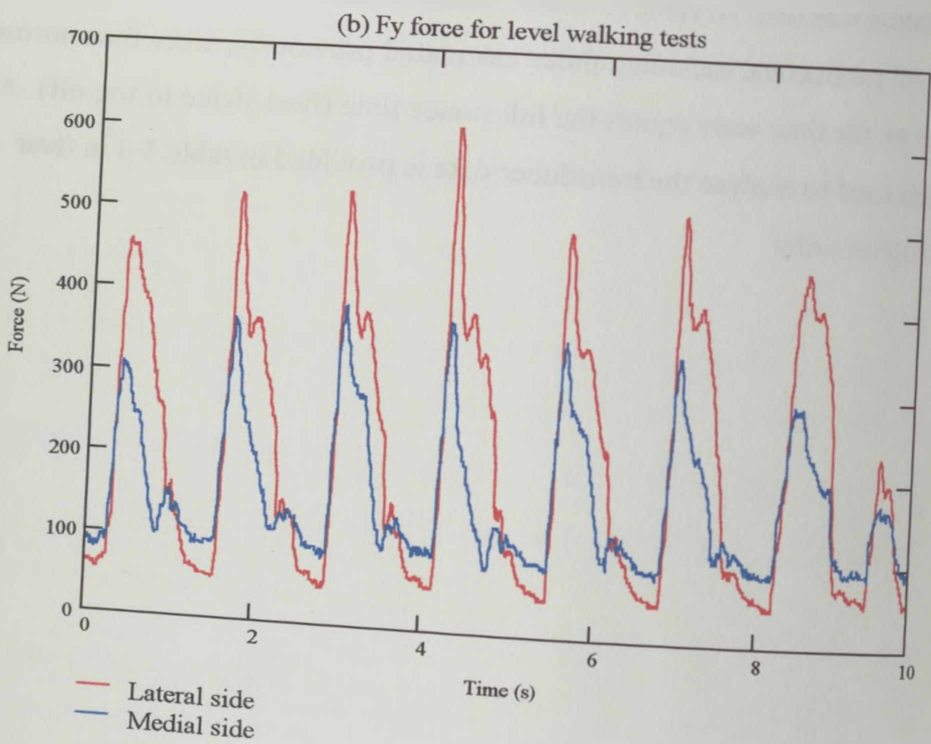

CHAPTER 6 RESULTS

The data recorded in the experimental trials for subjects X and Z are given in this chapter together with the results obtained through the data processing and analysis. Due to the incongruous nature of the results from the two subjects it was considered necessary to provide examples of both concurrently. From observation of the subject's walking patterns during the tests it appeared that subject Z was initially very conscious of trying to step on the force plate and had problems walking in a consistent manner. Analysis of the results showed that one trial was clearly not representative of the subject's gait. For this reason, the data from only 9 trials for this subject were processed. For ease of understanding a consistent colour scheme was used throughout this chapter. For figures 6.1 and 6.2 where forces on the medial and lateral transducers are compared, all loads on the lateral transducer are in red and on the medial one are in blue. However for the rest of the chapter (figs. 6.3 to 6.13), three colours are used. For values calculated from the force plate data all forces, moments, joint angles, etc. about or along the x axis were plotted in blue. Similarly red and green were used for graphs plotted about the y and z-axis respectively. Forces recorded by the transducers and then converted into the shank reference system were plotted in black.

6.1 TRANSDUCER DATA

The data were initially analysed using the Mathcad software package. A program was written which took the bridge voltages, gain and cross-talk effects into account. The program is given in appendix A4. Graphs displaying the six components of the calculated load output against the experimental time were plotted for each subject. Figures 6.1 and 6.2 (a) to (f) show the results obtained for subjects X and Z respectively. These graphs allow the difference in the magnitude and nature of the output recorded by the lateral and medial transducers to be clearly observed. All graphs show a small offset from zero, the

Figure 6.1: (Subject X)

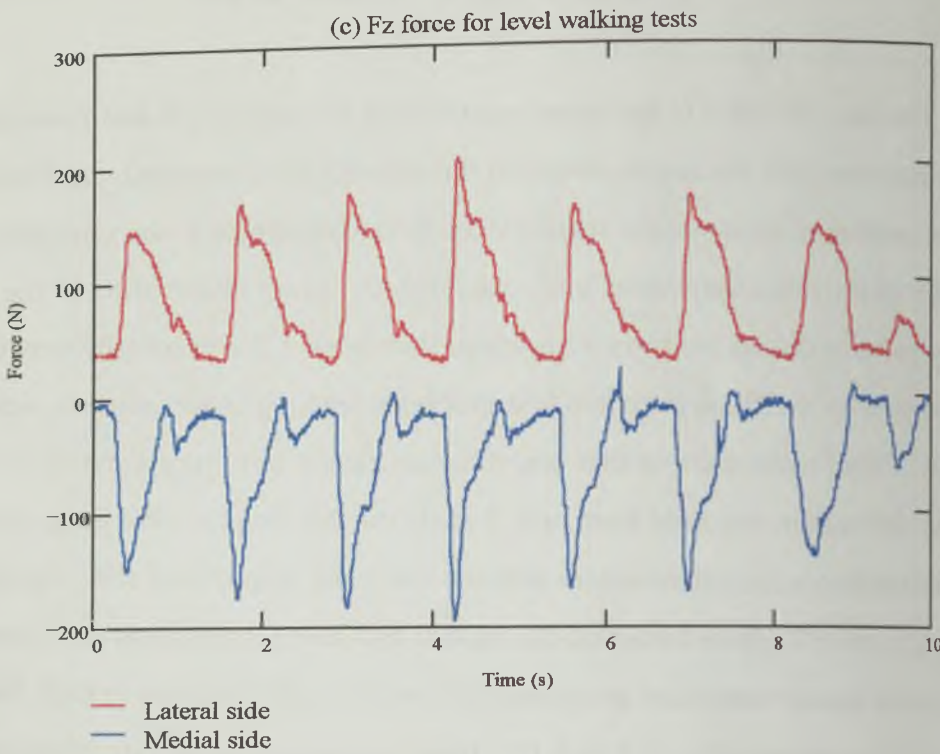

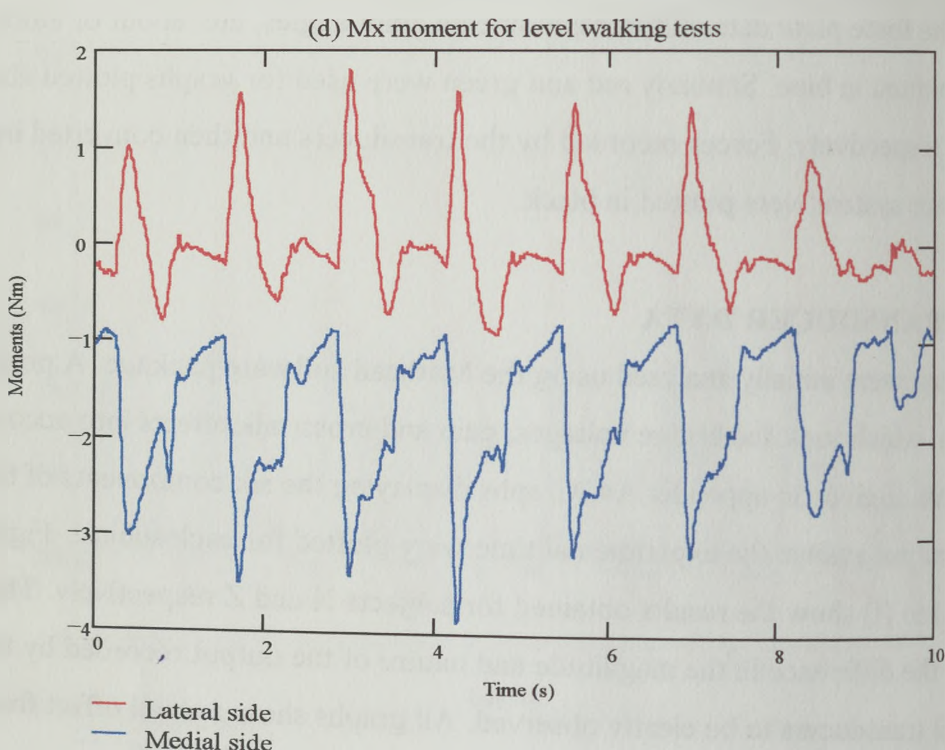

Figure 6.1: (Subject X)

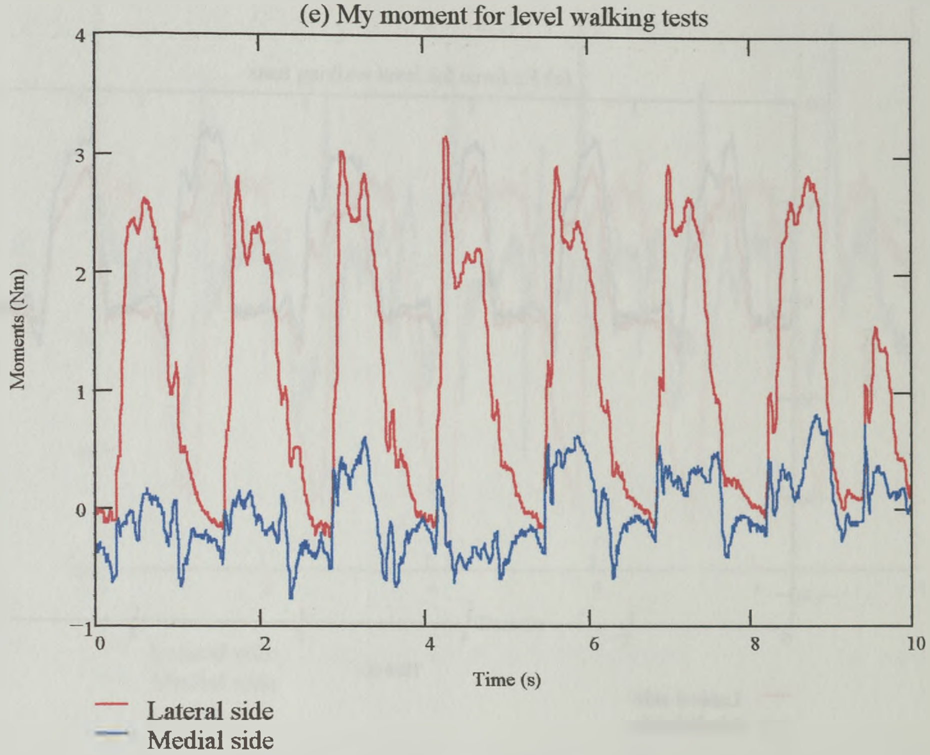

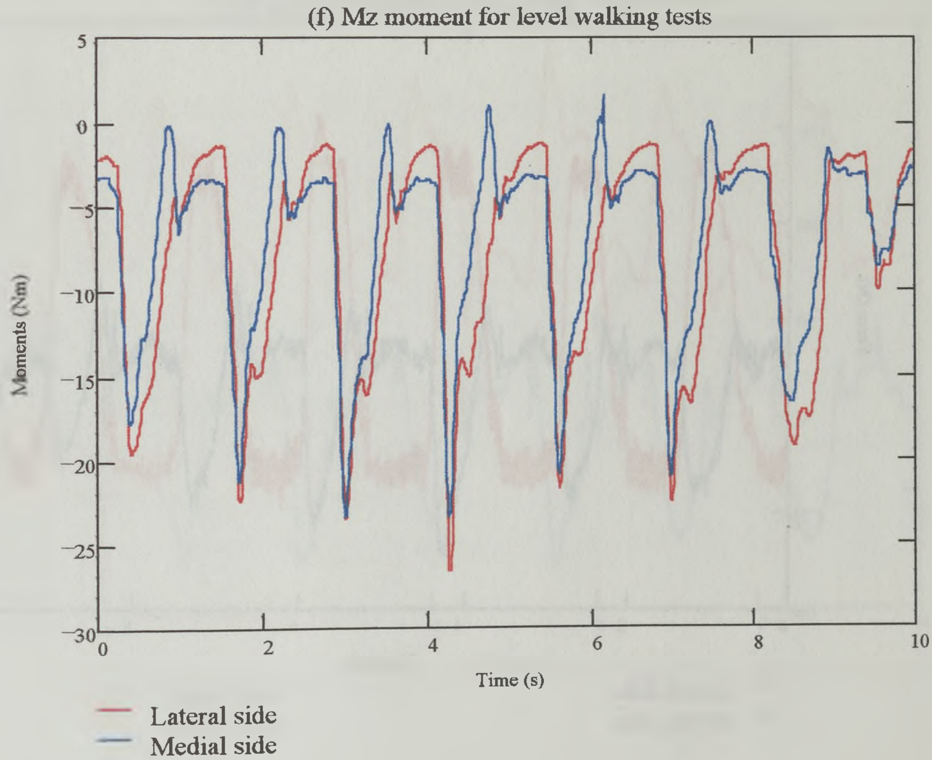

Figure 6.2
Six components of the transducer load on the medial and lateral uprights of subject Z

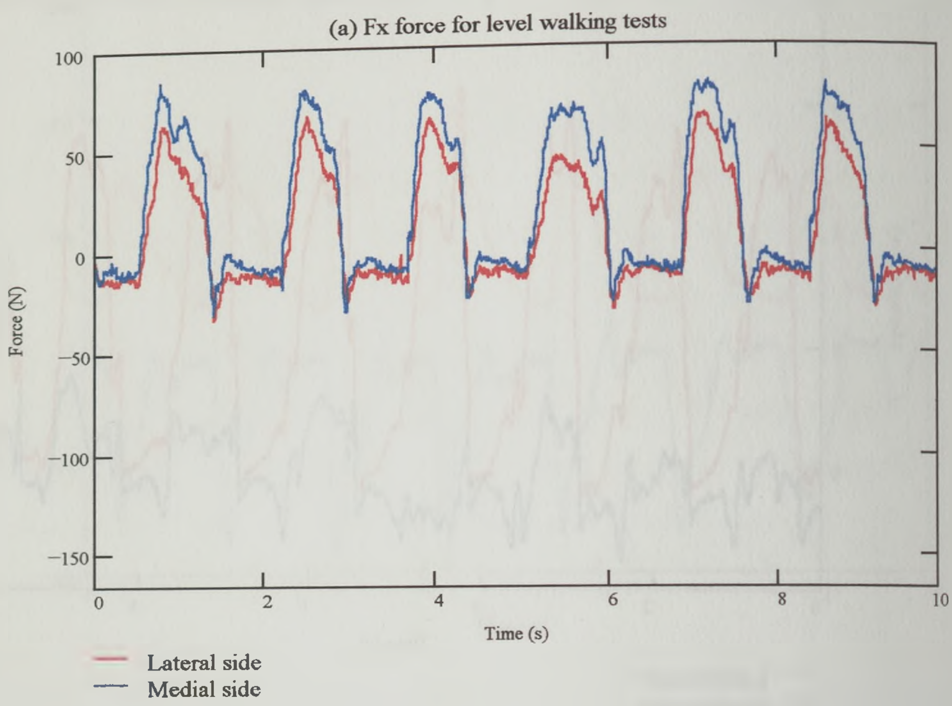

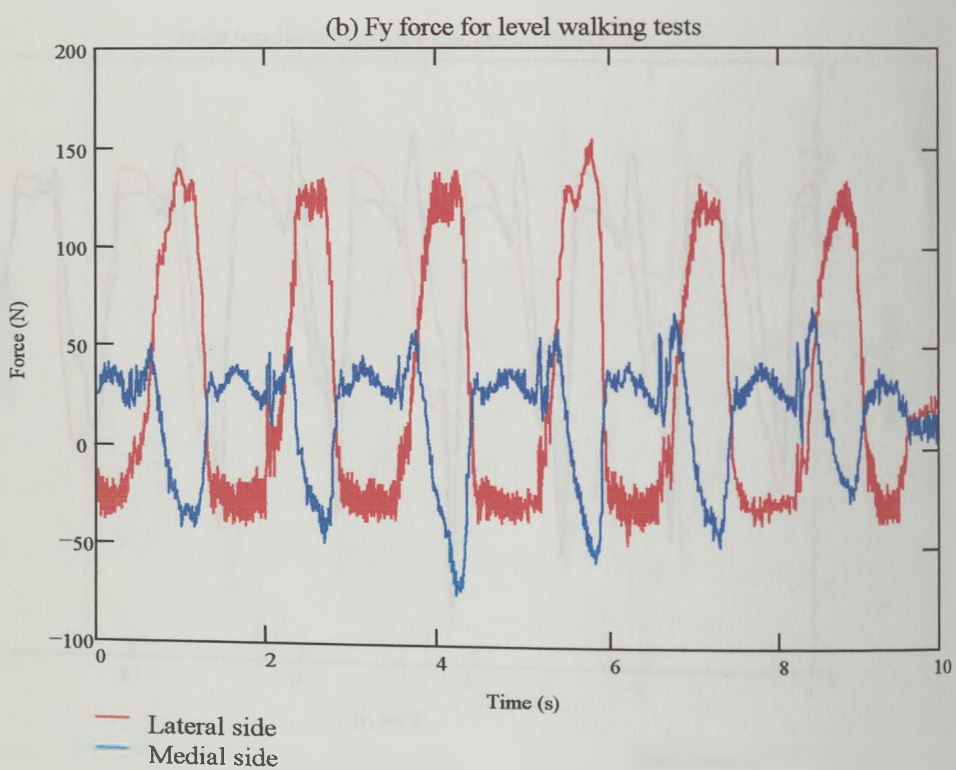

Figure 6.2: (Subject Z)

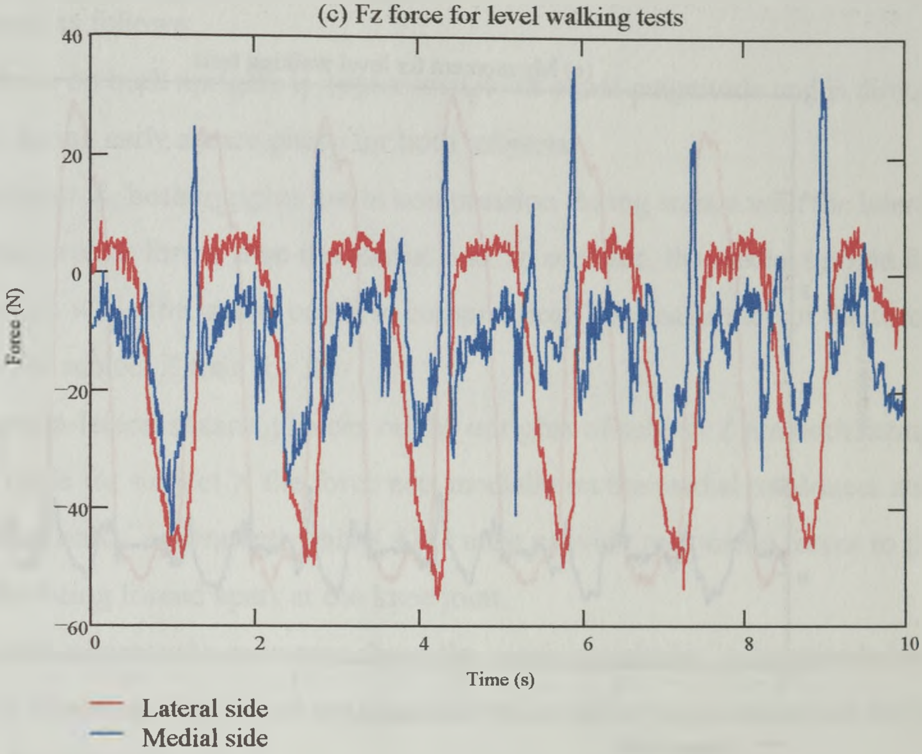

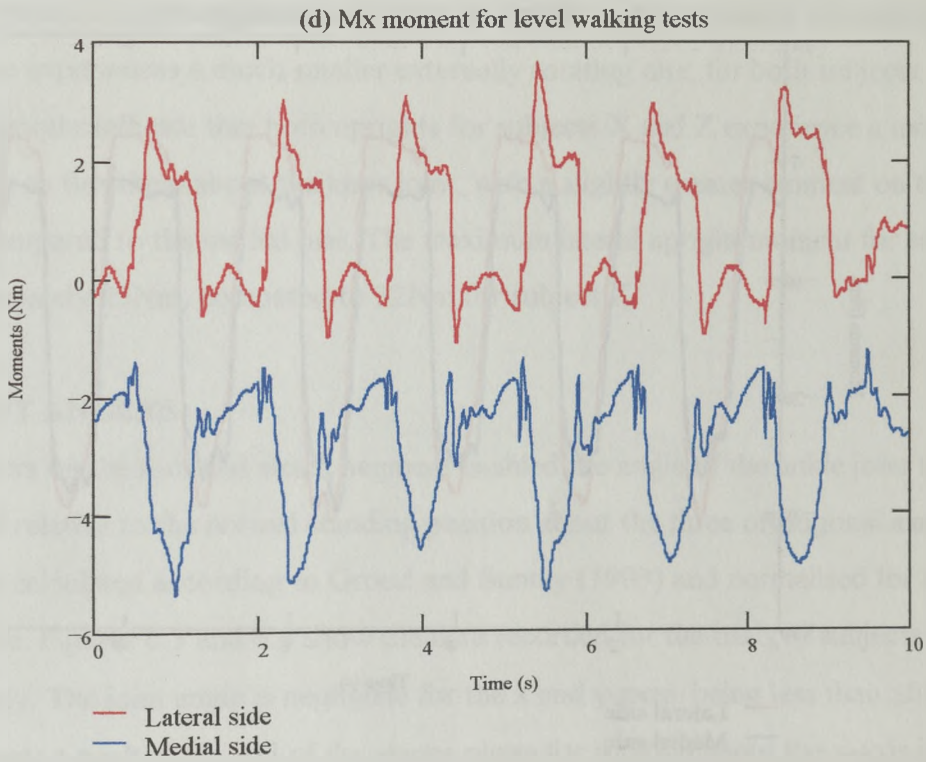

Figure 6.2: (Subject Z)

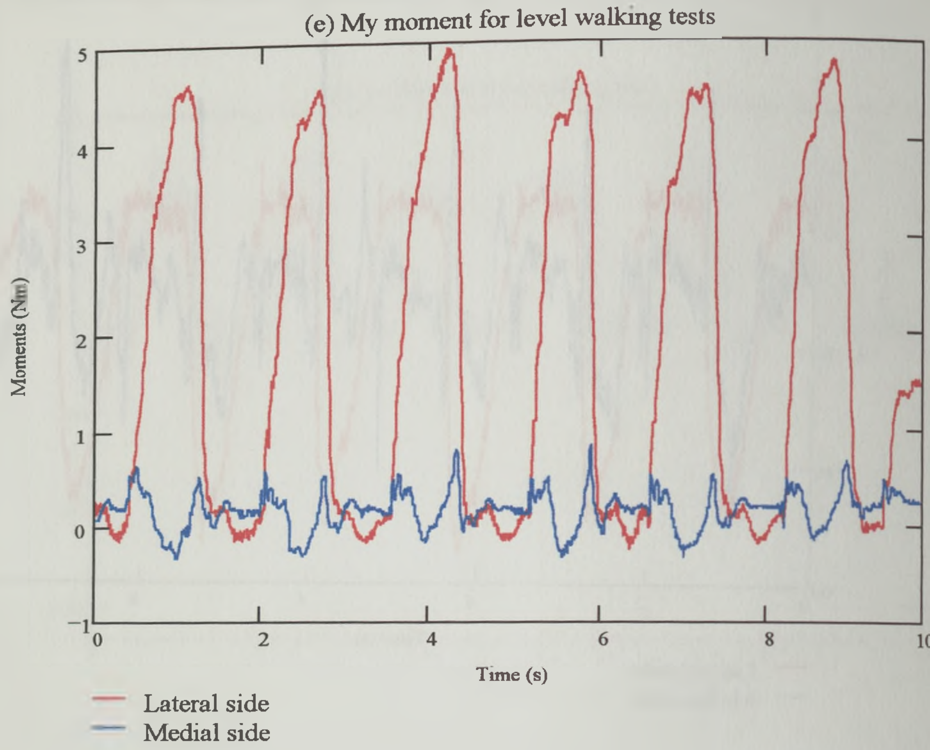

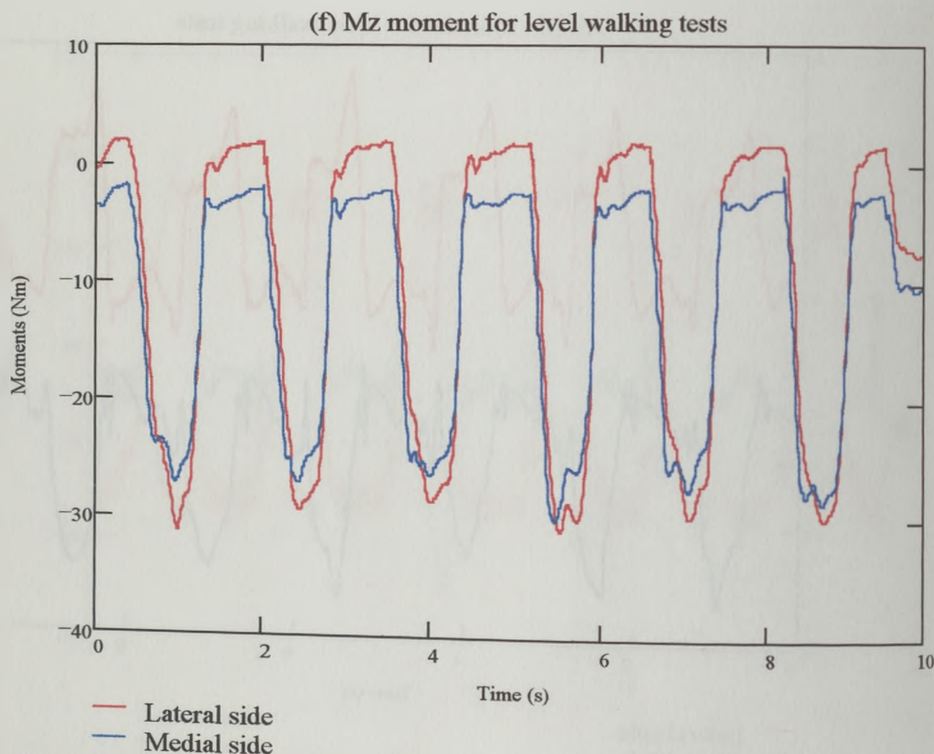

magnitude of which varies between each channel. The results may be summarised for each channel as follows:

Fx: The force on both uprights is approximately of equal magnitude and is directed anteriorly during early stance phase for both subjects.

Fy: For subject X, both uprights are in compression during stance with the lateral upright transmitting greater forces than the medial one. In contrast, the medial upright for subject Z is in tension while the lateral one is in compression. The magnitude of the forces are much less for subject Z than for X.

Fz: The medio-lateral shearing forces on the uprights of subject Z are both acting medially, while for subject X the force acts medially on the medial transducer and laterally on the lateral one. Consequently this KAFO must provide restraining forces to prevent the uprights being forced apart at the knee joint.

Mx: For both subjects the moments about the x-axis are similar in magnitude but opposite in direction. The lateral upright exhibits an adducting moment and the medial one an abducting moment.

My: The lateral upright experiences a large internally rotating moment whereas the medial one experiences a much smaller externally rotating one, for both subjects.

Mz: The graphs indicate that both uprights for subjects X and Z experience a moment which tries to flex them about the knee joint, with a slightly greater moment on the lateral upright compared to the medial one. The maximum lateral upright moment for subject X is approximately 25Nm, compared to 32Nm for subject Z.

6.2 JOINT ANGLES

The markers on the foot and shank segment enabled the angle of the ankle joint to be calculated relative to the normal standing position about the three orthogonal axes. The angle was calculated according to Grood and Suntay (1993) and normalised for the stance time. Figures 6.3 and 6.4 show the data recorded for the trials of subjects X and Z respectively. The joint angle is negligible for the x and y-axes, being less than $\pm 0.8°$. For both subjects a peak at the end of the stance phase for rotation about the x-axis indicates

Figure 6.3
Clinical angles calculated for the ankle joint complex (calculated according to Grood and Suntay, 1983) for 10 trials of subject X. Positive angles are external rotation, figure 6.3 (a); inversion, figure 6.3 (b); and dorsiflexion, figure 6.3 (c).

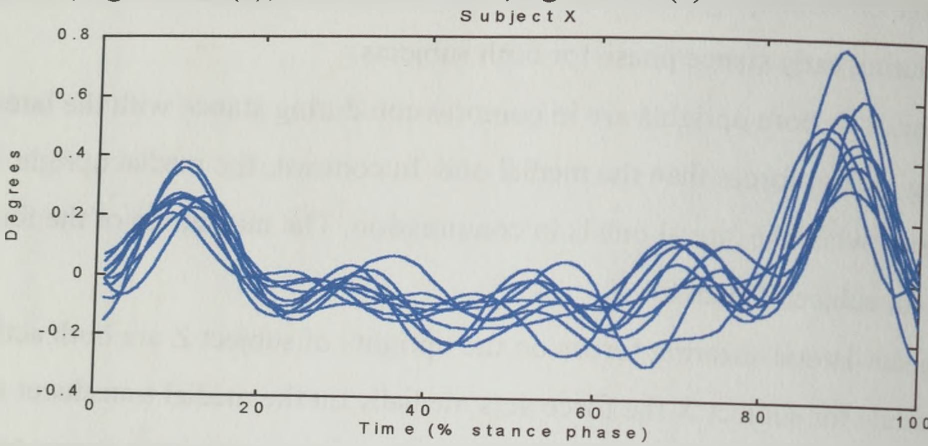

Figure 6.3 (a)

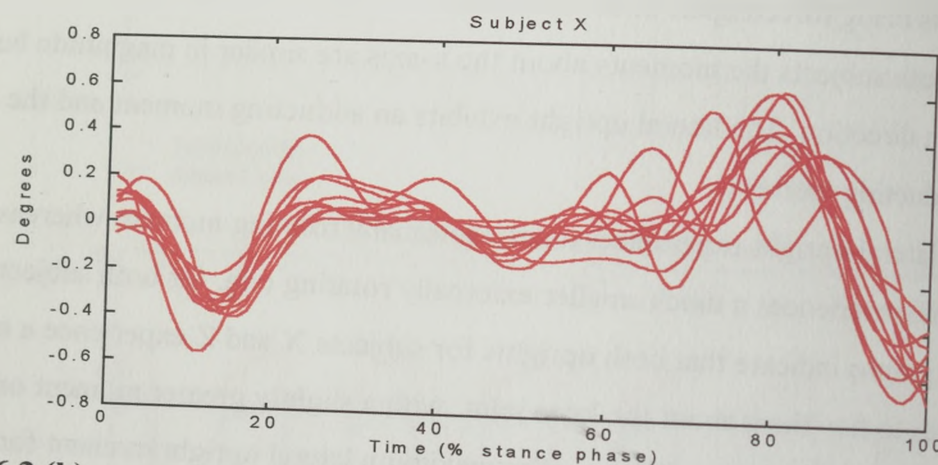

Figure 6.3 (b)

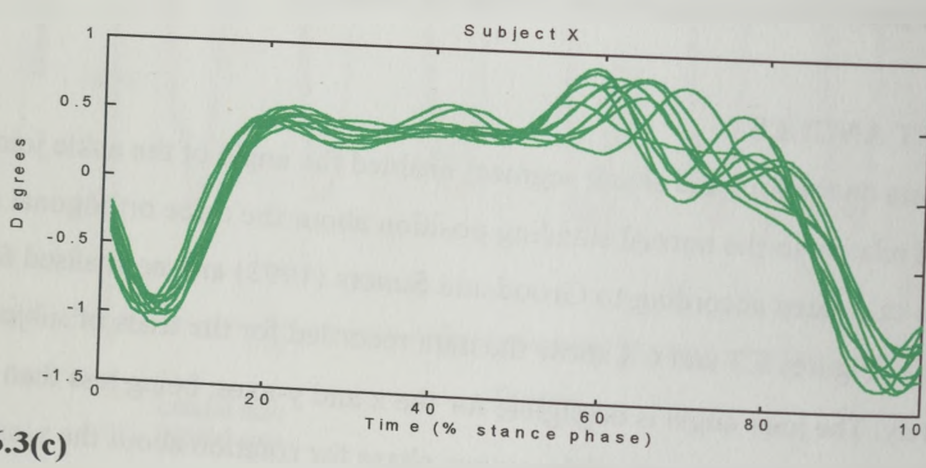

Figure 6.3(c)

Figure 6.4

Clinical angles calculated for the ankle joint complex (Grood and Suntay, 1983) for 10 trials of subject Z. Positive angles are external rotation, Fig 6.4 (a); inversion, figure 6.4 (b); and dorsiflexion, figure 6.4 (c).

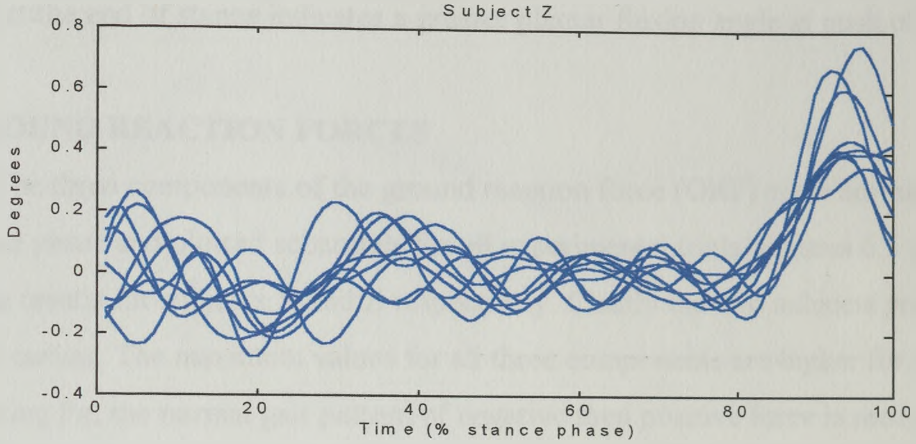

Figure 6.4 (a)

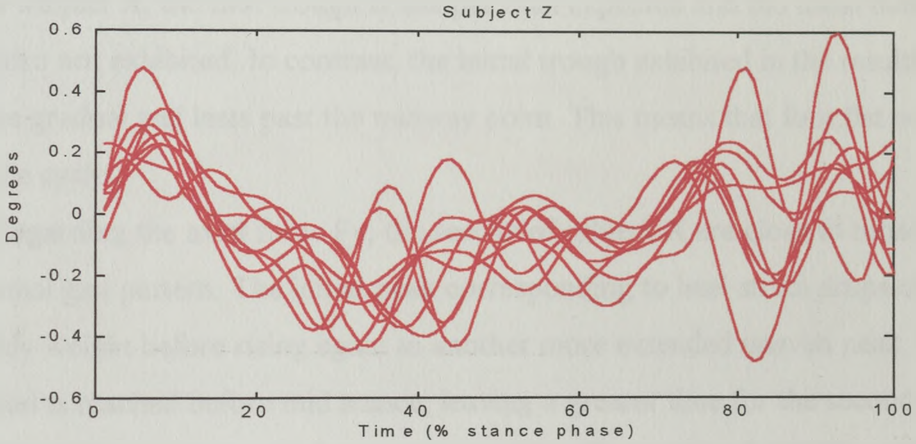

Figure 6.4 (b)

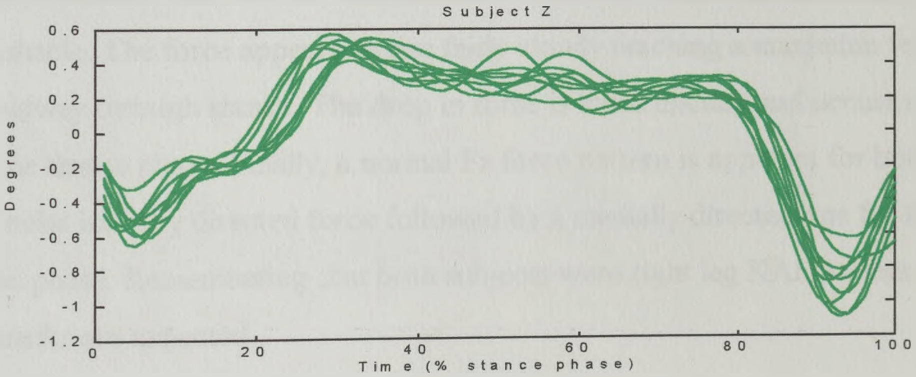

Figure 6.4 (c)

the point of maximum external rotation. The most significant result concerns the dorsi/plantar flexion movement about the z-axis. The initial trough indicating plantar flexion is followed by an extended period of dorsi flexion. A second, larger trough of up to -1.5° at the end of stance indicates a greater plantar flexion angle at push off.

6.3 GROUND REACTION FORCES

The three components of the ground reaction force (GRF) were normalised for the stance phase and plotted separately for all experimental trials. Figures 6.5 and 6.6 show the results for subjects X and Z respectively. Clearly the two subjects produce very different curves. The maximum values for all three components are higher for subject X. Considering Fx, the normal gait pattern of negative then positive force is recognisable. Both subjects also display an initial positive force corresponding to forwards force on the foot. For subject X, the first trough is sharper than expected and the usual delay at zero force is also not exhibited. In contrast, the initial trough exhibited in the results of subject X is more gradual and lasts past the midway point. This means that foot flat occurs much later in the cycle.

Regarding the axial force Fy, the results of subject X are close to those observed for a normal gait pattern. The initial peak corresponding to heel strike drops off to about 0.7% body weight before rising again to another more extended uneven peak. The flat foot period is reached before mid stance, leaving a greater time for the second peak which is much longer and more bumpy than normal. For subject Z, the Fy pattern is completely different than normal, with neither of the two peaks nor the trough distinguishable. The force appears to rise fairly slowly reaching a maximum value just before midway through stance. The drop in force is more distinct and occurs at about 75% of the stance phase. Finally, a normal Fz force pattern is apparent for both subjects with an initial laterally directed force followed by a medially directed one for the rest of the stance phase. Remembering that both subjects were right leg KAFO users, these similar results are expected.

Figure 6.5
Ground reaction forces at the knee joint in shank reference system for trials of subject X. Positive forces are directed anteriorly for Fx force figure 6.5 (a); vertically upwards for axial Fy force, figure 6.5 (b); and laterally for Fz force, figure 6.5 (c).

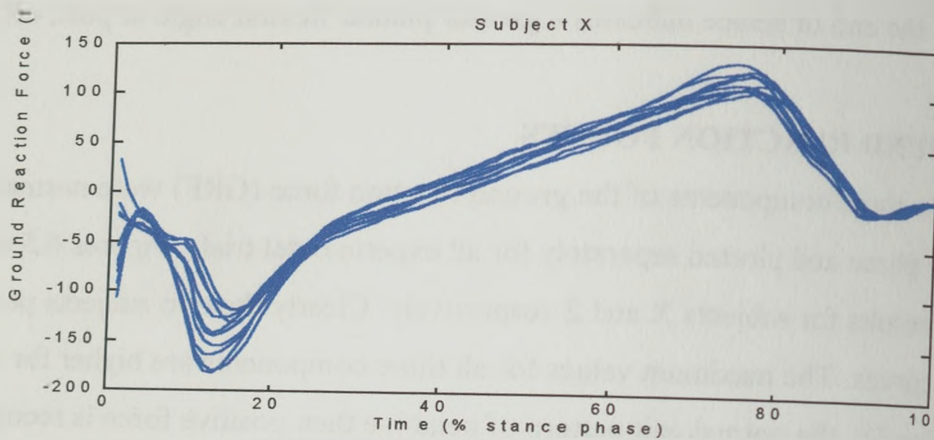

Figure 6.5 (a): Fx

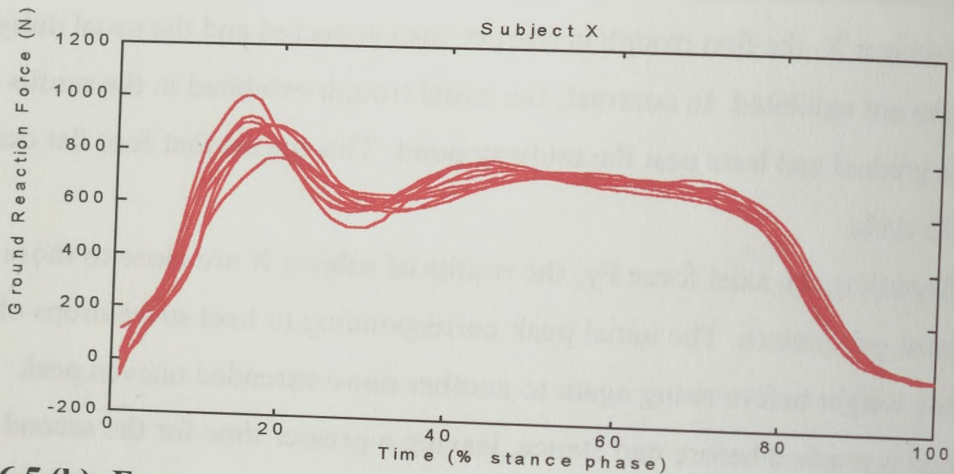

Figure 6.5 (b): Fy

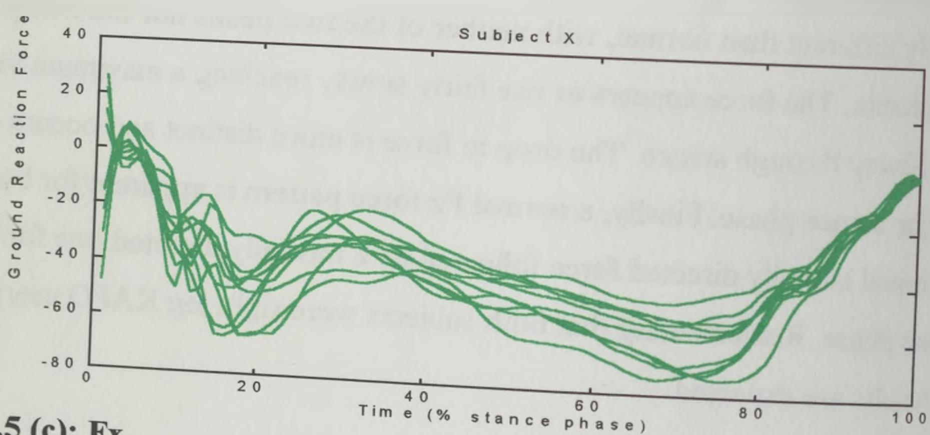

Figure 6.5 (c): Fx

Figure 6.6
Ground reaction forces calculated at the knee joint in shank reference system for trials of subject Z. Positive forces are directed anteriorly for Fx force, figure 6.5(a); vertically upwards for axial Fy force, figure 6.5(b); and laterally for Fz force, figure 6.5(c).

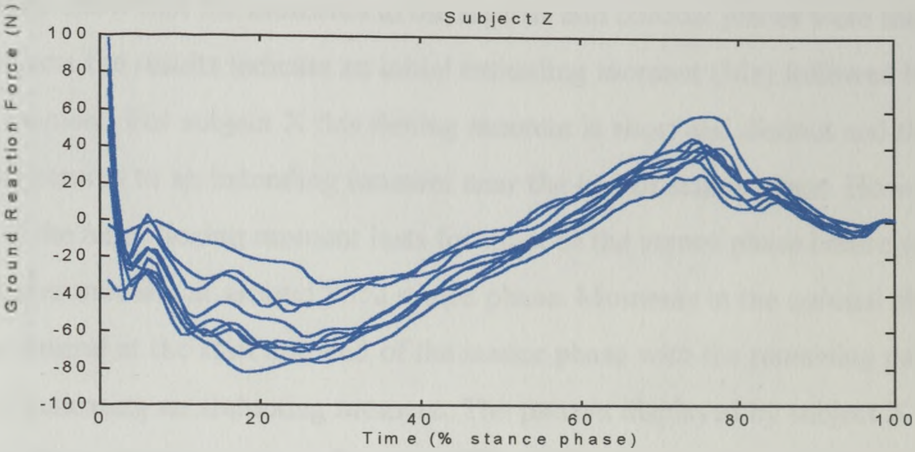

Figure 6.6(a): Fx

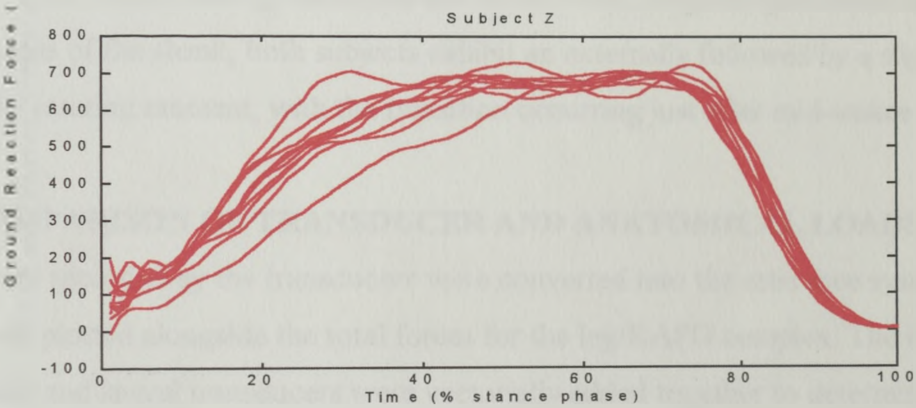

Figure 6.6(b): Fy

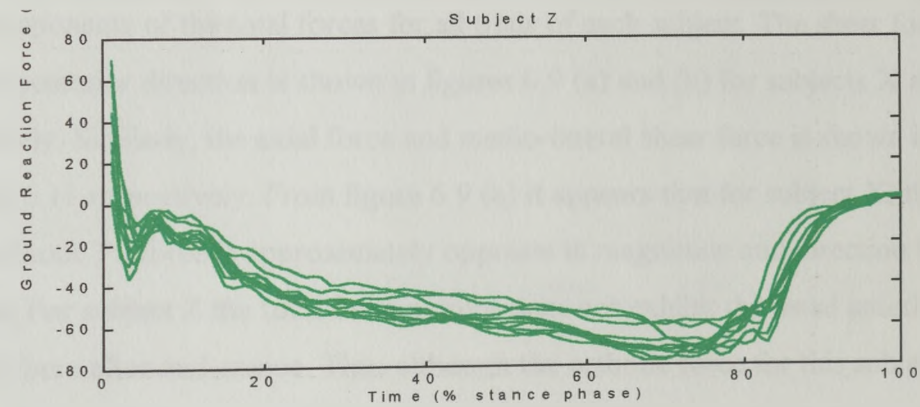

Figure 6.6(c): Fz

6.4 INTERSEGMENTAL MOMENTS

The three components of the intersegmental moments at the knee joint were normalised over the stance phase and plotted for each subject. The graphs (fig 6.7 and 6.8) clearly show that the moments in the sagittal and coronal planes were the largest. For both subjects the results indicate an initial extending moment (Mz) followed by a negative flexing moment. For subject X this flexing moment is short and distinct and then gradually returns to an extending moment near the end of stance phase. However for subject Z the large flexing moment lasts for most of the stance phase before steeply rising to a positive moment at around 85% stance phase. Moments in the coronal plane (Mx) are near neutral at the start and end of the stance phase with the remaining part being negative indicating an abducting moment. The pattern displayed by subject X is more distinct with a maximum value of around 25Nm. For subject Z the maximum moment is around 35Nm with a more gradual rise and fall in value. Regarding moments about the vertical axis of the shank, both subjects exhibit an externally followed by a slight internally rotating moment, with the transition occurring just after mid-stance.

6.5 COMPARISON OF TRANSDUCER AND ANATOMICAL LOADS

The forces recorded by the transducers were converted into the reference system of the shank and plotted alongside the total forces for the leg/KAFO complex. The forces from the medial and lateral transducers were vectorially added together to determine the total orthotic forces. The three components of the transducer forces were plotted against the three components of the total forces for all trials of each subject. The shear force in the anterior-posterior direction is shown in figures 6.9 (a) and (b) for subjects X and Z respectively. Similarly, the axial force and medio-lateral shear force is shown in figures 6.10 and 6.11 respectively. From figure 6.9 (a) it appears that for subject X, the pattern of the orthotic Fx force is approximately opposite in magnitude and direction to the total Fx force. For subject Z the total force pattern does not exhibit the usual anteriorly directed force after mid-stance. Thus although the orthotic force for this subject also

Figure 6.7
Total intersegmental distal moments at the knee joint for 10 trials of subject X in the shank frame of reference. Positive moments are adducting Mx moment, figure 6.7 (a); internally rotating My moment, figure 6.7 (b); and extending Mx moment, figure 6.7(c).

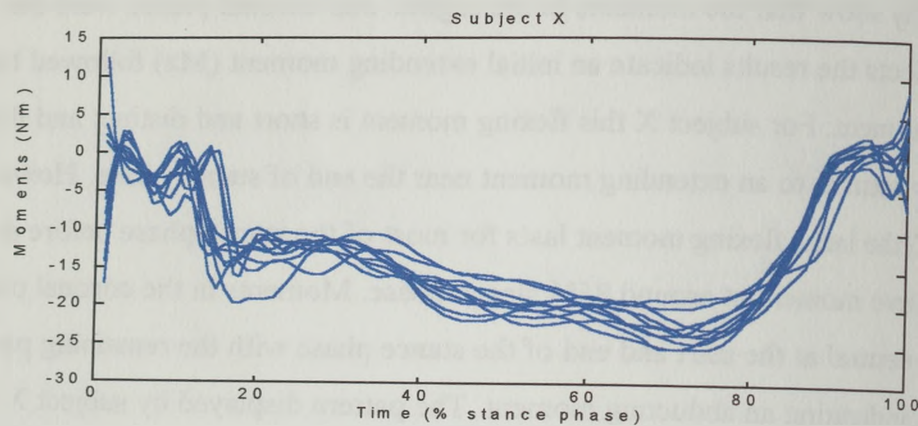

Figure 6.7(a): Mx

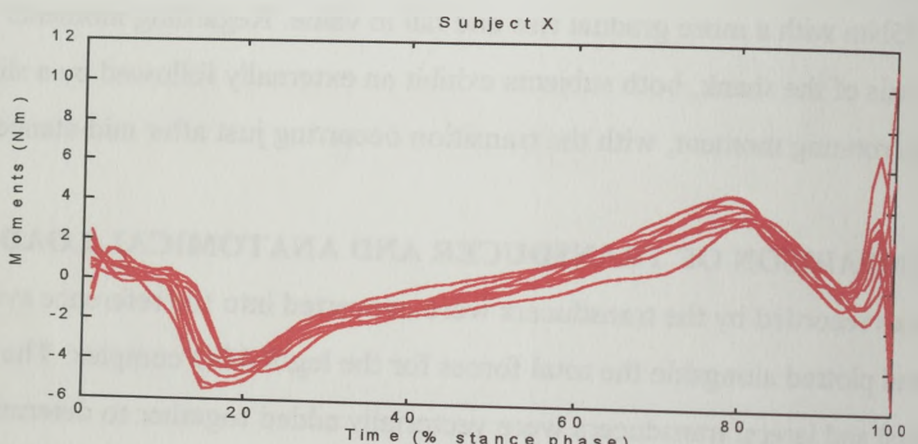

Figure 6.7(b): My

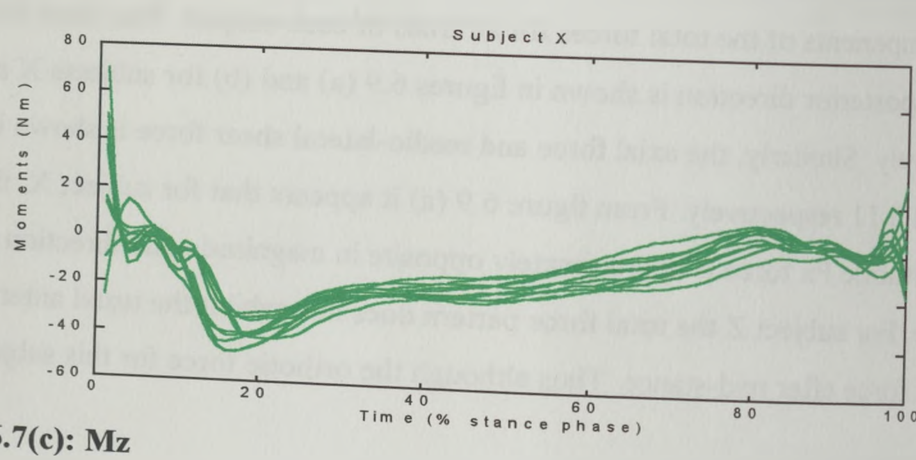

Figure 6.7(c): Mz

Figure 6.8

Intersegmental distal moments at the knee joint for 10 trials of subject Z in shank frame of reference. Positive moments are adducting Mx moment, figure 6.8(a); internally rotating My moment, figure 6.8(b); and extending Mx moment, figure 6.8(c).

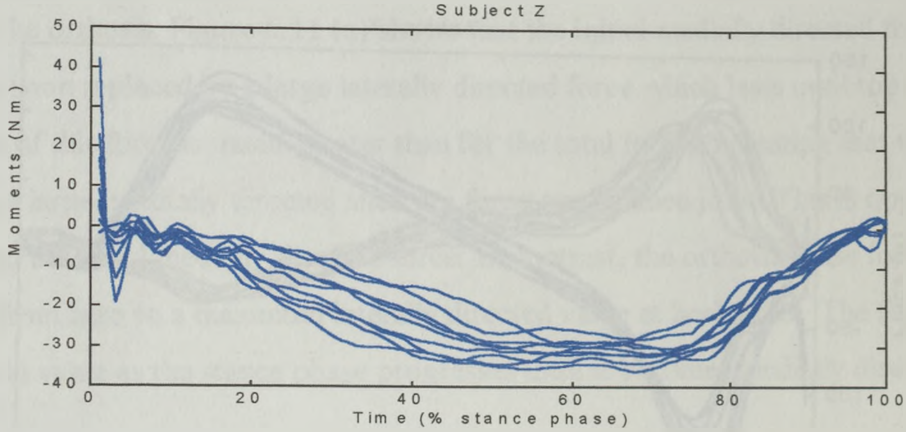

Figure 6.8(a):Mx

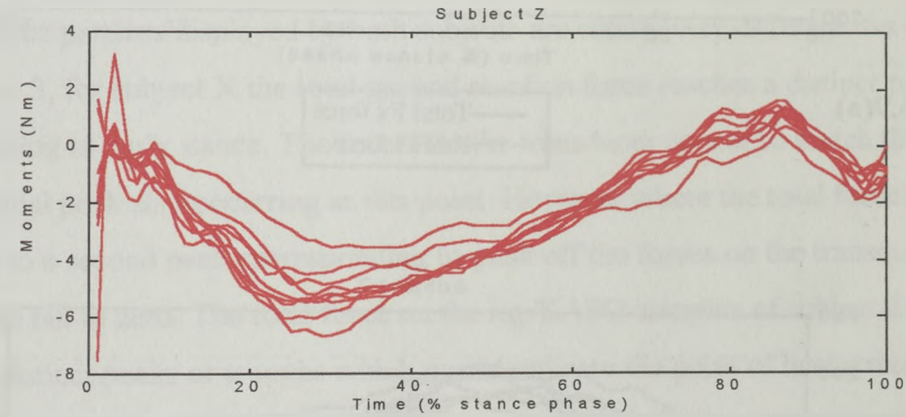

Figure 6.8(b):My

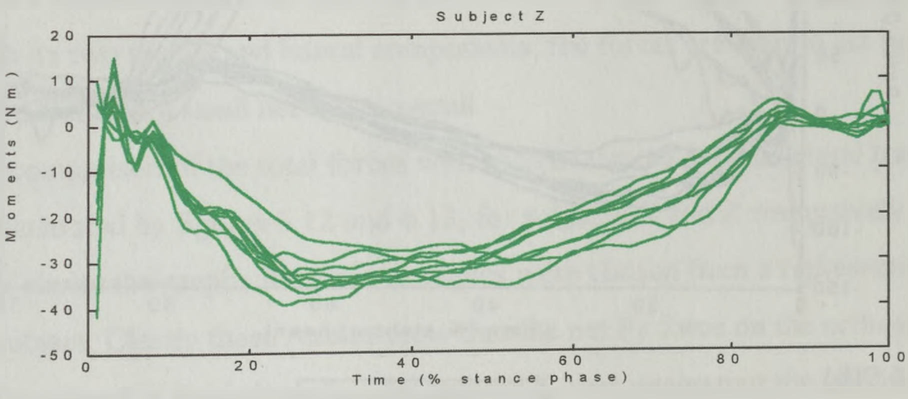

Figure 6.8(c):Mz

Figure 6.9
Comparison of the transducer and total (leg/KAFO complex) anterior-posterior Fx forces at the knee joint. Both forces in shank reference frame with positive forces acting anteriorly. Figure 6.9 (a) and (b) for trials of subjects X and Z respectively.

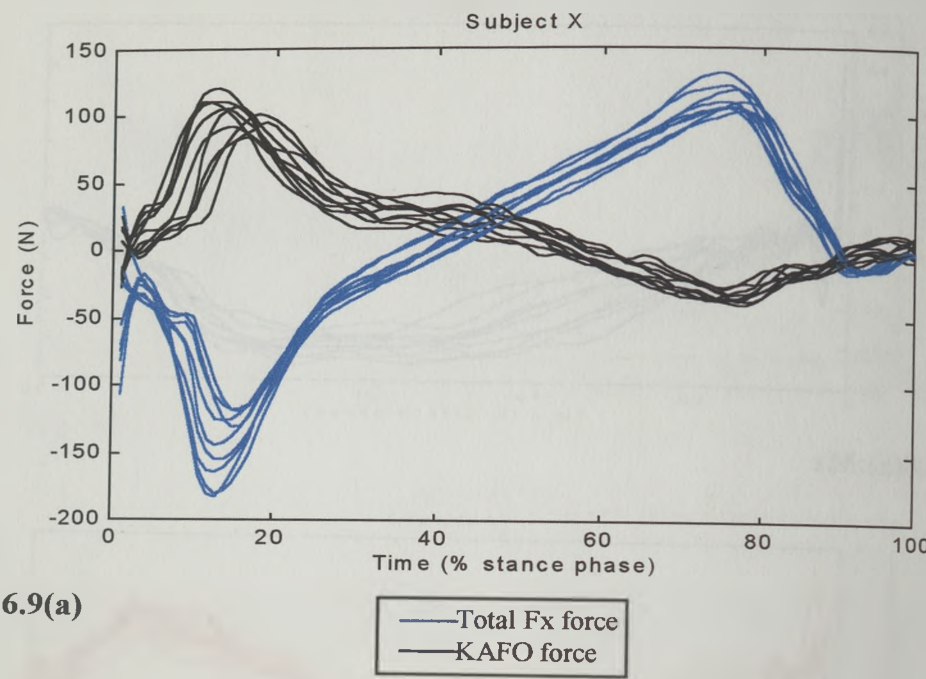

Figure 6.9(a)

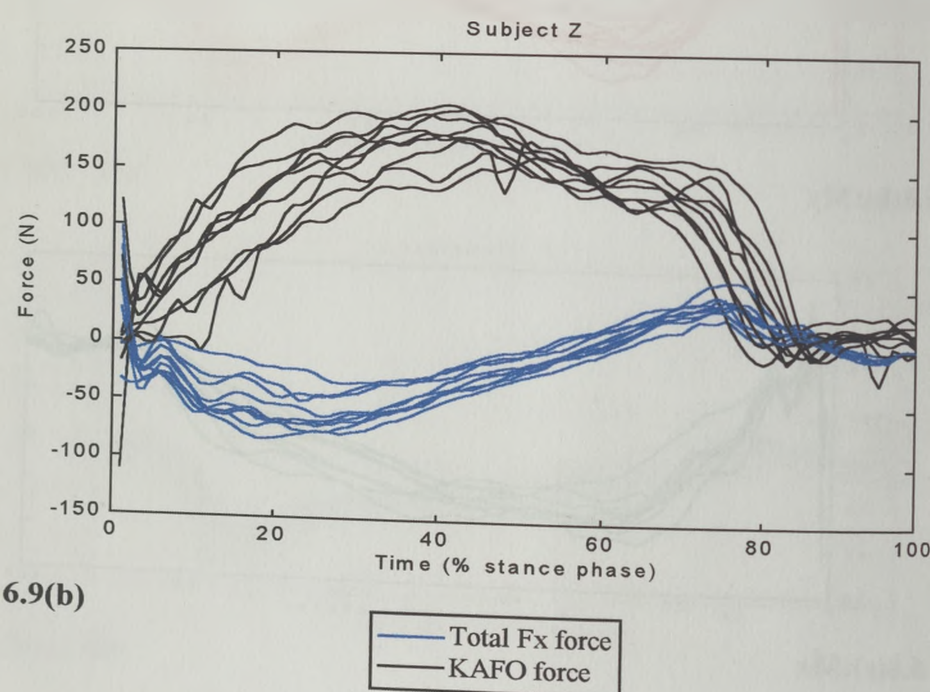

Figure 6.9(b)

appears opposite in direction to the total force, it does not display the same pattern as for subject X.

Examining the medio-lateral Fz force next (fig 6.11), the graphs indicate that a similar total force for the whole complex for each subject does not result in the same forces on the orthosis. Figure 6.11 (a) shows that the initial medially directed force on the orthosis is soon replaced by a large laterally directed force which lasts until toe off. The magnitude of this force is much greater than for the total force, indicating that the KAFO is causing a large, medially directed shearing force on the knee joint. This is opposite in direction to the usual medially directed force. In contrast, the orthotic force for subject Z increases from zero to a maximum laterally directed value at heel strike. The force then decreases in value as the stance phase progresses until it becomes medially directed at toe off.

Lastly considering the axial Fy force, (fig. 6.10 (a), (b)) the total force and orthotic force patterns displayed by both subjects are clearly very different. As explained in section 6.3, for subject X the total ground reaction force reaches a distinct peak corresponding to early stance. The forces on the transducer appear to match this pattern, with an initial peak also occurring at this point. However where the total force falls and then rises to a second peak corresponding to push off the forces on the transducer continue to fall to zero. The total force on the leg/KAFO complex of subject Z does not have any distinct peaks or troughs which would indicate the point of heel strike and toe off. The force on the orthosis of this subject appears negligible in comparison to the total force, with a maximum value of approximately 100N. However when this orthotic force is split into its two medial and lateral components, the forces are seen to act in opposite directions producing a small net force overall.

A comparison of the total forces with each of the medial and lateral transducer forces is illustrated by figures 6.12 and 6.13, for subjects X and Z respectively. For reasons of clarity the graphs for these examples were chosen from a representative trial for each subject. Clearly these results show that the net Fy force on the orthosis is additive for subject X but subtractive for subject Z, thus generating the graphs seen in

Figure 6.10
Comparison of the transducer and total (leg/KAFO complex) axial load, Fy. Both forces in shank reference frame with positive forces acting upwards. Figure 6.10 (a) and (b) for trials of subjects X and Z respectively.

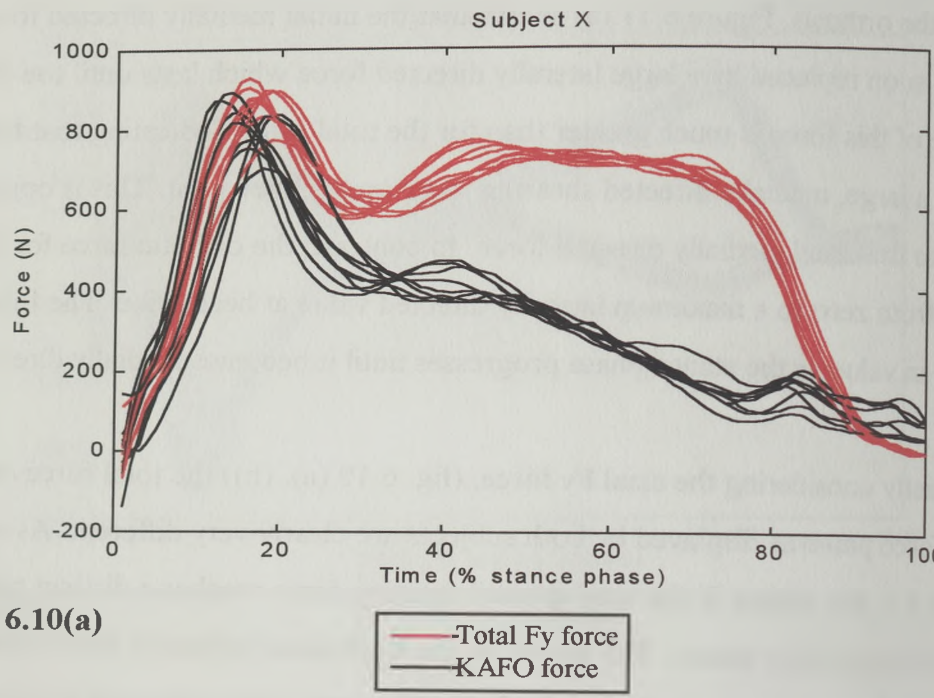

Figure 6.10(a)

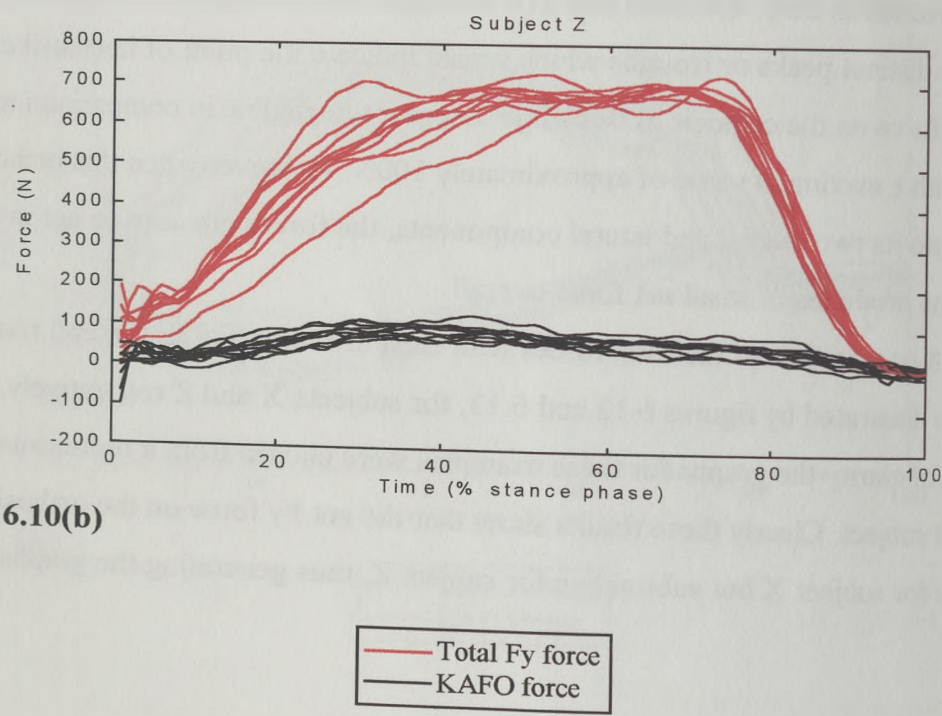

Figure 6.10(b)

Figure 6.11

Comparison of the transducer and total (leg/KAFO complex) medio-lateral load, Fz. Both forces in shank reference frame with positive forces acting upwards. Figure 6.11 (a) and (b) for trials of subjects X and Z respectively.

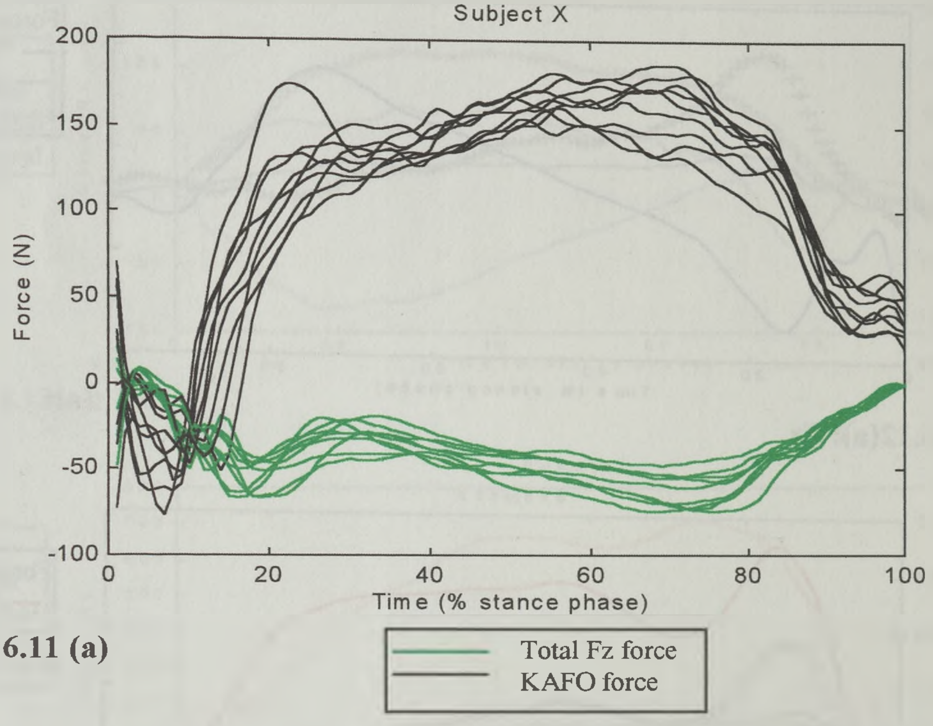

Figure 6.11 (a)

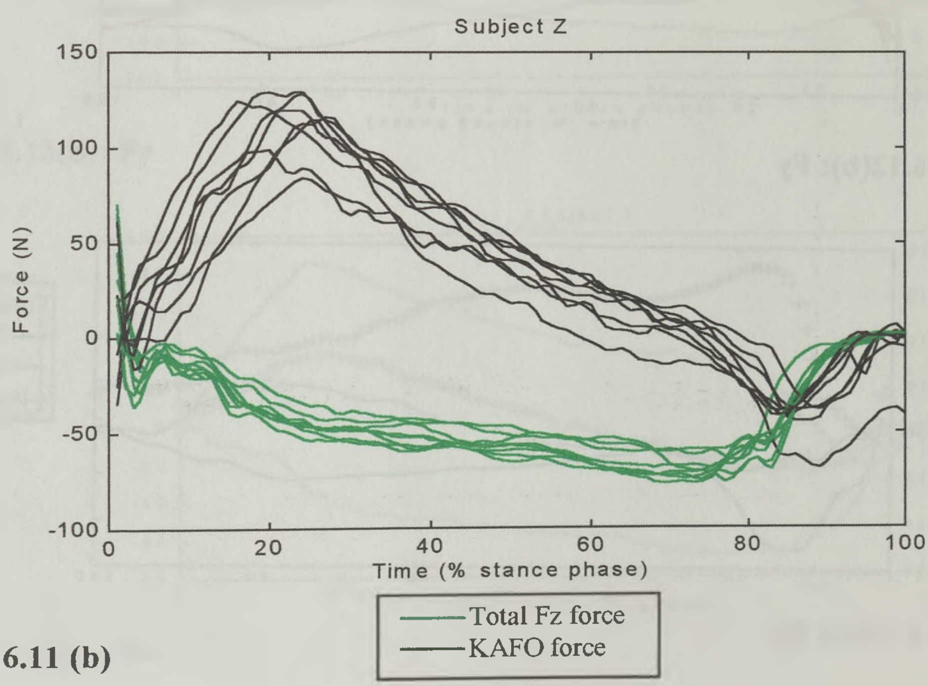

Figure 6.11 (b)

Figure 6.12
Comparison of the loads recorded by the transducers with those calculated for the total leg/KAFO complex. Positive forces for Fx act anteriorly figure 6.12 (a); Fy vertically upwards figure 6.12 (b); and Fz laterally figure 6.12 (c).

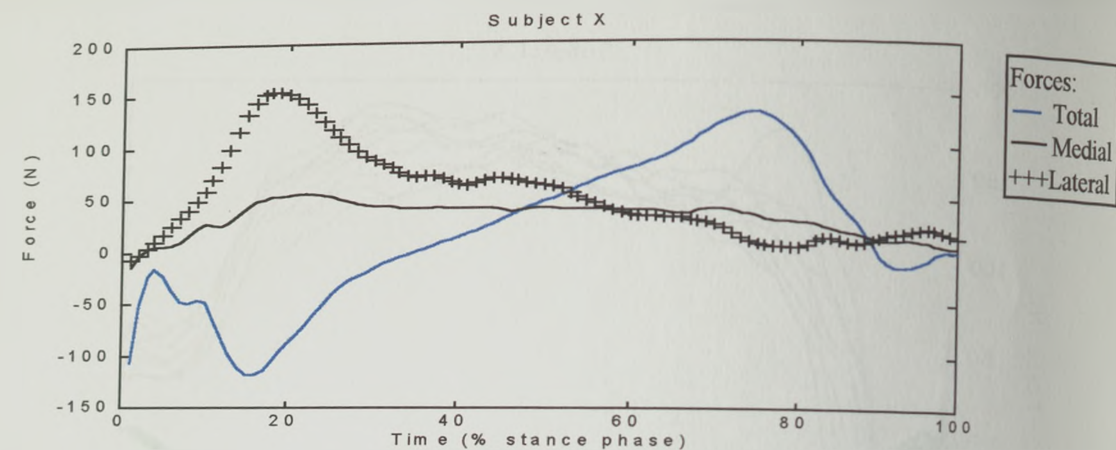

Figure 6.12(a): Fx

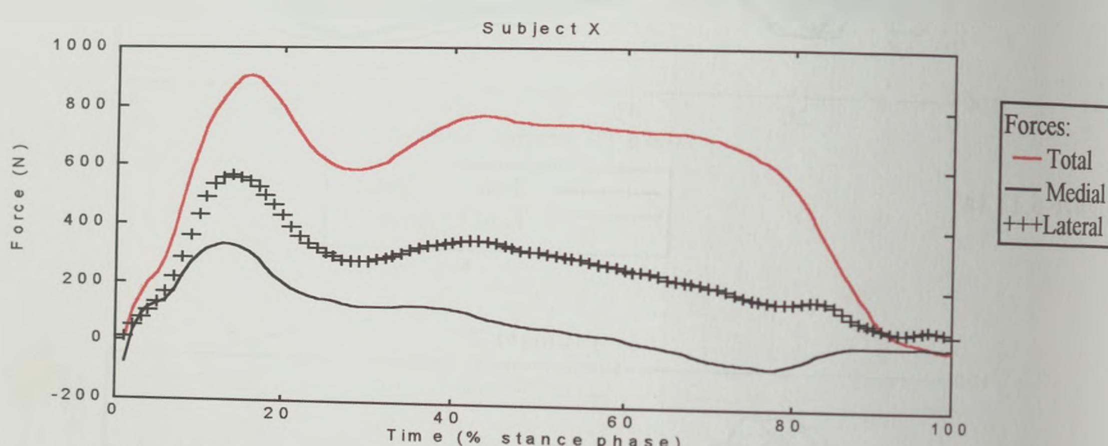

Figure 6.12(b): Fy

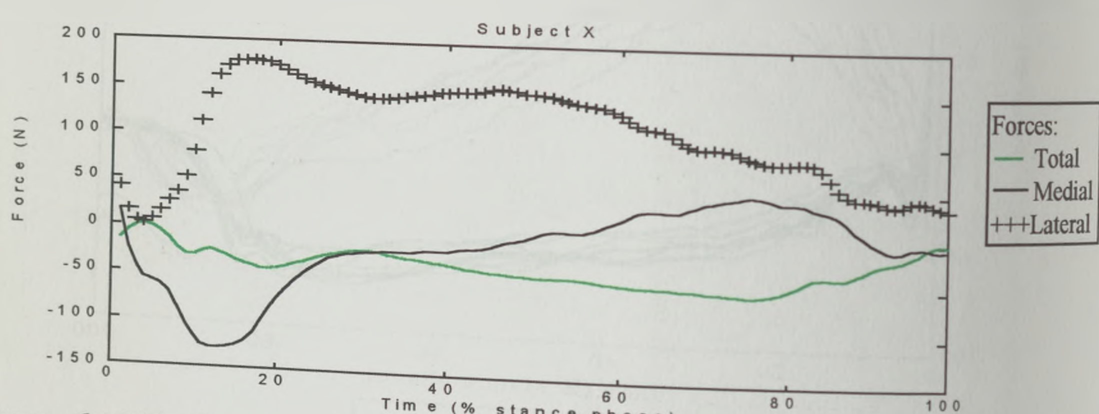

Figure 6.12(c): Fz

Figure 6.13
Comparison of the loads recorded by the transducers with those calculated for the total leg/KAFO complex. Positive forces for Fx act anteriorly figure 6.13(a); Fy vertically upwards figure 6.13(b); and Fz laterally figure 6.13(c).

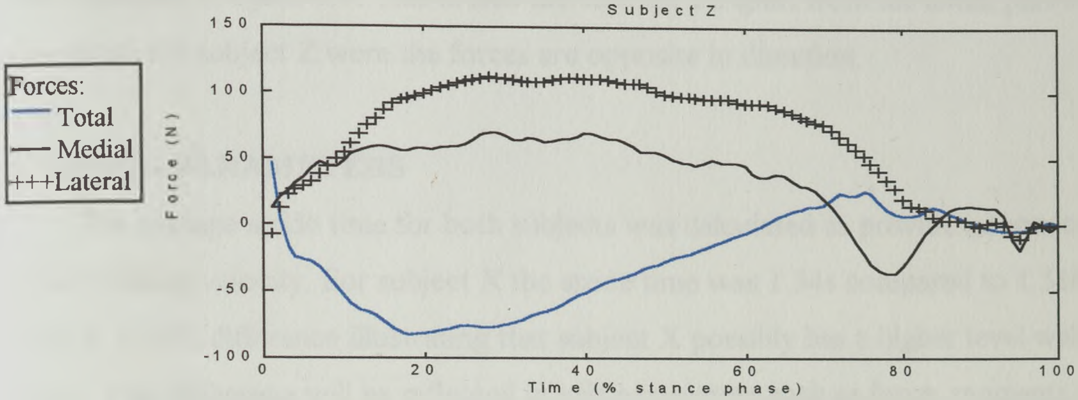

Figure 6.13(a): Fx

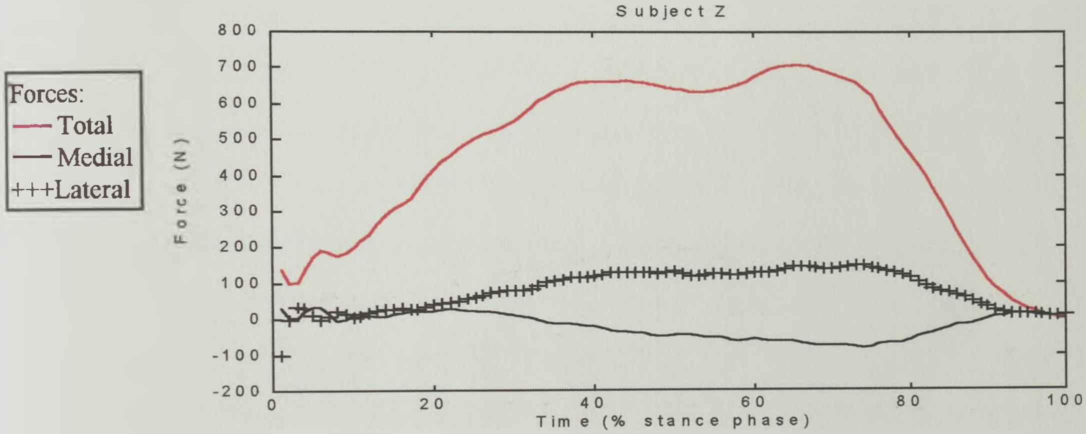

Figure 6.13(b): Fy

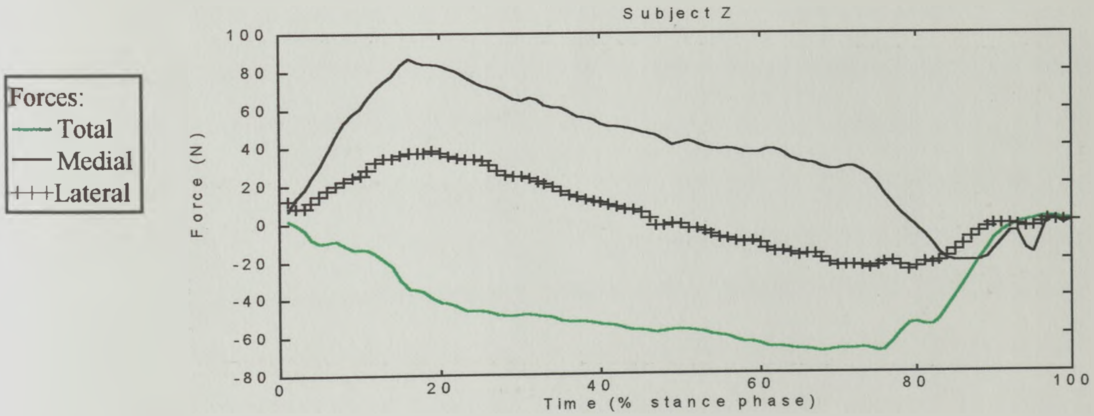

Figure 6.13(c): Fz

figures 6.10 (a) and (b). Similar graphs were plotted for the anterior-posterior and medio-lateral shear forces. Again for the Fx component, figures 6.12 (a) and 6.13 (a) show that the forces recorded from the transducers have an additive effect causing the large orthotic forces displayed in figure 6.9. This is also the case for Fz apart from the initial part of the stance phase for subject Z were the forces are opposite in direction.

6.6 TIMING PARAMETERS

The average stride time for both subjects was calculated to provide information on their walking velocity. For subject X the stride time was 1.34s compared to 1.51s for subject Z, a 13% difference illustrating that subject X possibly has a higher level walking velocity. This difference will be reflected in gait parameters such as force, moments, etc. due to the higher resulting accelerations.

CHAPTER 7: DISCUSSION

This chapter discusses the results obtained in the experimental trials. Since just two subjects were tested, with each exhibiting quite different loading patterns, both sets of results will be discussed simultaneously. The first part of the chapter examines the loadings recorded by the transducers. The deformation of the KAFO is then discussed in the section detailing the ankle joint angle. Next the intersegmental forces and moments on the total leg/KAFO complex are discussed. Finally with both the total loads and the transducer loads in the local reference system of the shank a direct comparison is made.

7.1 TRANSDUCER DATA

The results from the initial analysis are presented in the local reference system of each transducer using the right-handed Cartesian co-ordinate system described in appendix A1. Figures 6.1 and 6.2 illustrate an initial load offset for each channel just before heel strike, i.e. before weight bearing. This occurs despite the fact that the channels were set to zero prior to testing and so must result from the donning of the KAFO. It is believed that the tightening effects of the KAFO strapping are enough to produce these loading effects. The magnitude of this offset varies between the channels and ranges from nearly zero for the My moments to 90N for the lateral Fy force of subject X. A swing phase loading pattern was also seen in the study done by Lippert (1971). He attributed the loading (fig. 6.1 (b)) to the muscle forces voluntarily exerted against the confines of the KAFO. In the research done by Kirkpatrick *et al.* (1969), they considered the early swing phase axial load pattern occurred as a result of their subject trying to bend his leg as the foot rises for the next step. Maqsood (1996) obtained similar results in the level walking tests that she conducted. However, she also recorded the load output when the subject suspended the limb bearing the KAFO. Obviously in these tests the muscles in the limb were not active and as such could not exert a force on the KAFO other than the forces due gravity. Yet, again her results showed loadings slightly offset from zero, suggesting that Lippert's proposal that they were a result of muscle forces was incorrect. Similar loading patterns recorded by Lim (1985) were attributed to the effect of the tight KAFO strapping. For this study, the larger offset values recorded for subject X may indicate that this subject had his KAFO strapping much tighter which caused the uprights to be in an initial state of bending. Lim (1985) also proposed that the orthotic fitting would effect the initial loading pattern.

In terms of the actual loading pattern recorded during the stance phase, the uprights of both orthoses experience a positive force in the anterior-posterior direction, during early stance. This shows the considerable forces imposed on the KAFO at heel strike. In each case the force on the medial upright is greater than that on the lateral one with a difference of approximately 30% for X and just 10% for Z. The greater medial upright loading is considered to be due to the abducted gait and valgus thrust of the knee commonly exhibited by post-polio patients. Lim (1985) and Maqsood (1996) also measured larger Fx forces for the medial upright as did Lippert (1971) who suggested that use of lighter designs with only one medial upright may be possible.

It should be noted that these KAFOs are designed to redistribute the anterior-posterior loads at the anatomical knee joint to more proximal and distal sections, i.e. to the ankle and thigh. This is also true for the medio-lateral loads. For subject X the medio-lateral forces on the KAFO at the level of the knee joint are tending to push the lateral upright laterally and the medial one medially (fig. 6.1 (c)). This is probably due to the weight of the subject bearing down on the orthosis, trying to buckle the bars. The magnitude of these forces are high, approximately 130N laterally and 180N medially and so the KAFO must resist these forces to prevent the uprights from failing. For subject Z a medio-lateral instability was found to occur, figure 6.2 (c), where both uprights act to prevent the knee collapsing in the medial direction during the stance phase. The Mx moments for both subjects act positively on the lateral upright and negatively on the medial one (fig. 6.1, 6.2 (d)). This again suggests the reaction of the uprights against a medio-lateral instability at the knee. The My moments tend to internally rotate the lateral bars. A double peak pattern is seen similar to that generated for the Fy channel. Negligible loading of approximately 0.5Nm occurs on the medial uprights for both subjects.

As explained in section 2.3, the anterior-posterior Mz moment is the most important one as it is where the highest moments are seen to occur. The results reveal negative moments on both uprights as the KAFO resists the moment caused by the ground reaction force which tends to flex the orthosis during the early part of the stance phase. These results thus verify the previous findings for the Fx component that the KAFO acts to prevent the knee from buckling. The magnitude of all three components of the forces, measured for each subject are higher for X. In contrast, the magnitude of all three components of the moments are greater for subject Z compared to subject X.

Finally, very high axial loads in the positive direction were recorded on the uprights of subject X, especially on the lateral side with values of up to 500N recorded. This correlates well with the findings of Maqsood (1996) for this patient but contradicts the studies done by Anderson (1977, 1974) and Trappitt (1979) who both found that the medial upright experienced higher axial loads. Figure 6.2 (b) indicates that the medial upright is actually in tension while the lateral one is in compression. This compares well to the results obtained by Scott *et al.* (1971) for their research on the UCLA functional KAFO. A similar result also occurred for two of the patients used in Lim's (1985) study. It is considered that this pattern is a direct result of the excessive lateral trunk bending exhibited by subject Z.

Overall, the results show that it is difficult to generalise on the loading pattern exhibited by different patients. Although the weight of the two subjects differs by only 10N the magnitude of the axial force measured on the uprights of subject X, the aggressive walker, is approximately three times greater than that recorded for subject Z, the more careful walker. Hence these results tend to agree with the findings of Lim (1985) who suggested that a variety of factors including: the shape of the orthosis, the patients fitness level and their style of walking, all affect the amount of axial load experienced by the KAFO. For the other components of the load, the pattern is also affected by these factors but perhaps more strongly by the individuals own physical impairment and compensatory gait manoeuvres, e.g. medio-lateral instability, etc. This contradicts the suggestion by Scothern & Johnson (1984) who proposed that the strength of the orthosis could be related to the patient's weight.

The accuracy of the measurements which the transducers could record is related to their design and construction. As explained in section 3.4.1, a careful balance between the accuracy of the Fy force and the ability to record the high Mz moments must be decided upon. Each channel was designed to measure within a defined range with loads exceeding these values likely to damage the transducers. Moments of 32Nm were recorded for the Mz channel. These values approach the design limit of 35Nm for this channel. Although both subjects tested in this study were of average weight (approx. 785N), occasionally during testing the force on the Fz channel exceeded its design load of 200N, reaching a maximum of 240N on the lateral transducer during one test. It is likely that heavier subjects would produce greater loads, exceeding the maximum design limits and possibly damaging the transducers. The construction of new transducers which could withstand higher loadings would be useful if future patient tests are to be conducted.

7.2 JOINT ANGLES

The orthoses used in this study were both of the rigid ankle and locked knee type. Thus the angle of the ankle joint was not a major parameter to be studied. However it was considered that by determining its value some knowledge would be gained of the deformation of the KAFO structure during gait. The graphs plotted (fig. 6.3, 6.4) illustrated that maximum bending of the KAFO occurred due to the plantar and dorsi flexion of the ankle about the z-axis with angles of up to $\pm 1.5°$ recorded. Generally a reduced form of the pattern exhibited during normal gait is generated with initial plantar flexion at heel-strike (HS) being followed by an extended period of dorsi flexion from flat-foot (FF) to toe-off (TO), finishing in plantar flexion at push-off (PO). The small movements about the other axes of about $\pm 0.5°$ was considered beyond the accuracy of these tests to be considered significant. In the tests performed by Lim (1985), an assumption was made that the orthoses do not experience excessive deformation. It is interesting to note that the results from this study indicate otherwise although his tests involved conventional metal and leather KAFOs the uprights of which are less likely to deform than the plastic sections of cosmetic KAFOs. However it is possible that more movement may occur within the soft leather strapping.

7.3 GROUND REACTION FORCES

The ground reaction forces (GRF) recorded by the force plate are in agreement with the recordings by the transducers in that the magnitude of the forces for subject X is much greater than those measured for Z, particularly for the Fy forces. The higher walking velocity of X is considered to be partly responsible for these differences. For the Fy force, higher upward and downward accelerations will generate the higher peaks and lower troughs displayed in the graphs. The initial peak corresponding to HS occurs at around 20% of stance for subject X, which is about 5% earlier than for normal gait. The force rises to a peak value of approximately 105% body weight (BW) compared to 112% BW for normal gait (Smidt, 1990). The trough corresponds to the force falling to approximately 80% BW during FF.

A definite second peak corresponding to the upward acceleration between FF and TO is not seen, indicating a less effective PO. Instead the earlier transition between braking and propulsion resulting in an extended period corresponding to PO may indicate compensatory techniques by the subject to compensate for the lower maximal vertical component. A completely different Fy pattern is exhibited by subject Z where neither peaks nor troughs may be distinguished. Instead the propelling action of the opposite limb acts to cause an upward acceleration on the bodies centre of gravity producing the graph seen in figure 6.6 (b). The Fy graph generated for this subject has a similar pattern to those produced in the studies of Kirkpatrick *et al.* (1969) and Lehmann *et al.* (1970b). However no information is given in either study of the functional impairment of the subject tested.

The Fx graphs for both subjects have a similar pattern to those produced for a normal subject. An immediate positive, forward force on the foot is a result of the impact caused by the foot hitting the ground hard at heel strike. This is followed by a period of backward force of approximately 15-20% BW. The transition to a forward force occurs around mid-stance as the foot tries to push backwards against the frictional resistance of the ground.

The Fz graphs indicate an initial laterally directed GRF on the foot (figs. 6.5, 6.6(c)). This occurs at HS as the abducted leg tries to adduct as it hits the ground. However, the force is soon reversed to a medially directed one in an effort to balance the moment caused by the position of the centre of gravity of the body.

7.4 INTERSEGMENTAL MOMENTS

The magnitude of the intersegmental moments at the knee joint is approximately equal for both subjects, although the patterns displayed are slightly different with greater variability among the trials for subject Z. Clearly moments in the sagittal and coronal planes dominate with the magnitude of the My force only about 10% of the Mx and Mz moments. The negative Mx moment suggests that the leg/KAFO complex is in an abducted gait. An initially externally rotating torque corresponds to HS where the foot is prevented from internally rotating due to the frictional forces from the ground. This moment is reversed during the FF to TO period where the force required at PO tends to externally rotate the foot causing an internally rotating force on the foot.

Finally the Mz component of the load illustrates the moment in the sagittal plane, due to the GRF which passes behind the knee joint centre during early stance and thus tends to cause the knee to flex (figs. 6.7, 6.8 (c)). This moment has a magnitude of 40Nm which is approximately equal to the sum of the two forces recorded for the medial and lateral uprights of approximately 20N each. Although these moments are not in the same reference frame, this result does suggests that the KAFO is stabilising the knee joint in the anterior-posterior direction, as required. It was noted that the patients could not walk without their KAFOs unless they aided their leg extensor muscles by applying a posteriorly directed force on the front of their thigh which again indicates that the KAFOs are performing their knee stabilising function.

7.5 COMPARISON OF TRANSDUCER AND TOTAL LOADS

7.5.1 Forces

When both sets of forces, i.e. total GRF and transducer forces are translated into the reference system of the shank then a direct comparison between their magnitude and direction can be made.

Figure 6.9 illustrates that the Fx component of the total and KAFO loads are acting in opposite directions. This suggests that the KAFO is causing an extra posteriorly then anteriorly directed shear force on the knee joint during stance phase. The GRF is approximately 30% and 25% BW for subjects X and Z respectively compared to the usual ±15% BW seen during normal gait. However the extended backwards force followed by a much reduced forward force for subject Z suggests that the majority of the effort is used to decelerate the body after heel strike. This is followed by an ineffective PO. The initial shock effect occurring at HS is directed anteriorly for both the total and transducer forces, indicating that the anatomy is protected from this shock effect by the use of the KAFO.

A comparison of the medio-lateral shear forces again reveals that the KAFO does not transmit the medially directed load. Instead the KAFO generates its own force in the lateral direction thereby increasing the medial force on the anatomy up to 25% BW, 10% greater than for normal gait. Kirkpatrick *et al.* (1969) reported similar findings for the Fx and Fz forces when they investigated the load sharing properties of an ischial weight bearing KAFO. However Trappitt (1979) found that the Fx and Fz transducer forces were generally of greater magnitude but in the same direction as the GRF which produced forces on the anatomy which were opposite in direction than those normally experienced during gait.

A comparison of the difference in the axial loads will provide the clearest indication of the load sharing capability of the KAFOs. For subject X the KAFO appears to transmit approximately 85% of the axial load in early stance thus reducing the compressing forces on the anatomy at this point. Following the trough associated with the FF to TO period, the transducer forces continue to decrease while the total force rises again. Thus the KAFO stops relieving the anatomy as the centre of pressure on the foot moves towards the metatarsal heads where active loading occurs during PO.

Similar results were reported by Lehmann *et al.* (1970b) for their investigation of the axial loading on a free ankle, fixed knee KAFO. Lippert (1971) found that the HS to FF period was prolonged and that the heel bore the full impact of the forces which again agrees with the results of subject X. Lim (1985) also determined that the orthosis was most effective at the early stages of the stance phase. The high degree of weight relief offered by the fixed knee and ankle, high brimmed KAFO worn by this subject compares well with the study by Lehamnn *et* al. (1970b) where they reported that more weight relief was offered by a fixed knee compared to the free knee design. However Lippert (1971) disagreed with these findings when he reported that orthoses with fixed ankle assemblies showed less weight relief.

On first glance, figure 6.10 (b) seems to indicate that the results for subject Z totally contradict all previous studies with the orthosis offering practically no weight relief. However when it is remembered that the medial upright is actually in tension during the stance phase while the lateral one experiences compressive forces, the counteractive nature of these results can be understood. As explained in section 7.1, this loading pattern is thought to be due to the excessive lateral trunk bending exhibited by this subject. Since his KAFO is non-weight bearing the tightness of the strapping at the thigh and calf bands will have a greater affect on the ability of the KAFO to transmit the forces through the soft tissue of the leg.

The results from this study would lead the author to disagree with the views of Lehneis (1969) and Lippert (1971) that KAFOs are overdesigned. Although KAFOs may contain more metal than is required, the high axial and medio-lateral forces recorded at the knee joint indicate that, if anything the uprights are not strong enough at this point and that a complete revision of the standards used in their design and manufacture are required. The high Mz moments reinforce this view.

7.5.2 Moments

When determining the moments recorded at the orthotic knee joint by the transducer in the local reference system of the shank, consideration must also be given to the effect of the forces recorded by the transducer. The moments due to the forces are calculated from the product of the forces multiplied by the perpendicular distances from the knee joint centre (pivot). Unfortunately due to the time restrictions of this project, these additional moments were not calculated. Thus an accurate comparison of the moments recorded by the transducer with the total moments calculated from the force plate data for the leg/KAFO complex could not be made. However the length of the vector between the knee joint centre and each transducer origin was calculated to be 63mm. This distance is resolved into its three orthogonal components to obtain the lever arms about which the forces act and hence their maximum value is also 63mm. Since this is relatively low when compared to the overall anatomical distances, the extra moments at the knee due to the forces at the transducer will also be small.

When processing the transducer data it was also noticed that the rotation matrices between the shank and transducer local reference systems were close to unity, again indicating that the forces at the transducer will not significantly alter the moments at the knee centre. In conclusion, it is believed that if the moments calculated from the force plate data were compared with those calculated from the transducer data the difference in the flexing moments about the z-axis of the knee joint would be zero. As discussed in section 2.2, the ground reaction force causes a flexing moment at the knee during the early part of the stance phase. A zero anatomical moment would indicate that the KAFO is transferring this extending moment away from the knee joint and onto the thigh and ankle section and thus preventing the knee joint from buckling. This would verify the view that the KAFO is performing its desired function of providing knee stability during weight bearing.

6.5 ACCURACY

The accuracy of the recorded marker co-ordinates will depend on the accuracy of the VICON equipment and the magnitude of the residual errors generated by the initial calibration procedure. Considerable effort was spent positioning the cameras during calibration to ensure that these errors were as small as possible.

The accuracy of the equipment used to record the orthotic loading was discussed in section 3.4.2 which detailed the calibration of the transducers. The graphs plotted from the results showed the transducers to have satisfactory linearity and repeatability, with no signs of hysteresis during repeated loading.

In this study, segment parameters such as the mass, centre of gravity and moments of inertia were calculated from the values proposed by Contini (1971). These parameters were derived from studies on normal subjects. However the subjects used in this study both suffer from post-poliomyelitis syndrome, causing flaccid paralysis and atrophy of the impaired limb. This will result in minor inaccuracies in the calculated mass and moments of inertia of the body segments but is unlikely to alter the position of the centre of gravity.

The foot and shank were assumed to be rigid body segments. For this assumption to be valid the position of the markers on the segments should not alter during the gait cycle. The markers for the foot segment had to be attached to the shoe. Subject X wore more flexible sports shoes compared to the more rigid shoes worn by subject Z and hence the inaccuracies in the marker co-ordinates for X are likely to be greater. These errors may have a significant effect on the angle calculated for the ankle joint but due to the insignificant mass of the foot and shoe, will have a negligible effect on the total loads at the knee joint. The repeatability of the distance between the two markers on the calibration stick will provide a good indication of the accuracy of the VICON equipment and of the data processing software in determining the other marker co-ordinates. This distance was measured to be 200mm (±1mm) by hand. However using the co-ordinates recorded by the VICON data, the distance was calculated to range between 197.3 and 200.1mm.

CHAPTER 8: CONCLUSIONS

All channels recorded an initial offset load before heel strike when no weight was applied to the orthosis. Since the transducers were initially zeroed prior to patient donning, these loads are considered to arise from the tightening effects of the strapping during donning of the KAFOs. The control of the patient over this effect results in the different offsets seen between the two patients. Overall higher loads were recorded on the lateral upright compared to the medial one.

The results for each subject varied significantly in the magnitude and nature of the loading pattern. The greater loads for patient X were probably due to a combination of his high brimmed orthosis, tighter strapping loads and higher walking velocity. The extremely high loads of up to 600N recorded for patient X occasionally exceeded the maximum design limits for the transducers in the Fz direction.

Comparison of the anterior-posterior moments, reveal that the KAFO prevents the knee from flexing (and therefore buckling) during early stance for both patients. The KAFO thus adequately performs its joint stabilising function. The axial force results for patient X wearing an high brimmed KAFO suggest that the orthosis relieves the anatomy by up to 90% during early stance. As the gait cycle progresses this weight sharing ability falls to approximately 20% at late stance. The intense lateral trunk bending exhibited by patient Z generated a tensile force on the medial upright but a compressive force on the lateral one. Consequently, when the loads were vectorially added the results showed that this KAFO offered practically no weight-bearing relief.

RECOMMENDATIONS FOR FUTURE WORK

The accuracy of the tests could be improved by use of five markers on each segment. Thus the loss of a marker during recording would not be so crucial. Further improvements to the accuracy of the tests could be made by deriving algorithms which would reduce the noise of the kinematic data, possibly by using a polynomial to model the gait cycle.

A more complete biomechanical analysis could be made by recording the ground reaction forces of the sound leg and by using markers on the thigh of both limbs and the pelvis. This could show the effect of wearing an orthosis on the sound limb and would allow a comparison of the total loads between both limbs to be made. It would also be interesting to conduct the tests at different walking speeds to determine the effect of walking velocity on the total and orthotic loads. Testing on different days would enable the difference between the initial offset loads to be examined.

For a full evaluation of the functional performance of KAFOs a larger study using a wide range of patients with different medical impairments should be conducted.

Finally, since the forces on the transducers occasionally exceeded their maximum design limits, the construction of new, stronger transducers would be useful for any future KAFO tests.

REFERENCES

American Academy of Orthopaedic Surgeons -AAOS (1985), Orthopaedic appliances atlas, 2nd edition. The C.V, Mosby company, Missouri.

Anderson EG, Frank PL, Henshaw JT & Rae HG (1977), Clinical assessment of a new weight-relieving brace. J Bone Joint Surg 59B:439-445

Bowker P (1987), Biomechanics of orthoses. Physiotherapy 73(6):270-274.

BS 2574:Part 2 (1972), Lower limb orthoses: Specification for metal knee joints, British Standards Institution, London.

Cappozzo A, Catani F, Della Croce U & Leardini A (1995), Position and orientation in space of bones during movement: anatomical frame definition and determination. Clin Biomechanics 10(4):171-178.

Challis JH (1993), An examination of procedures for determining body segment attitude and position from noisy biomechanical data. Med Eng Phys 17(2):83-90.

Condie DN (1987), Biomechanics of orthoses. Physiotherapy; 73(6):275-279.

Condie DN, Meadows C B (1993),Ankle-foot orthoses. In 'Biomechanical basis of Orthotic Management', eds Wallace WA, Bowler P, Condie DN, Bader DL, Pratt DJ, Butterworth-Heinemann Ltd.

Contini R (1970), Body segment parameters (phatologies). Technical Report No 1584.03. New York University research division.

Dittmer DK, MacArthur-Turner DE & Jones K, (1993), Orthotics in stroke. Phys Med Rehabil: State Art Rev 7:161-177.

Elias E (1994), Application of design methodology to the development of knee and ankle mechanisms for an orthosis. PhD Thesis, University of Strathclyde, Glasgow.

Engen TJ (1989), Lightweight modular orthosis. Prost & Orthot Int 13:125-129.

Esquenzai A & Hirai BA, (1994), Assessment and Management of gait dysfunction in patients with spastic stroke or brain injury. Phys Med Rehabil: State Art Rev 8:523-533.

Gozal D (1986), Load analysis of the knee joints of the cosmetic type knee-ankle-foot orthosis. MSc Thesis, University of Strathclyde, Glasgow.

Granata C, DeLollis A, Campo G, Piancastelli L, Merlini L (1990), Analysis, design and development of a carbon fibre reinforced plastic knee-ankle-foot orthosis prototype for myopathic patients. J. Eng Med 204:91-96.

Grood ES & Suntay WJ (1983), A joint co-ordinate system for the clinical description of three-dimensional motions: Application to the knee. J Biomechanical Engineering 105:136-144.

Harris EE (1973), A new orthotic terminology. Orthot Prosthet 27:6-19.

Henshaw JT (1970), Design and development of a cosmetic calliper. Biomed Eng 5:60-64.

Kirkpatrick GS, Day EE, Lehmann JF (1969), Investigation of the performance of an ischial load-bearing brace. Experimental Mechanics, January 1-5.

Korsah KG (1990), Surgical Pathology, Assessment and Management of Poliomyelitis. JCRPO Journal 1(3):114-146.

Lehmann JF & Warren CG (1976), Restraining force in various designs of knee-ankle orthoses: Their placement and effect on the anatomical knee joint. Arch Phys Med Rehabil 57:430-437.

Lehmann JF (1979), Biomechanics of Ankle-Foot Orthoses: Prescription and Design. Arch Phys Med Rehabil Vol 60:200-207.

Lehmann JF, Warren CG, DeLateur BJ, Simons BC, Kirkpatrick GS (1970b). Biomechanical evaluation of axial loading in ischial weight-bearing braces of various designs. Arch Phys Med & Rehabil 51:331-337.

Lehmann JF, Warren CG, Hertling D, McGee M, Simons BC & Dralle A (1976), Craig-Scott orthosis: A biomechanical and functional evaluation. Arch Phys Med Rehabil 57:438-442.

Lehmann JF, Warren CG, Hertling D, McGee M, Simons BC, Dralle A (1970a), Craig-Scott Orthosis: A biomechanical and functional evaluation 57:438-442.

Lehneis HR (1969), New concepts in Lower Extremity Orthotics. Med Clin N Am 53(3):585-92.

Lehneis HR (1972), New Developments in Lower-Limb Orthotics Through Bioengineering. Arch Phys Med Rehabil 53:303-322.

Lim SYE (1985), A study of the biomechanical performance of Knee-Ankle-Foot orthoses in normal ambulatory activities. PhD Thesis, University of Strathclyde, Glasgow.

Lippert FG (1971), A long-leg brace for comprehensive force measurement. Acta Orthop Scand 42, suppl 138.

Mann RA (1988), Gait Analysis. In 'The Foot', volume 1, ed Helal B & Wilson D, Churchill Livingstone, Edinburgh 96-107.

Maqsood T (1996), Load analysis of a knee-foot-ankle orthosis of the cosmetic type. MSc Thesis, University of Strathclyde, Glasgow.

McHugh B, Campbell J (1987), Below-knee Orthoses. Physiotherapy 73(8):380-385.

Merritt JL (1987), Knee-Ankle-Foot Orthotics: Long leg braces and their practical applications. Phys Med Rehabil State Art Review 1(1):67-82.

Murdoch G (1976), The Advance in Orthotics. Edward-Arnold (Publishers) Ltd, London.

Nicol AC & Paul JP (1988), Biomechanics. In 'The Foot', volume 1, ed Helal B & Wilson D, Churchill Livingstone, Edinburgh 75-86.

Perry J (1967), The mechanics of walking - a clinical interpretation. In 'Principles of lower extremity bracing', ed Perry J & Hislop HJ, American Physical Therapy Association, Alexandria, Virginia 33-35.

Platts RGS (1988/89), Long leg callipers or KAFOs - who needs them? Orthopaedic Product News; Dec 88/Jan/Feb89:18-19.

Scothern RP & Johnson GR (1984), A method for determining the mechanical characteristics of orthotic knee joints. Prosthet & Orthot Int 8:16-20.

Scott BA (1971), Engineering principles and fabrication techniques for the Scott-Craig long leg brace for paraplegics. Orthot and Prosthet 25(4):19-24.

Smidt GL (1990), Gait in Rehabilitation. Churchill Livingstone, New York.

Trappitt AE & Berme N (1981), A transducer for the measurement of lower limb orthotic loads. Engineering in medicine 10(3):149-158.

Trappitt AE (1979), Load measuring system developed for patient-orthosis tests. PhD Thesis, University of Strathclyde, Glasgow.

Trautman P (1980), Lower limb orthotics. In 'Orthotics etcetera', ed Redford J. Waverly Press, Inc, Baltimore.

Tuck WH (1974), The Stanmore cosmetic calliper. J. Bone Joint Surgery 56B:115-120.

Van der Linden ML (1995), A biomechanical investigation into the effects of various energy storing prosthetic feet on transfemoral amputee gait: A pilot study. Internal report, University of Strathclyde, Glasgow.

Veldpaus FE, Woltring HJ & Dortmans LJMG (1988), A least-squares algorithm for the equiform transformation from the spatial marker co-ordinates. J Biomechanics 2:45-54.

APPENDICES

A1: SIGN CONVENTION

The Cartesian right-handed co-ordinate system is applied to the ground reference system and all local reference systems including: the shank, foot, medial and lateral transducers. It is defined as:

Linear measurements:

X-axis: horizontal and positive in the direction of progression

Y-axis: vertical and positive upwards

Z-axis: horizontal and positive from left to right

Angles measurements:

Clockwise rotations when viewed along the positive direction of the axis are defined as positive rotations (right hand screw rule).

Loads:

Loads are applied by an external device to the distal end of a body segment. Forces act in the positive direction of a co-ordinate axis. Moments act on the body in accordance with the right-hand rule for angular directionality.

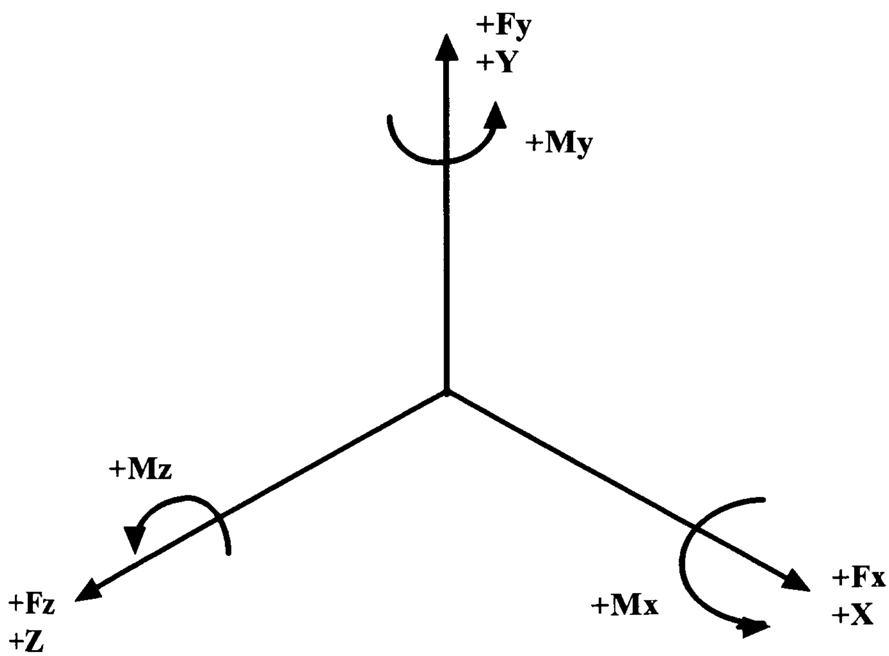

Figure A1: Cartesian right-handed co-ordinate system

A2: CALIBRATION FACTOR CALCULATIONS

Example 1

The first example illustrates the method used to determine the principal sensitivity coefficient $C_{11}$and the five cross-talk co-efficients C_{21} C_{31} C_{41} C_{51} C_{61} when the Fx channel was loaded. The load was increased from 0 to 98.7N and the output on the digital voltmeter (DVM) was recorded.

Fx loaded

Load (N)	Fx (mV)	Fy (mV)	Fz (mV)	Mx (mV)	My (mV)	Mz (mV)
0	0.4	0.1	0	-0.2	0	0.3
98.7	194.6	-12.2	6.9	-1.3	-2.9	4.6

Since the only load is in the positive Fx direction all other loads in equation 4.3 equal zero. Hence:

$$SF_x = C_{11}F_x \qquad \text{Equation A2.1}$$

where: SF_x = voltage difference

C_{11} = unknown calibration factor

F_x = applied load

The first step is to divide the output voltage by the bridge voltage (bv) and gain settings for each individual channel.

For C_{11} (Fx):

Measured output $=SF_x/$ (bv*gain) = (194.6-0.4)(x 10^{-3})/(3 *2000) = 32.37 x10^{-6}

Substituting into equation A2.1

$$32.37 \times 10^{6} = C_{11}*98.7$$

$$C_{11} = 0.328 \times 10^{-6}\ VN^{-1}$$

For ease of comparison this result is multiplied by 10^8 to convert the value into the same units used by Lim (1985), i.e. $C_{11} = 32.8$

Using the bridge voltage, gain and output voltage for each particular channel the same method may be applied to determine the cross-talk effects for all other channels, e.g.

For C_{21}(Fy output from Fx load):

Measured output $=SF_y/ (bv*gain) = (12.2-(-0.1))(x\ 10^{-3})/(6 *1000) = 2.05\ x10^{-6}$

Substituting into equation A2.1

$$2.05 \text{ x } 10^6 = C_{21}*98.7$$

$$C_{21} = 20.7 \text{ x}10^{-9}\ VN^{-1}$$

Example 2

All six calibration factors for the Fy, Fz and My channels can be determined using the method described above. However, when the Mx and Mz channel are loaded the small displacement of the shear force strain gauges will induce a load in the Fz and Fx channels respectively. From equation 4.2, the calibration factors for these channels are determined using the following equations:

Mx loaded (C_{14} to C_{64}):

$$SF_x = C_{13}F_z + C_{14}M_x$$

$$SF_y = C_{23}F_z + C_{24}M_x$$

$$SF_z = C_{33}F_z + C_{34}M_x$$

$$SM_x = C_{43}F_z + C_{44}M_x$$

$$MF_y = C_{53}F_z + C_{54}M_x$$

$$MF_z = C_{63}F_z + C_{64}M_x$$

where: F_z: is the force applied to the Fz channel.

M_x: is the moment applied to the Mx channel

C_{13} to C_{63}: are the calibration factors determined by loading Fx previously

SF_x to SM_z: are the output voltages from the Fx to Mz channels with each of the respective bv and gains taken into account.

Mz loaded (C_{16} to C_{66}):

$$SF_x = C_{11}F_x + C_{16}M_z$$
$$SF_y = C_{21}F_x + C_{26}M_z$$
$$SF_z = C_{31}F_x + C_{36}M_z$$
$$SM_x = C_{41}F_x + C_{46}Mz$$
$$SM_y = C_{51}F_x + C_{56}M_z$$
$$SM_z = C_{61}F_x + C_{66}M_z$$

where: F_x: is the force applied to the Fx channel.

M_z: is the moment applied to the Mz channel

C_{11} to C_{61}: are the calibration factors determined by loading Fz previously

SF_x to SM_z: are the output voltages from the Fx to Mz channels with each of the respective bv and gains taken into account.

A3: ANATOMICAL REFERENCE SYSTEMS

List of definitions of the local reference systems from the anatomical landmarks (Cappozzo *et al.*,1995)

SHANK

Origin: The origin is the midpoint of the line joining the lower ends of the lateral and medial malleoli (LM and MM).

Y-axis: The landmarks of the malleoli and the head of the fibula define a plane which is quasi-frontal. A quasi-sagittal plane, orthogonal to the quasi-frontal plane is defined by the midpoint between the malleoli and tibial tuberosity (TT). The y-axis is defined by the intersection between the above mentioned planes with its positive direction proximal.

Z-axis: The z-axis lies in the quasi-frontal plane with its positive direction from left to right.

X-axis: The x-axis is orthogonal to the yz plane with the positive direction forward.

FOOT

Origin: Calcaneus landmark (CA).

Y-axis: The calcaneus and the first and fifth metatarsal heads (FM and VM) define a plane which is quasi-transverse. A quasi-sagittal plane, orthogonal to this latter plane is defined by the calcaneus landmark and the second metatarsal head (SM). The y-axis is defined by the intersection of these two planes and its positive direction is proximal.

Z-axis: The z-axis lies in the quasi-transverse plane and its positive direction is from left to right.

X-axis: The x-axis is orthogonal to the yz plane and its positive direction is dorsal.